# Numerical Investigations of Discrete Models for Traffic Flow

Inaugural – Dissertation
zur
Erlangung des Doktorgrades
der Mathematisch – Naturwissenschaftlichen Fakultät
der Universität zu Köln

vorgelegt von
**Ludger Santen**
aus Haren

Köln 1999

| | |
|---|---|
| Berichterstatter: | Prof. Dr. J. Zittartz |
| | Prof. Dr. M. Schreckenberg |
| Tag der mündlichen Prüfung: | 9. Februar 1999 |

# Contents

# Chapter 1

# Introduction

## 1.1 Modeling Complex Phenomena

In the first part of this century physical research was mainly characterized by the development of more and more sophisticated methods which allowed to get a very deep understanding of the fundamental laws of nature. In recent years several theoretical concepts have been developed in physical research which can also be applied in other fields of interest, e.g. sociology, economics, or biology. In particular the tools of statistical physics have been successfully generalized to other fields of interest.

Obviously for complex systems like the stock market the interactions between the agents cannot be deduced from first principles. But it turns out that in many cases a phenomenological definition of the microscopic dynamics is appropriate. The phenomenological laws often have a stochastic component which compensates the incomplete description of the dynamics of the individual species. This way of modeling allows for a description of rather complex problems with simple stochastic models.

A powerful approach for the modeling and simulation of complex phenomena which has been widely used in recent years are cellular automaton (CA) models. The basic idea was already proposed by John von Neumann in the late 40's, but extensive applications were worked out only after the publication Wolfram's famous book in 1986 [1] where the first systematic investigation of CA models has been presented. It became clear that CA models are well suited to analyze even complex phenomena [2]. By design CA models allow for high performance implementations because discrete variables are used. Therefore very efficient coding techniques can be applied. This allows to simulate large systems with an enormous efficiency which is necessary for a systematic investigation of many complex phenomena.

An analysis of CA models is not only possible by computer simulation but also analytical techniques have been developed. Nevertheless an analytical treatment of CA models is often difficult. Beyond the fact that generally a treatment of an interacting particle system is a formidable task, an additional difficulty is that often systems far from equilibrium are described where dissipative processes are important. Therefore the standard methods of statistical mechanics cannot be used. In contrast the master equation which describes the time evolution of such processes has to be analyzed directly. The master equation can be viewed as the analogue of the Schödinger equation for stochastic systems and it turns out that this analogy is indeed very useful. E.g. the generalization of methods which were originally developed for the treatment of interacting quantum systems have been successfully applied in order to obtain exact solutions for the stationary state of stochastic systems.

One interesting field for the application of CA models is the modeling of traffic flow. In that field CA models have been first proposed by Cremer [3] and by Nagel and Schreckenberg [4]. In particular the model of Nagel and Schreckenberg (NaSch model) is widely used to date. The NaSch model is a stochastic CA model which is defined by a simple set of update rules. Therefore the possible computational performance is much higher than for other microscopic modeling approaches which exist in that field. Albeit its simplicity, this model gives a quite realistic description of traffic flow.

From a theoretical point of view the NaSch model is of interest as an example of a system far from equilibrium, i.e. even the stationary state is not described by equilibrium statistical mechanics. Moreover, also analytical results have been found which is of special interest because those are rare in that field.

## 1.2 Overview

The aim of this work is to describe the behavior of discrete one-dimensional stochastic systems and to discuss their application for the modeling of traffic flow.

In chapter 2 the experimental facts and existing modeling approaches for traffic flow will be reviewed. Then analytical techniques for the treatment of discrete one-dimensional stochastic systems will be explained in chapter 3.

In chapter 4 the parameter dependence of a phase transition for a CA model for traffic flow will be analyzed. The phase transition describes the transition from a free-flow state at low densities to a high-density state where jams are present.

In the following chapter the effects of local impurities in a periodic lattice will be discussed for different models as well as for different implementations of the impurities. Here phase-separation effects can be observed in different density regimes. Driven systems with open boundary conditions are considered in section 6. Here so-called boundary induced phase transitions, i.e. phase transitions which are governed by the choice of the boundary conditions, can be observed.

In the following chapters we concentrate on realistic applications of the investigated models. Experimental observations on traffic flow show the existence of meta-stable states. These states are not described by the Nagel-Schreckenberg (NaSch) model. Therefore generalizations of the NaSch model which are able to reproduce this phenomenon are introduced in chapter 7. In chapter 8 the effect of different types of cars in two-lane systems will be analyzed. In particular, several variants of lane-changing rules and the bulk dynamics will be discussed. In the final section a summary and discussion of the results will be given.

# Chapter 2

# Traffic Flow: Experimental Facts and Modeling Approaches

This chapter summarizes the experimental findings and modeling approaches for traffic flow. The first section gives an overview of empirical facts which have been revealed in several experimental studies. In the following section the most important theoretical approaches of highway traffic will be introduced briefly.

## 2.1 Empirical Results

Although the systematic investigation of traffic flow has a surprisingly long history [5–10] (first experimental investigations have been performed already in 1935 by Greenshields) the experimental situation is still discussed controversially. Nevertheless some basic facts which will be discussed in this section seem to be well established.

Obviously traffic flow phenomena strongly depend on the occupancy of the road. At low densities interactions between cars are rare and therefore an undisturbed movement of each car is possible. At high densities the situation is different because the drivers strongly interact. Beyond this trivial observation some nontrivial effects have been observed which will be discussed in the following.

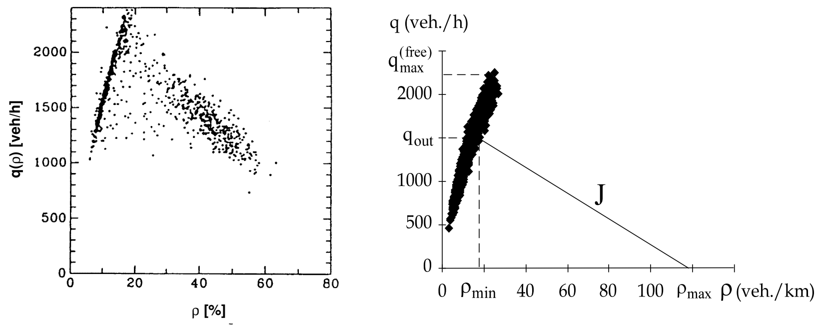


Figure 2.1: Fundamental diagrams from different measurements. The left part of the figure shows the flow $q(\rho)$ dependent on the relative occupancy $\rho$. The data have been obtained on a Japanese highway (from [7]). The low density branch of the right fundamental diagram shows measurements from German highways while the high density branch is depicted schematically (from [11]). Here the density is given in units of vehicles per kilometer.

The most important quantitative result which one gains from traffic measurements is the relation between the average velocity $v(\rho)$ and the occupancy of the road $\rho$. Clearly the maximal value $v_{max}$ of $v(\rho)$ can be observed at rather low density where the cars move freely. At high densities the velocity of cars is drastically reduced. Finally in a compact jam of density $\rho_{max}$ cars cannot move at all. For intermediate densities one expects

$$\frac{dv(\rho)}{d\rho} \leq 0 \tag{2.1}$$

because interactions between cars lead to a reduction of the average velocity.

Even more characteristic for the capacity of the road at a given density of cars is the density dependence of the average flow which is given by

$$q(\rho) = v(\rho)\rho. \tag{2.2}$$

The flow-density relationship determines the so-called "fundamental diagram". At first sight one can distinguish two parts of the fundamental diagram (see Fig. 2.1). For low densities the flow increases linearly with the average density because all vehicles move with their desired velocity. While the linear part at low densities was confirmed in several investigations, the form of the fundamental diagram at higher densities is less clear. An often suggested form is the "inverse lambda" shape [8, 11]. In this case the high-density or "jammed" branch of the fundamental diagram is a linearly decreasing function of the density. Although this form of the fundamental diagram is widely accepted several alternative shapes of the fundamental diagram are compatible with the empirical results (see [8] for an overview).

The right part of Fig. 2.1 shows another characteristic feature of empirical fundamental diagrams. Close to the optimum density $\rho_{opt}$, i.e. the density where the flow takes its maximal value $q_{max}^{(free)}$, the flow does not depend uniquely on the density. This non-unique behavior of the flow is closely related to the existence of hysteresis effects and meta-stable states. In the context of traffic flow hysteresis effects have the following meaning. If a measurement starts in the free-flow regime an increase of the density leads to an increase of the flow until $\rho_{opt}$ is reached. A further increase of the density leads to a discontinuous reduction of the flow ("capacity drop") and jams emerge. The high flow values of the homogeneous state can only be reached if the density is noticeably reduced so that the jams dissolve.

New experimental results of highway traffic indicate the existence of a third state of traffic flow. This third state, denoted as synchronized flow, is often observed in congested traffic. So far no clear definition of synchronized traffic exists, but some characteristics can be obtained from experimental data [12–15]. Synchronized traffic is observable at high densities where interactions between cars are important. Although the average velocity of the cars is drastically reduced compared to the free-flow regime [12] the flow by synchronized states can be close to the maximal value. This means that synchronized states are not dominated by jams but often by cars which move with small distances and moderate

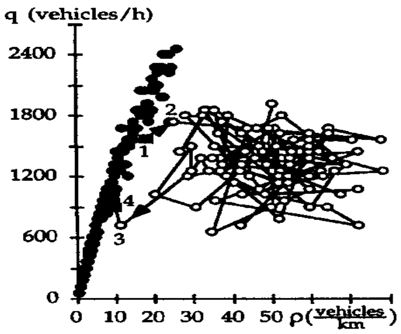


Figure 2.2: Fundamental diagram with synchronized states. In the high density regime no systematic density dependence of the flow is observable (from [12]). The lines connect consecutive measurements of high density states. Each data point corresponds to an one minute aggregate of local measurements of the density and flow.

velocities. Finally, measurements show an irregular pattern in the flow density plane (see Fig. 2.2) where no systematic density dependence of the average flow is observable.

On a microscopic level the formation of traffic jams is one of the most important points which has to be explained in traffic flow theory. Jams often emerge at hindrances or bottlenecks. But also the formation of jams without obvious reason has been observed.

The first experimental study which has shown this effect was performed by Treiterer [16] who analyzed a series of aerial photographs of a multi-lane highway. The analysis of these photographs allows for the identification of trajectories of individual cars. Fig. 2.3 shows that a jam is induced by fluctuations rather than due to a hindrance. For some time the jam remains stable and it disappears without any obvious reason.

A more detailed analysis of jams was done by Kerner and coworkers [11, 17] who summarized the characteristics of wide jams, i.e. jams which are considerably larger than the up- and downstream fronts of the jam. They noticed that the outflow from a jam is reduced compared

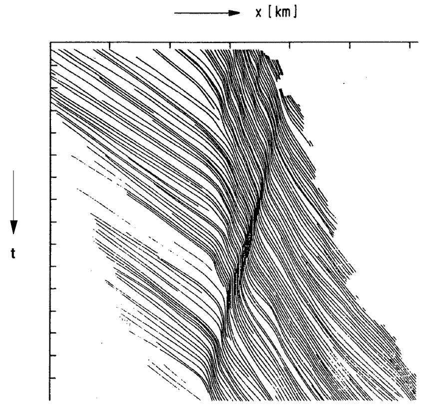


Figure 2.3: Spontaneous formation and resolution of a jam (from [16]). Each line corresponds to a trajectory of an single car.

to the maximal flow. Experimentally $\frac{q_{max}^{(free)}}{q_{out}} = 1.5$ was observed, where $q_{max}^{(free)}$ denotes the maximum possible flow and $q_{out}$ the outflow from a jam. The reduced outflow from jams leads to the capacity drop observable in the fundamental diagram. As shown in Fig. 2.3 jams are moving downstream. The downstream velocity of the jam front is surprisingly constant and in particular does not depend on the size of the jam. Therefore two or more jams can exist simultaneously and may form complex stable structures [11].

## 2.2 Modeling Traffic Flow

Throughout the past decades several theoretical approaches have been developed in order to describe traffic flow (see [24] for an overview). Two classical approaches still used are macroscopic and car-following models. Car-following models are based on the assumption that drivers tend to move with the same velocity as the leading car while macroscopic models are formulated in analogy to the hydrodynamical description of compressible viscous fluids.

Recently as an alternative microscopic description cellular automaton [3, 4] models came into play. Cellular automaton models are designed for very efficient implementations on computers and therefore allow to simulate large scale networks with microscopic models. In the following a short overview of the different concepts will be given.

### Macroscopic Models

The size and the complexity of realistic traffic networks does not allow to follow all routes of individual cars. Therefore it is reasonable to introduce a coarse-grained picture where the microscopic degrees of freedom are neglected. Using the coarse-grained picture the system is characterized in terms of macroscopic variables. For traffic flow problems it is straightforward to exploit the analogies to classical fluid dynamics. This approach allows for the calculation of macroscopic quantities, i.e. the average flow, for arbitrary system sizes.

Starting point of every macroscopic model is to formulate in analogy to fluid dynamics a continuity equation which represents the conservation of the number of cars [18, 19]. This leads (in the absence of sources and sinks) to the following local condition:

$$\frac{\partial \rho(x,t)}{\partial t} + \frac{\partial q(x,t)}{\partial x} = 0, \tag{2.3}$$

where $\rho(x,t)$ denotes the density of cars and $q(x,t)$ the local flow at time $t$ and position $x$. The time evolution of the density profile $q(x,t)$ can be obtained from eq. (2.3) if one assumes a stationary flow-density relationship [18, 19]. Note, that the stationary fundamental diagram has to be calculated from a microscopic model or alternatively a fundamental diagram which was determined experimentally may be chosen.

For realistic applications an additional velocity equation has to be considered [20]. Although various models with different velocity equations have been suggested [21–23] the structure of the velocity equation often is similar:

$$\frac{\partial V(x,t)}{\partial t} + V\frac{\partial V(x,t)}{\partial x} = -\frac{1}{\rho}\frac{\partial \mathcal{P}^e(x,t)}{\partial x} + \nu(\rho)\frac{\partial^2 V(x,t)}{\partial x^2} + \frac{1}{\tau(\rho)}\left[V_e(\rho) - V(x,t)\right], \quad (2.4)$$

where $V(x,t)$ denotes the local velocity at time $t$.

The terms in eq. (2.4) may be interpreted with respect to their hydrodynamical analogue:

- $-\frac{1}{\rho}\frac{\partial \mathcal{P}^e(x,t)}{\partial x}$: Due to its form this term is usually denoted as traffic pressure. Often $\mathcal{P}^e(x,t)$ is related to the velocity variance. The form of the pressure term depends on the specific model.

- $\nu(\rho)\frac{\partial^2 V(x,t)}{\partial x^2}$: A term, parametrized by the "viscosity" $\nu(\rho)$, which leads to the reduction of spatial inhomogeneities of the velocity field.

- $\frac{1}{\tau(\rho)}\left[V_e(\rho) - V\right]$: This term describes the relaxation to the stationary velocity $V_e(\rho)$. The time scale of this process is determined by the density dependent relaxation time $\tau(\rho)$.

The various model parameters serve as fit parameter, which have to be adjusted in order to reproduce the empirical results.

An example is given in Fig. 2.4 , where the time evolution of a density profile $\rho(x,t)$ for the Kühne-Kerner-Konhäuser model [17] is shown. For the chosen density, spatial inhomogeneities are amplified, and a shock profile emerges. The formation of shock fronts corresponds to the formation of jams in real traffic.

In principle one could treat arbitrary networks with this approach but the results have to be handled with care because of the enormous number of free parameters. A calculation of these parameters from first principles is not possible for obvious reasons. Moreover terms like the viscosity are not even directly observable and are only justified because they improve the accuracy of the model results. Therefore an adjustment of these parameters has to be done -at least in principle- for each specific application. The use of macroscopic models is limited also for principle

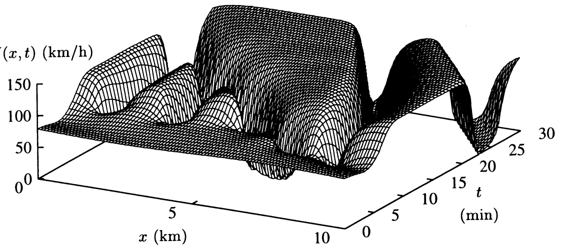


Figure 2.4: Time evolution of a density profile in the Kühne-Kerner-Konhäuser model. Initially an approximately constant density profile is assumed. The figure shows that the homogeneous state is not stable already for small deviations from a flat profile (from [24]).

reasons[1]. In order to measure quantities which are related to single cars a microscopic model has to be considered. But often quantities of that kind are highly relevant for modern applications, i.e. calculating traveling times is essential for route guidance systems.

### Car-following Models

Car-following models use the simplest driving strategy which includes three elements. First, as mentioned above, drivers tend to move with the same velocity as the leading car. Second, accidents are avoided by the drivers and finally at low densities drivers move with their desired velocity.

The first car-following models have been introduced by Reuschel [26, 27] and Pipes [28]. The basic idea of this approach is to calculate a safe velocity depending on the distance to the leading vehicle. A safe

[1] The derivation of macroscopic models from microscopic equations is the goal of the gas-kinetic approach of vehicular traffic [24, 25]. But also this approach does not lead to a macroscopic approach which is based on first principles because already the microscopic equations are of phenomenological nature. Moreover one has to use several approximations in order to derive the macroscopic models.

distance $s_{i+1}(t) := x_i(t) - x_{i+1}(t)$ is given by

$$s_{i+1}(t) := s_0 + Tv_{i+1}(t), \tag{2.5}$$

where $s_0$ denotes the minimal spacing of cars in a dense jam and $x_i(x_{i+1})$ the position of the leading (following) car. The parameter $T$ determines the time-scale of the model and is of the order of the reaction time. Then in the simplest version of the model the acceleration of vehicle $i+1$ at time $t$ is given by the first derivative of equation (2.5):

$$\frac{\mathrm{d}v_{i+1}(t)}{\mathrm{d}t} = \kappa[v_i(t) - v_{i+1}(t)], \qquad \kappa = \frac{1}{T}. \tag{2.6}$$

The constant $\kappa$ determines the magnitude of the acceleration at time $t$. Therefore $\kappa$ is often called *sensitivity.* It turned out that this ansatz is too simple to obtain realistic results.

Chandler, Herman, and Montroll [29] argued that velocity fluctuations of the leading car do not lead to an instantaneous reaction of the following vehicle. Therefore an acceleration of the following car is observable only after a certain reaction- or delay-time $\tau$.

Another unrealistic feature of the original model is the constant sensitivity. A realistic sensitivity takes into account the velocity of the car $v_{i+1}(t)$ and the distance to the leader $s_{i+1}(t)$. Currently car-following models have the following form [30, 31]:

$$\kappa_{i+1} = \frac{\kappa_0 \left[v_{i+1}(t+\tau)\right]^m}{\left[s_{i+1}(t)\right]^l}, \tag{2.7}$$

where $\kappa_0, l, m$ serve as fit parameters[2]. Then the density dependence of the average velocity can be obtained inserting (2.7) in (2.6) in the generalized velocity equation

$$\frac{d}{dt}v_{i+1}(t+\tau) = \kappa_{i+1}\left[v_i(t) - v_{i+1}(t)\right]. \tag{2.8}$$

The stationary solutions of (2.8) have to be compared with fundamental diagrams obtained from empirical observations.

[2]Using the velocity at time $t+\tau$ instead of $v_{i+1}(t)$ allows for an analytical treatment of eq. (2.7).

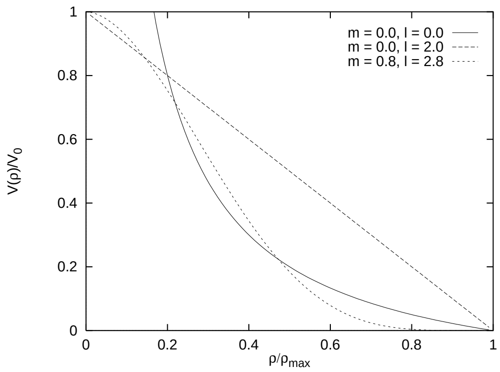


Figure 2.5: Stationary velocity-density relations for different values of the parameters $m, l$. The choice $m = 0.8$ and $l = 2.8$ was obtained from a fit of experimental data for an American highway, $m = 0$, $l = 0$ was chosen by Pipes [28]. Note, that this choice leads to diverging average velocities at low densities. $V(\rho)$ depends linearly on the density for $m = 0$ and $l = 2$ (this choice of $m, l$ was used by Greenshields [5]).)

Fig. 2.5 shows some stationary solutions of (2.8) for different parameter values $m, l$. It turned out that the choices $m = 0.8$ and $l = 2.8$ are in good agreement with measurements on American highways. Therefore one can state, that quite realistic stationary fundamental diagrams can be obtained using car-following models. Nevertheless on a microscopic level the car-following models fail to reproduce realistic results.

A slightly different approach was introduced by Bando et al. [32, 33] the so-called *optimal velocity* (OV) model. Depending on the *distance* to the leading vehicle the driver moves with an optimal velocity which is calculated from the stationary fundamental diagram. Explicitly the velocity update is determined by the following equation

$$\frac{dv_i(t)}{dt} = \kappa_0 \left[ V(\Delta x_i(t)) - v_i(t) \right], \tag{2.9}$$

where $V(\Delta x_i(t))$ denotes the OV-function, $v_i(t)$ the velocity of the car $i$, and $\Delta x_i$ the distance to the leading car. Time and also the space coordinate are considered as continuous variables. One obtains the OV-function by fitting experimental data for the fundamental diagram.

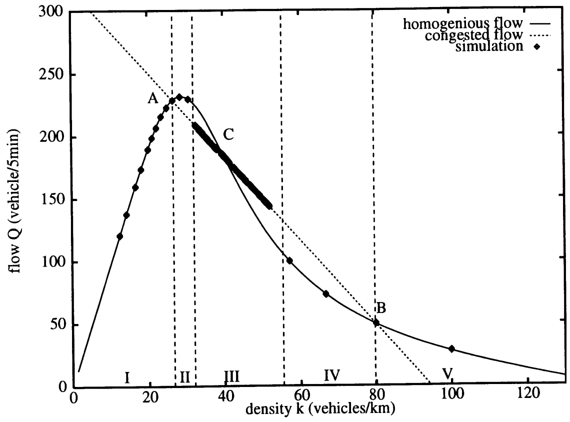


Figure 2.6: Fundamental diagram of the OV-model. The solid line shows the OV-function and the dots simulation data. One can distinguish five different density regimes with respect to their stable stationary states (from [32]).

The OV-model is able to describe the propagation of cars without accidents. Moreover one can distinguish different density regimes with respect to the stability of microscopic states. At low and at high densities close to $\rho_{max}$ homogeneous configurations form stable states. For intermediate densities one can distinguish three regimes (see Fig. 2.6). In contrast to the high and low density regimes jammed states exist. The regions differ in the sense that in region III only the jammed state is stable while for the intervals II and IV both homogeneous and jammed states form stable structures. Beyond the formation of jams also hysteresis effects have been observed. In conclusion, the OV-model is able to reproduce many aspects of the experimental findings. But nevertheless, from a theoretical point of view, the fact that an OV-function has to be assumed is quite unsatisfactory because then the number of free parameters of the model is infinite.

### Cellular Automaton Models

The first cellular automaton (CA) model for traffic flow was introduced by Cremer [3]. CA models are *microscopic* models which are by definition well suited for computer simulations. To date the CA approach is well established because it enables computer simulation of large scale networks in real time [34–36] a task which is impossible to handle with traditional microscopic models. Compared to macroscopic models CA have the advantage that measurements on individual cars can be performed.

Meanwhile several CA models have been suggested [37–41]. The most prominent example was introduced by Nagel and Schreckenberg (NaSch model). The NaSch model [4, 42] is a probabilistic cellular automaton. Space and time (and hence the velocities) are discrete. The road is divided into cells of length 7.5 m. Each cell can either be empty or occupied by just one car. The state of car $j$ ($j = 1, \dots, N$) is slso discrete and is characterized by its momentary velocity $v_j$ ($v_j = 0, 1, \dots, v_{max}$). The configuration of the system at time $t+1$ can be obtained from the state at time $t$ by applying the following four rules to all cars at the same time (parallel dynamics):

**R1:** Acceleration: $v_j(t) \to v_j(t+\frac{1}{3}) = \min\{v_j(t)+1, v_{max}\}$

**R2:** Braking: if $v_j(t+\frac{1}{3}) > d_j(t)$ then $v_j(t+\frac{1}{3}) \to v_j(t+\frac{2}{3}) = d_j(t)$

**R3:** Randomization: $v_j(t+\frac{2}{3}) \xrightarrow{p} v_j(t+1) = \max\{0, v_j(t+\frac{2}{3})-1\}$ with probability $p$

**R4:** Driving: car $j$ moves $v_j(t+1)$ cells.

Here $d_j(t)$ denotes the number of empty cells in front of car $j$, i.e. the gap or headway. One time-step $t \to t+1$ corresponds to approximately 1 sec in real time [4] if $v_{max} = 5$ and $p \approx 0.5$.

The NaSch model is able to reproduce some basic features of traffic flow, e.g. the spontaneous formation of jams. Also the form of the fundamental diagram is quite realistic but in order to observe meta-stable states or synchronized flow additional rules must be considered [40]. In that sense the NaSch model is a minimal model for traffic flow because every simplification of the rules leads to more unrealistic results.

## Chapter 3

# Analytical Methods

In this chapter a selection of analytical methods which have been successfully applied to discrete stochastic systems is presented. In addition the conceptional similarities between stochastic systems and quantum many particle systems are discussed.

The dynamics of stochastic systems, i.e. the time-evolution of the probability distribution, is governed by the master equation. In the first section the basic properties of the master equation will be discussed and it will be shown that strong similarities to the Schrödinger equation exist. The following section concerns the introduction of the matrix-product ansatz (MPA) which can be used in order to calculate exact and nontrivial stationary states for stochastic processes. The MPA was first introduced in order to calculate exact groundstates for quantum spin chains. In 1993 Derrida et al. [43] have shown that a generalization of this method can be applied to calculate the exact stationary state of the totally asymmetric exclusion process (TASEP) with open boundary conditions. Writing the stationary state as a product measure of local states is a frequently used concept in the context of stochastic systems. In the final section of this chapter product measures in terms of local lattice and particle states are introduced. For the NaSch model both methods lead to exact (for $v_{max} = 1$) or approximative solutions of high accuracy (for $v_{max} > 1$).

## 3.1 Master Equation and Quantum Formalism

Traditionally statistical mechanics has been used to describe systems which are in thermal equilibrium or which are at least close to an equilibrium state. "Close to an equilibrium state" means that the deviations from the stationary state can be treated in a pertubative manner, e.g. using linear response theory. For these kind of problems a well established formalism exists. On the other hand for complex systems far from equilibrium no general theory exists. However these processes play an important role in different fields of interest e.g. biological systems, growth processes, reaction-diffusion problems, and traffic flow [44, 45].

Here we concentrate on the description of stochastic processes which are defined on a one-dimensional lattice of length $L$. These kind of systems are characterized by the probability distribution $P(\{\tau\}, t)$, where $\{\tau\} = \{\tau_1, \tau_2, ..., \tau_L\}$ denotes a possible configuration of the lattice. The dynamics of such a process is governed by a master equation of the following form [46]:

$$P(\{\tau\}, t + \Delta t) = \sum_{\{\tau'\}} p(\tau' \to \tau) P(\{\tau'\}, t) \tag{3.1}$$

where $p(\tau \to \tau')$ denotes the probability of a transition from $\{\tau\}$ to $\{\tau'\}$ during the time interval $[t, t + \Delta t]$.
It turns out that it is very useful to rewrite eq. (3.1) in vector notation [46]. As a first step one has to introduce a suitable basis in the configuration space $\{\tau\}$ given by

$$|\tau\rangle = |\tau_1, ..., \tau_L\rangle \tag{3.2}$$

with $\langle\tau'|\tau\rangle = \delta_{\tau',\tau}$. Then the complete probability distribution at time $t$ is represented by the vector

$$|P(t)\rangle = \sum_{\{\tau\}} P(\{\tau\}, t)|\tau\rangle \tag{3.3}$$

which implies that $P(\{\tau\}, t) = \langle\tau|P(t)\rangle$. This allows to rewrite the master equation in a very compact notation using a transfer matrix $T$.

The diagonal elements of $T$ are given by

$$\langle\tau|T|\tau\rangle = 1 - \sum_{\{\tau\}\neq\{\tau'\}} p(\tau \to \tau') \tag{3.4}$$

and the off-diagonal elements by

$$\langle\tau|T|\tau'\rangle = p(\tau' \to \tau). \tag{3.5}$$

Using these definitions the master equation is simply given by

$$|P(t+\Delta t)\rangle = T|P(t)\rangle. \tag{3.6}$$

By construction each column of the transfer matrix must add up to one which guarantees probability conservation. This also implies that $\sum_{\{\tau\}}\langle\tau|$ is a *left* eigenvector with eigenvalue 1.

While discrete time steps are frequently used in computer simulations often a continuous time variable is more convenient for analytical calculations. In order to rewrite the time variable $t = n\Delta t$ in continuous form one has to take the limit $\Delta t \to 0$ and $n \to \infty$ keeping $t$ fixed. This can be done with ease writing the transfer matrix in the form $T = 1 - H\Delta t$.

The limiting procedure leads to the master equation in continuous time

$$\frac{\partial}{\partial t}|P(t)\rangle = -H|P(t)\rangle. \tag{3.7}$$

Then the diagonal elements of the stochastic "Hamiltonian" $H$ are given by

$$\langle\tau|H|\tau\rangle = \sum_{\{\tau\}\neq\{\tau'\}} w(\tau \to \tau') \tag{3.8}$$

and the off-diagonal elements by

$$\langle\tau|H|\tau'\rangle = -w(\tau' \to \tau), \tag{3.9}$$

where $w(\tau \to \tau')$ denotes the transition rates $w(\tau \to \tau') = p(\tau \to \tau')/\Delta t$. Now probability conservation demands that all columns of $H$ add up to zero. The time-continuous form of the master equation (3.7) is closely related to the Schrödinger equation of an interacting many particle system in imaginary time but in general the "Hamiltonian" may not be hermitean.

It is illustrative to discuss how stochastic processes in continuous and in discrete time can be implemented in computer simulations. A continuous time variable corresponds to a random-sequential update of the lattice, i.e. a pair of sites is chosen randomly and then a local update is performed. For processes in discrete time several variants of the update-procedure exist. Two variants which are discussed in the following section are the site-sequential and the parallel update. If the site-sequential update is applied the local updates are performed in a fixed order. In contrast using the parallel update all sites are updated synchronously.

## 3.2 Matrix-Product States

The quantum formalism for stochastic processes suggests the application of analytical methods which were originally developed for the treatment of quantum many-body problems, i.e. the Bethe Ansatz [47–49]. Beyond this advantage of the quantum formalism one can use the similarities between stochastic and quantum problems even more directly. E.g. it has been shown that a large subset of the general two-state process with nearest neighbor interactions can be mapped onto a exactly solvable quantum chain [46]. Therefore the results which were originally obtained for the quantum problem may be used directly for the treatment of the stochastic system.

In the following the generalization of the matrix-product ansatz (MPA) for stochastic processes will be discussed. The MPA formalism has been introduced in order to construct exact ground-states of quantum spin chains [50–52]. In the context of stochastic systems the MPA was introduced by Derrida et al. [43] for the totally asymmetric exclusion process (TASEP) with open boundary conditions and random-sequential dynamics [53–56]. Using the MPA the stationary state of the TASEP was calculated exactly [43]. Meanwhile exact solutions of the stationary problem were obtained also for other implementations of the dynamics [57–61].

The TASEP has various applications in different fields of interest. Originally it was formulated as a simplified model for biopolymerisation

[62]. In the context of this work the TASEP can be viewed as a simplified model for traffic flow, e.g. if a parallel update is applied one recovers the NaSch model with $v_{max} = 1$.

As mentioned above the first exact solution of the TASEP with open boundary conditions was obtained for random-sequential dynamics [43, 56]. For this type of dynamics the TASEP on a one-dimensional lattice of $L$ sites is defined by the following transition probabilities:

$$\tau_i(t+dt) = \begin{cases} \tau_i(t) & \text{with prob. } 1-2wdt, \\ \tau_{i-1}(t) + \tau_i(t) + \tau_{i-1}(t)\tau_i(t) & \text{with prob. } wdt, \\ \tau_i(t)\tau_{i+1}(t) & \text{with prob. } wdt, \end{cases} \tag{3.10}$$

where $\tau_i = 0, 1$ and $i = 1, \ldots, L-1$. Obviously the hopping *rate* $w$ only rescales the time unit $dt$, as far as homogeneous hopping rates are considered. Therefore we can set $w = 1$ without loss of generality.

In order to give a complete definition of the TASEP with open boundary conditions particle injection and removal at the boundaries must be considered. Here we demand that particles are injected at the first site with probability $(1-\tau_1)\alpha dt$ and deleted with probability $\tau_L \beta dt$ on the last site.

The application of random-sequential dynamics corresponds to a continuous time variable. Therefore the Hamiltonian formalism must be applied. For a chain of $L$ sites the Hamilton-operator $H$ acts on a $2^L$-dimensional state space. The fact that only local interactions are included for the TASEP allows to rewrite the Hamiltonian $H$ as a sum of "local" Hamiltonians:

$$H = \bar{H}_1 + \sum_{j=1}^{L-1} H_j + \bar{H}_L. \tag{3.11}$$

The operators $\bar{H}_1, \bar{H}_L$ act nontrivially only on the boundary sites $1, L$ and the "bulk" Hamiltonian $H_j$ on the sites $j, j+1$. Explicitly the local

Hamiltonians are given by

$$\begin{aligned}
\bar{H}_1 &= \bar{h}_1 \otimes \underbrace{\mathbf{1} \otimes \ldots \otimes \mathbf{1}}_{L-1}, \\
\bar{H}_L &= \underbrace{\mathbf{1} \otimes \ldots \otimes \mathbf{1}}_{L-1} \otimes \bar{h}_L, \\
H_j &= \underbrace{\mathbf{1} \otimes \mathbf{1} \ldots}_{j-1} \otimes h_j \underbrace{\otimes \mathbf{1} \ldots \otimes \mathbf{1}}_{L-j-1},
\end{aligned} \tag{3.12}$$

where $\mathbf{1}$ denotes the two-dimensional identity matrix. The nontrivial terms of the tensor products are given by:

$$\bar{h}_1 = \begin{pmatrix} \alpha & 0 \\ -\alpha & 0 \end{pmatrix}, \qquad \bar{h}_L = \begin{pmatrix} 0 & -\beta \\ 0 & \beta \end{pmatrix}, \tag{3.13}$$

for the boundaries and

$$h_j = \begin{pmatrix} 0 & 0 & 0 & 0 \\ 0 & 0 & -1 & 0 \\ 0 & 0 & 1 & 0 \\ 0 & 0 & 0 & 0 \end{pmatrix} \tag{3.14}$$

for the bulk.

Now in order to determine the stationary state one has to find an eigenvector of the $H$ with eigenvalue zero[1]. This can been done most elegantly for the TASEP by the MPA [43]. The crucial idea of the MPA for stochastic systems is to write the stationary weight of a configuration $\{\tau\}$ as a product of matrices which represent a single site state of the lattice:

$$P_0(\{\tau\}) = \frac{1}{Z_L} \langle W| \prod_{j=1}^{L} \left[\tau_j D + (1-\tau_j) E\right] |V\rangle, \tag{3.15}$$

where $Z_L = \langle W|C^L|V\rangle$ denotes the normalization constant and $C$ is simply given by $C = D + E$. The dimension of the matrices $E$ and $D$ is in general arbitrary.

[1] Obviously finding a stationary state of the stochastic process is closely related to the groundstate problem of a quantum spin chain.

Then the complete probability vector $|P_0\rangle$ is given by

$$|P_0\rangle = \frac{1}{Z_L}\langle\langle W|A \otimes \cdots \otimes A|V\rangle\rangle\,, \tag{3.16}$$

where $A = \begin{pmatrix} E \\ D \end{pmatrix}$. The brackets $\langle\langle ... \rangle\rangle$ indicate that the scalar product is taken for each entry of the vector $A \otimes ... \otimes A$. So far, (3.16) is just an ansatz for the stationary state. It can be shown easily that $|P_0\rangle$ indeed represents the stationary state if

$$h_j(A \otimes A) = \bar{A} \otimes A - A \otimes \bar{A} \tag{3.17}$$

holds for the bulk matrices and

$$\langle W|\bar{h}_1 A = -\langle W|\bar{A} \quad , \quad \bar{h}_L A|V\rangle = \bar{A}|V\rangle\,, \tag{3.18}$$

for the boundaries [63]. The additional vector $\bar{A}$ is given by $\bar{A} = \begin{pmatrix} \bar{E} \\ \bar{D} \end{pmatrix}$, where $\bar{E}, \bar{D}$ are arbitrary matrices acting in the same vector space as $E, D$. Now an exact expression for the stationary distribution is found if one can solve the algebraic equations generated by (3.17) and (3.18).

It turns out that the choice $\bar{E} = \mathbf{1} = -\bar{D}$ leads to a much simpler form of the algebra:

$$\begin{aligned} DE &= D + E \quad , && (3.19)\\ \alpha\langle W|E &= \langle W| \quad , && (3.20)\\ \beta D|V\rangle &= |V\rangle \quad . && (3.21) \end{aligned}$$

A representation of the algebra (3.19-3.20) was found by Derrida et al. [43][2].

For arbitrary values of the input rates representations $E, D$ are infinite-dimensional matrices. But nevertheless for a subset of the in- and output rates, i.e. if $\alpha + \beta = 1$, a one-dimensional representation of the algebra can be found.

[2] In fact in [43] it was shown directly that a stationary state is obtained if $D, E$ fulfill the algebra by inserting (3.19-3.21) into the master equation.

Using the MPA the calculation of physical quantities is straightforward, e.g. the two point-correlation function is simply given by

$$\langle \tau_i \tau_{i+n} \rangle = \frac{\langle W | C^{i-1} D C^{n-1} D C^{L-i-n-1} | V \rangle}{\langle W | C^L | V \rangle}. \tag{3.22}$$

A detailed discussion of the physical properties will be given in a later chapter of this work.

Meanwhile it has been shown that the stationary solution of the master equation for a general stochastic processes with n-site interactions and random-sequential dynamics can always be written in terms of the MPA [64, 65].

The MPA can also be applied in the framework of the transfer matrix formalism. Two examples of updates which are discrete in the time variable will be discussed in the remaining part of this section. First the ordered-sequential update procedure and second the fully-parallel dynamics.

The ordered-(site)-sequential dynamics is implemented in the following fashion: First a particle at site $L$ is deleted with probability $\beta$. Then a particle at site $L-1$ moves to site $L$ with probability $q$ if this site is empty. This will be done gradually for site $L-1$ to site 1. Finally a particle is injected with probability $\alpha$ if the first site is empty. Alternatively one could also perform the update starting with the injection at site 1.

Analogous to the Hamiltonian of the TASEP with a continuous-time variable the transfer matrix can be written in terms of "local" matrices which have a nontrivial effect only on a single site (boundaries) or a pair of sites. But in contrast to the random sequential case, the transfer matrix $T_{\leftarrow}$ is given as a *product* of "local" transfer matrices,

$$T_{\leftarrow} = L \cdot T_1 \cdot \ldots \cdot T_{L-1} \cdot R, \tag{3.23}$$

where

$$\begin{aligned} L &= \mathcal{L} \otimes \mathbf{1} \otimes \ldots \otimes \mathbf{1}\,, \\ R &= \mathbf{1} \otimes \ldots \otimes \mathbf{1} \otimes \mathcal{R}\,, \\ T_j &= \mathbf{1} \otimes \mathbf{1} \ldots \otimes \mathcal{T} \otimes \mathbf{1} \ldots \otimes \mathbf{1}\,. \end{aligned} \tag{3.24}$$

Again $\mathbf{1}$ denotes the identity matrix.

Analogous to the local Hamiltonian $H_j$ the matrix $T_j$ acts non-trivially on the pair of sites $(j, j+1)$. The local operators $\mathcal{T}$ are simply given by

$$\mathcal{T} = \begin{pmatrix} 1 & 0 & 0 & 0 \\ 0 & 1 & q & 0 \\ 0 & 0 & 1-q & 0 \\ 0 & 0 & 0 & 1 \end{pmatrix}, \tag{3.25}$$

and the boundary operators by

$$\mathcal{R} = \begin{pmatrix} 1 & \beta \\ 0 & 1-\beta \end{pmatrix}, \qquad \mathcal{L} = \begin{pmatrix} 1-\alpha & 0 \\ \alpha & 1 \end{pmatrix}. \tag{3.26}$$

For the sequential update a different canceling mechanism must be used in order to guarantee stationarity given by

$$\mathcal{T}\left(A \otimes \hat{A}\right) = \hat{A} \otimes A, \tag{3.27}$$

$$\langle W|\mathcal{L}\hat{A} = \langle W|A, \qquad \mathcal{R}A|V\rangle = \hat{A}|V\rangle. \tag{3.28}$$

Again one ends up with a set of algebraic equations for the matrices $E, D, \hat{E}, \hat{D}$. It turns out that this algebra can be solved if one demands that

$$\hat{D} = D - \lambda\mathbf{1}, \tag{3.29}$$
$$\hat{E} = E + \lambda\mathbf{1}. \tag{3.30}$$

Then effectively the algebra (3.19-3.21) is recovered. This mapping is already a complete solution of the stationary problem because eq. (3.29) can be fulfilled for all $q < 1$ and arbitrary in- and output probabilities.

Analytical calculations for the TASEP using a parallel update are difficult because no simple decomposition of the transfer matrix is possible. Nevertheless a local mechanism can be obtained if one introduces a third state which marks the particles which already moved in that time step [58]. Then one can introduce a mechanism analogous to the site-sequential update which leads to a quadratic algebra. Unfortunately, so far no representation for this algebra has been found.

Very recently an exact solution for the TASEP with synchronous update was found using an alternative approach [60, 61]. Starting from the explicit solution of small chains it has been shown that stationary states demand for the following relations between the matrices $E, D$

$$\begin{aligned}
EDEE &= (1-q)EDE + EEE + qEE\,, &(3.31)\\
EDED &= EDD + EED + qED\,, &(3.32)\\
DDEE &= (1-q)DDE + (1-q)DEE + q(1-q)DE\,, &(3.33)\\
DDED &= DDD + (1-q)DED + qDD\,. &(3.34)
\end{aligned}$$

in the bulk. Combining this with boundary terms which involve three and two sites one ends up with a complete set of algebraic equations. Again one has to find explicit representations for this algebra. This was done using the following ansatz for the matrices $D, E$

$$D = \begin{pmatrix} D_1 & 0 \\ D_2 & 0 \end{pmatrix}, \quad E = \begin{pmatrix} E_1 & E_2 \\ 0 & 0 \end{pmatrix}. \tag{3.35}$$

Inserting this into the original algebra one ends up with a quadratic algebra analogous to the random-sequential update which can be solved.

The example of the TASEP shows that the MPA provides an elegant method for the solution of discrete stochastic processes. Beyond the explicit results for this particular process also more general results could be obtained using the MPA, e.g. the relation between the ordered sequential updates and the sub-lattice parallel update was shown rigorously [66]. Also generalizations of the MPA for the time-dependent problem are possible [49].

## 3.3 Approximative Methods

In the remaining part of this chapter analytical methods are discussed which can be used to calculate approximative solutions for the dynamics as well as for the stationary state of realistic traffic models like the NaSch model (see [67] for an overview). In order to illustrate the methods they are introduced by the example of the NaSch model with $v_{max} = 1$ and periodic boundary conditions where most of the methods which are introduced in this section lead to exact results for the stationary state.

### Mean-Field Analysis

The most simple analytical treatment of the NaSch model is given by a mean field (MF) theory [42]. In MF treatment correlations between neighboring sites are completely neglected and the probability distribution in the state space given as a product measure of the local states. Then for $v_{max} = 1$ the MF equations for the NaSch model are given by

$$\rho_0 = (\rho + p\overline{\rho})\rho, \tag{3.36}$$

$$\rho_1 = q\rho\overline{\rho}, \tag{3.37}$$

where $\rho_\alpha$ denotes the density of cars with velocity $\alpha$, $\rho$ ($\overline{\rho} = 1 - \rho$) the average density, and $p$ ($q = 1 - p$) the braking parameter. Obviously the MF result for the flow is simply given by $f(c) = \rho_1 = q\rho\overline{\rho}$. A generalization of the MF approach to higher velocities is straightforward.

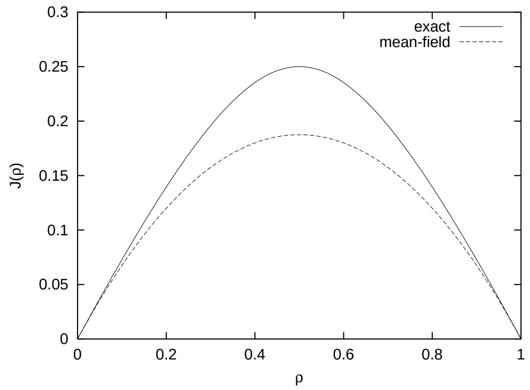


Figure 3.1: Comparison of the exact and the mean-field solution for the NaSch model for $v_{max} = 1$ and $p = 0.25$. Obviously the correlations lead to an increase of the stationary flow.

Fig. 3.1 shows the MF result in comparison with the exact result. Obviously the MF approximation underestimates the flow for the parallel update, or, alternatively speaking, the correlations lead to an increase of the flow at a given density [69].

The failure of the MF theory also for the simplest variant of the NaSch model is due to the use of a parallel update. In contrast, the MF approach gives correct results for $v_{max} = 1$ if one considers a random-sequential update [42]. Therefore correlations are induced only by the update procedure.

An important property of the parallel dynamics is the existence of configurations which cannot be reached dynamically. These states are called Garden of Eden (GoE) states motivated by the fact that they have no predecessor. Of course such states have no weight in the stationary state. Therefore the consideration of GoE states should considerably improve the accuracy of the analytical results.

For the case of $v_{max} = 1$ GoE states are configurations which contain the two-site states $(0, 1)$ or $(1, 1)$ after a full system update. The numbers denote the velocity of a car at a given lattice site. The first configuration is excluded because the occurrence of this state would demand a double occupancy of the first site. This violates the exclusion principle and the second configuration cannot be reached due to the breaking rule **R2**.

Considering the GoE states the modified MF equations read [68]

$$c_0 = \mathcal{N}(c_0 + pd)c, \tag{3.38}$$

$$c_1 = \mathcal{N}qcd, \tag{3.39}$$

where the normalization $\mathcal{N}$ can be calculated using $\rho = \rho_0 + \rho_1$. Solving these equations one obtains $f(\rho, p) = \rho_1 = \frac{1}{2}\left(1 - \sqrt{1 - 4q(1-\rho)\rho}\right)$, which turns out to be the exact expression for the flow [42]. The exactness of this results implies that the additional correlations are due to the reduction of the available configuration space.

For the case of $v_{max} > 1$ the GoE approximation does not lead to the exact stationary solution but it is still a considerable improvement of the MF theory [68]. Therefore one can state that the reduction of the configuration space still has an important effect. But beyond that correlations exist which cannot be neglected.

In order to illustrate the accuracy of this method the GoE results are compared with simulation data for $v_{max} = 2$ in Fig. 3.2. Obviously for the chosen parameter combination the GoE results are in good agreement with the simulation results but closer to the deterministic limits the accuracy of the approximative results is less satisfactory.

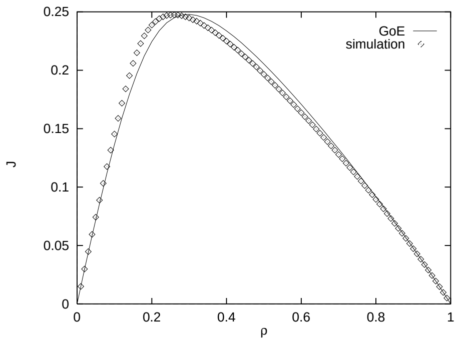


Figure 3.2: Simulation results in comparison with the GoE approximation for $v_{max} = 2$ and $p = 0.50$ (from [68]).

### Cluster Approximation

The cluster approximation [42, 69] is a systematic improvement of the mean-field method where correlations between nearest-neighbor sites are taken into account. In the $n$-cluster approximation the probability to find the configuration $P(\sigma_1, \sigma_2, \ldots, \sigma_L)$ is given by

$$P(\sigma_1, \sigma_2, \ldots, \sigma_L) \propto \prod_i P(\sigma_i, \sigma_{i+1}, \ldots, \sigma_{i+n}). \qquad (3.40)$$

Then the first step beyond mean-field theory, i.e. the "single-cluster approximation", is the two-cluster approximation.

In order to determine the cluster probabilities one has to insert the ansatz (3.40) into the master equation. This can be done most conveniently after the acceleration step **R1** where the number of states per site is reduced to $v_{max} + 1$ because the minimal velocity of cars after the acceleration step is one. In general, the cluster-probabilities depend on the time and the lattice site but here we are interested in the stationary state of a translation-invariant system. From now on the simplest case, i.e. the two-cluster approximation for $v_{max} = 1$, is considered in order to keep the notation as simple as possible. For $v_{max} = 1$ the stationary probability to find the local configuration $(\sigma_i, \sigma_{i+1})$ is given by

$$P(\sigma_i, \sigma_{i+1}) = \sum_{\{\tau_j\}} W(\sigma_i, \sigma_{i+1} | \tau_{i-1}, \tau_i, \tau_{i+1}, \tau_{i+2}) P(\tau_{i-1}, \tau_i, \tau_{i+1}, \tau_{i+2}). \quad (3.41)$$

Obviously the probabilities $P_2(\{\sigma_j\})$ are related to the four site probabilities $P_4(\{\tau_j\})$ because the transition probabilities $W(\{\sigma_j\}|\{\tau_j\})$ depend non-trivially also on the state of the two nearest-neighbor sites. In order to calculate the four-site probabilities exactly one had to consider six-site probabilities and so forth because again the two neighboring sites have to be included. Therefore it is necessary to truncate this iterative scheme. This can be done in a self-consistent way expressing $P_4(\{\tau_j\})$ in terms of $P_2(\{\sigma_j\})$. Due to the non-vanishing overlap of the local clusters one has to introduce conditional probabilities in order to decompose the larger clusters. After all one has to solve a set of four coupled nonlinear equations. This can be done easily using the following symmetries of the model:

$$\begin{aligned} P(1, \circ) &= P(\circ, 1) \\ P(\circ, \circ) &= 1 - \rho - P(1, \circ), \\ P(1, 1) &= \rho - P(1, \circ), \end{aligned} \quad (3.42)$$

where $\circ$ denotes an empty site. The first equation is a consequence of the translational invariance of the lattice, while the following two equations are due to particle conservation. Finally, using the symmetries of the model (3.42), eq. (3.41) can be reduced to a single quadratic equation with the following solution:

$$P(\circ, 1) = P(1, \circ) = \frac{1 - \sqrt{1 - 4q\rho(1-\rho)}}{2q} \,. \quad (3.43)$$

This result directly leads to an analytical expression for the flow via $f(\rho, p) = qP(1, \circ)$, in fact the exact result [42] is recovered[3].

Applications of the cluster approximation to higher velocities yield no exact results but in particular the results of cluster approximations

[3]Note that in contrast to the order of this chapter the exact result for the stationary flow was first obtained by the cluster-approximation method [42] and not by GoE.

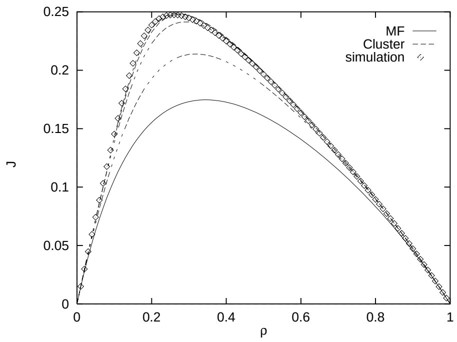


Figure 3.3: Results of the MF and $2 \ldots 5$-site cluster approximation for $v_{max} = 2$ and $p = 0.50$ (from [42]).

of higher order show an excellent agreement with simulation results (see Fig. 3.3). Moreover there is numerical evidence that the $(v_{max} + 1)$ cluster approximation is exact in the limit $p \to 0$ [71].

The cluster approximation can also be used in order to calculate spatial correlation functions [67].

### Car-Oriented Mean-Field Theory

While the cluster approximation introduced in the previous section is a systematic improvement of the MF approximation an alternative ansatz is introduced by the Car-Oriented Mean-Field (COMF) approximation [70].

Using the COMF approximation the master equation for the NaSch model is rewritten in terms of the distance variables. In order to illustrate the method an example will be presented in the following (again for the case $v_{max} = 1$). Consider a car $i$ at time $t$ with $n > 1$ empty cells in front. Then there are three different possible headways in the next time step. The first possibility is that the chosen car moves in the next time step while its predecessor does not move. Then the distance in the next time step is reduced by one unit. Conversely the car has $x + 1$ empty cells in front if the predecessor moves but the car $i$ does not. Finally the distance does not change if both cars have the same velocity in the next time step.

Introducing distance variables the master equation for an infinite translational invariant system can be written in the following form:

$$\begin{aligned} P_0(t+1) &= \bar{g}(t)\left[P_0(t) + qP_1(t)\right], \\ P_1(t+1) &= g(t)P_0(t) + \left[qg(t) + p\bar{g}(t)\right]P_1(t) + q\bar{g}(t)P_2(t), \quad (3.44) \\ P_n(t+1) &= pg(t)P_{n-1}(t) + \left[qg(t) + p\bar{g}(t)\right]P_n(t) \\ &\quad + q\bar{g}(t)P_{n+1}(t), \quad (n \geq 2) \end{aligned}$$

Here $P_n(t)$ denotes the probability to find exactly $n$ empty cells in front of a car at time-step $t$ and $g(t)$ ($\bar{g}(t) = 1 - g(t)$) the probability that the leading car moves one cell ahead (does not move). Obviously $g(t)$ is simply given by $g(t) = q[1 - P_0(t)]$ which is the probability that a car does not slow down neither in the randomization nor in the braking step. Please note that the probability that the leading car moves is considered to be independent of $P_n(t)$.

One can find stationary solutions of (3.45) using a generating function $P(z) = \sum_{n\geq 0} z^{n+1}P_n$ for the variables $P_n$. After multiplying each equation with $z^{n+1}$ and summing over all equations one gets the following expression for $P(z)$ [70]:

$$P(z) = \frac{q(\bar{g} + gz)zP_0}{q\bar{g} - pgz}. \quad (3.45)$$

The generating function must fulfill the normalization condition $P(1) = 1$. Moreover one can introduce the density dependence using $c^{-1} = \sum_{n\geq 0}(n+1)P_n = P'(1)$, where $P'(z)$ denotes as usual the first derivative of $P(z)$. Then the stationary distance distribution reads as follows [70]:

$$\begin{aligned} P_0 &= \frac{1}{2q\rho}\left[2q\rho - 1 + \sqrt{1 - 4q\rho(1-\rho)}\right], \\ P_n &= \frac{P_0}{p}\left(\frac{p(1-P_0)}{P_0 + p(1-P_0)}\right)^n \quad (n \geq 1), \quad (3.46) \end{aligned}$$

A comparison of the COMF results with the cluster method shows that the exact result is recovered for the case of $v_{max} = 1$.

In order to apply the COMF method to $v_{max} > 1$ one has to distinguish between cars with different velocities, i.e. cars that move one

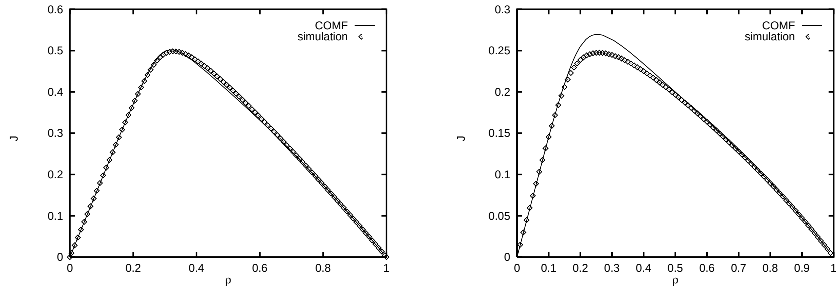


Figure 3.4: Comparison of the COMF results with simulation data for the NaSch model with $v_{max} = 2$ for two different values of the braking noise $p = 0.1$ (left) and $p = 0.5$ (right). Obviously for small braking parameters the COMF method gives very accurate results (from [70]).

or two sites at $v_{max} = 2$. Again the master equation can be written in terms of the distance variables and analyzed at least in principle in the same way than for the case of $v_{max} = 1$. In contrast to the former example for $v_{max} = 2$ the COMF results are not exact, but, at least for small values of the braking noise, an excellent approximation of the stationary state. The failure of the COMF theory for larger values of $p$ shows that also correlations between distances of cars exist for $v_{max} > 1$ and $p > 0$ [71].

## Chapter 4

# Jamming Transition

Simulation results of the NaSch model show that two different density regimes can be distinguished where a qualitatively different behavior of the model is observed. The aim of this chapter is to discuss the microscopic structure in the different density regimes and to show simulation results for the fundamental diagram and other quantities of interest. In particular, attention is paid to the influence of the model parameters $p$ and $v_{max}$. The discussion of the qualitative behavior in the different density regime is followed by a careful analysis of the transition regime. In the second section an order-parameter is introduced which shows a qualitatively different behavior in both density regimes. Then the relevant length scales are analyzed by measuring the two-point correlation function. In addition, the typical sizes of jams are calculated for different values of the model parameters. At the end of this chapter a critical discussion of the results will be given.

## 4.1 Free-Flow and Jammed States

The behavior of the NaSch model is determined by the model parameters $\rho$ ,$p$, and $v_{max}$. For given values of $p$ and $v_{max}$ the microscopic states of the model depend only on the occupation of the lattice and can be characterized as follows: At low densities cars can drive freely with their desired velocity while for larger densities interactions are important. Finally, at very high densities start-stop waves dominate the dynamics. In

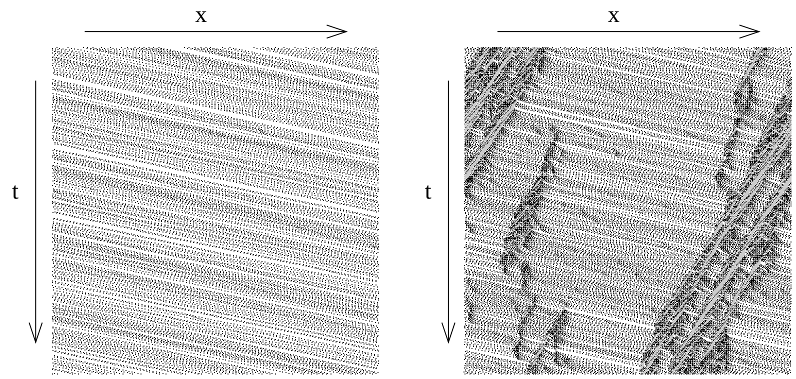


Figure 4.1: Space-time diagrams of the NaSch model in the stationary state. The left part of the figure shows the time evolution of the system in the free flow regime ($\rho = 0.08$) and the right part of the figure in the jammed state ($\rho = 0.20$).

Fig. 4.1 space-time diagrams of the NaSch model with $v_{max} = 5$ and $p = 0.25$ at two different densities ($\rho = 0.08, 0.20$) are shown. For low densities (left), obviously no jams are present in contrast to the high density state. At high densities one observes that the fluctuations lead to spontaneous formation of new jams in the outflow region of a jam ("stop-and-go" waves). On the other hand, fluctuations also lead to a finite lifetime of jams [72]. This characterization of high density states is valid only in the presence of noise. In contrast, jams present in the high density regime have infinite lifetimes for $p = 0$. Also for the other deterministic case, i.e. $p = 1$, a qualitatively different behavior compared to the nondeterministic case is observable. All initial configurations where one finds cars with velocity zero or gaps $d \leq 1$ lead to stationary states with vanishing flow. Nevertheless, considering homogeneous states at low densities ($\rho < 1/3$) also finite values of the stationary flow can be observed for $v_{max} > 1$. Then, for appropriate initial conditions, no spontaneous formation of jams is observable similar to the low density regime for $p = 0$.

Fig. 4.2 shows fundamental diagrams for $v_{max} = 5$ and different values of the braking noise. In the deterministic limit $p = 0$ the fundamental

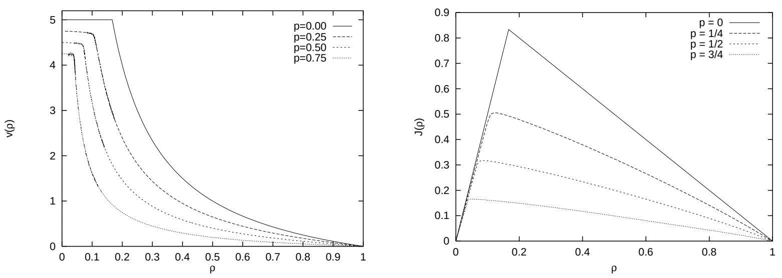


Figure 4.2: Fundamental diagrams for $v_{max} = 5$ and different values of the braking noise. On the left part of the figure the velocity-density relations are shown and on the right part the corresponding flow-density relations.

diagram is simply given by

$$J(\rho) = \min(\rho\, v_{max}, 1 - \rho) \tag{4.1}$$

because the system organizes at low densities so that every car can move with maximal velocity. This is only possible if there are enough empty cells available, i.e. for densities below $\rho_{max} = 1/(v_{max} + 1)$. For larger densities the flow is limited by the number of empty cells.

For $0 < p < 1$ the capacity of the system, i.e. the maximal flow which can be obtained for given $v_{max}$ and $p$, is drastically reduced and a nonlinear density dependence of the average flow is observable. Moreover already for densities below $\rho_{max}$, i.e. the density where the maximal flow is reached, interactions between cars lead to a reduction of the average velocity of cars (see the left part of Fig. 4.2).

Several attempts have been made to explain the nature of the transition in the NaSch model [72–78], but no consistent picture has been developed so far. The controversial discussion of this phenomenon is mainly for two reasons. First, no exact analytical treatment of the model for $v_{max} > 1$ is possible and furthermore no general theory of phase transitions in non-equilibrium systems has been established so far. Therefore the nature of the transition can be investigated exclusively via computer simulations. It turns out that large scale computer simulation must be performed in order to obtain a consistent description of the phase transitions. This is due to the fact that close to the density of maximum flow strong finite size effects can be observed, in particular for larger values of $v_{max}$ and $p$. Moreover, an average of a huge number of samples is needed. Therefore very efficient implementations of the model have to be used in order to obtain reasonable results. Here, a single-bit coding technique has been used [79], which leads to an extremely high numerical efficiency. The results of an extensive numerical investigation analyzing the parameter dependence of the transition will be shown in the following section.

## 4.2 Order Parameter

For a proper description of the transition one should introduce an order parameter which has a qualitatively different behavior within the two phases. A first candidate would be the analogue of the magnetization in the Ising model, i.e. the number of cars. However, since this quantity is conserved in the NaSch model it cannot serve as an order parameter. Therefore the density of nearest-neighbor pairs

$$m = \frac{1}{L} \sum_{i=1}^{L} n_i n_{i+1}, \tag{4.2}$$

with $n_i = 0$ for an empty cell and $n_i = 1$ for a cell occupied by a car (irrespective of its velocity), is the simplest choice of a local quantity with a nontrivial behavior at the transition density. Due to the braking rule (**R2**) $m$ gives the density of those cars with velocity 0 which had to brake due to the next car ahead.

An alternative choice of the order parameter was introduced in [73]:

$$\bar{M}_i = 1 - \frac{1}{2T\rho} \sum_{t=t_0+1}^{t_0+T} l_i(t), \tag{4.3}$$

where $l_i(t) = 1$ if the particle number at site $i$ and time $t$ has changed and zero else. Although $\bar{M}_i = \bar{M}$[1] is defined as a time-average it shows a quite similar behavior. For large time-periods it measures the densities of cars with velocity 0. Vilar et al. [73] only investigated the deterministic

[1]Note, that due to the translational invariance of the system $\bar{M}_i$ does not depend on the chosen site $i$.

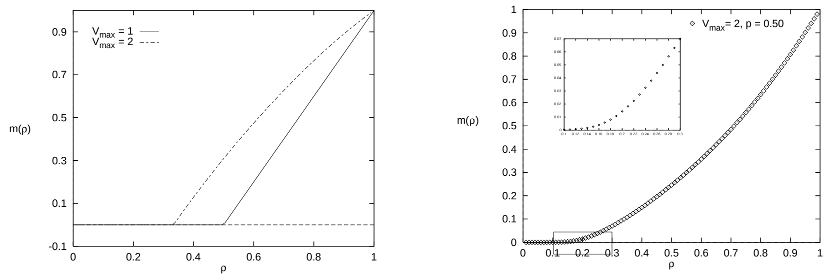


Figure 4.3: In the left part of this figures the order parameter for the deterministic model ($v_{max} = 1, 2$) is shown. Below the transition density $m$ vanishes exactly. In the right part of the figure the density dependence of $m(\rho)$ is shown in the presence of noise ($p = 0.5$). Here no clear identification of a transition density is possible.

case $p = 0$ for which their order parameter is identical to ours, but also in the presence of noise the values differ only slightly.

First, we will discuss the behavior of the order parameter $m$ in the case $p = 0$ (Fig. 4.3). Below the transition density

$$\rho_c = \frac{1}{v_{max} + 1} \tag{4.4}$$

the order parameter vanishes because every car has at least $v_{max}$ empty sites in front and propagates with $v_{max}$. Within the jammed phase the flow is limited by the number of empty cells. Therefore also stopped cars occur. In the presence of noise the behavior of the order parameter changes qualitatively in the vicinity of the transition density. Within this region $m$ growths exponentially as a function of $\rho$. The right part of Fig. 4.3 shows that the order parameter does not exhibit a sharp transition. Although it becomes rather small for small densities it is still different from zero. The situation is quite similar to the behavior of the order parameter in finite systems [80], but in our case we carefully checked that finite-size effects are excluded. Therefore, the transition in the NaSch model is smeared out by the noise and the transition density is shifted towards smaller values of $\rho$ with increasing values of $p$.

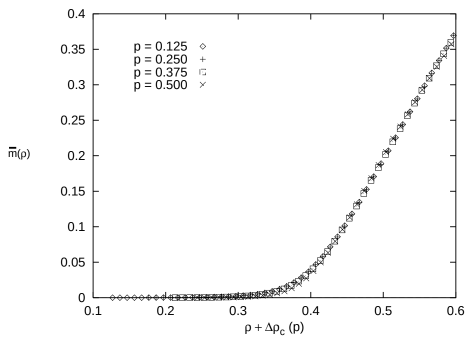


Figure 4.4: Scaling-plot of the order parameter for $v_{max} = 2$ and different values of $p$. In the vicinity of the transition density one gets a reasonable data collapse. The density shift determines the transition density for a given $p$.

In order to have a suitable criterion to locate the transition regime, we analyzed the scaling behavior of the order parameter near the "transition density" $\rho_c$[2]. Fig. 4.4 shows that one gets a quite reasonable data collapse using the scaling form

$$\overline{m}(\rho) = \Pi(p) m(\rho + \Delta\rho_c). \tag{4.5}$$

$\Pi(p)$ is a scaling factor and $\Delta\rho_c$ is the shift of the transition density compared to the deterministic value (4.4).

The values of the transition densities established by the scaling assumption are shown in Fig. 4.5. For all combinations of $p$, $v_{max}$ we took into account $\rho_c < \rho_{max}$ holds.

## 4.3 Spatial Correlations

A striking feature of second-order phase transitions is the occurrence of a diverging length scale at criticality and a corresponding algebraic

[2]In the presence of noise $\rho_c$ is merely a characteristic density which locates the density *regime* where the transition takes place.

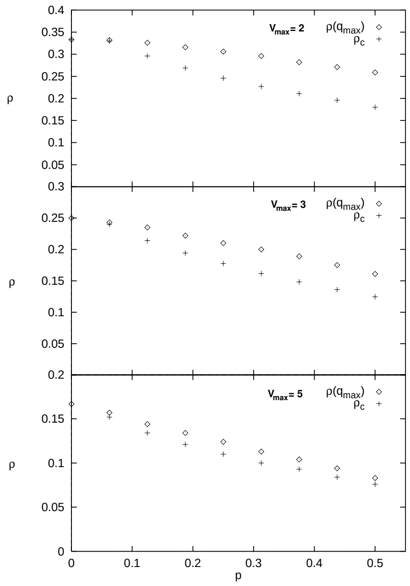


Figure 4.5: Values of the transition density for different maximum velocities and $p$ in comparison with $\rho_{max}$.

decay of the correlation function. Using lattice gas variables the density-density correlation function is defined by

$$G(r) = \frac{1}{L}\sum_{i=1}^{L} n_i n_{i+r} - \rho^2. \tag{4.6}$$

Again it is very instructive to consider the deterministic case ($p = 0$) first.

In the vicinity of the transition density one observes a decay of the amplitude of $G(r)$ for larger values of the distance between the sites (Fig. 4.6). Precisely at $\rho_c$, however, the correlation function is given by

$$G(r) = \begin{cases} \rho_c - \rho_c^2 & \text{for} \quad r \equiv 0 \mod(v_{max}+1) \\ -\rho_c^2 & \text{else,} \end{cases} \tag{4.7}$$

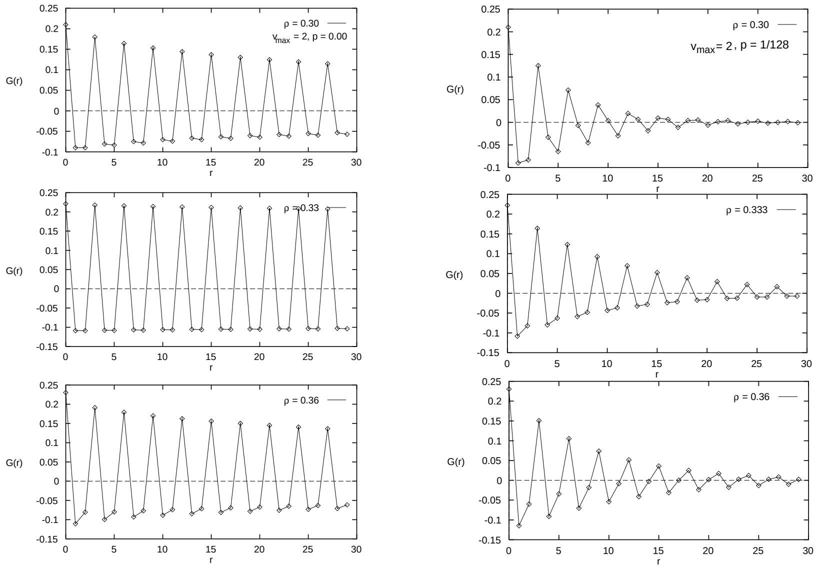

Figure 4.6: The left part of the figure shows the correlation function in the vicinity of the phase transition for $p = 0$. At $\rho = \rho_c$ the amplitude is independent of the distance $r$. The right part of the figure shows the correlation function in the presence of noise. The amplitude of the correlation function decays exponentially for all values of $\rho$.

because there are exactly $v_{max}$ empty sites in front of each car. Considering small, but finite, values of $p$ the correlation function has the same structure as in the deterministic case, but the amplitude decays exponentially for all values of $\rho$ (Fig. 4.6). The decay of the amplitude determines the correlation length for a given pair of $(p, \rho)$, which is finite for all densities in the presence of noise.

The maximal value $\xi_{max}$ of the correlation length determines the transition density for small values of $p$ (Fig. 4.7). Numerically we find (Fig. 4.8)

$$\xi_{max} \sim p^{-\frac{1}{2}}. \tag{4.8}$$

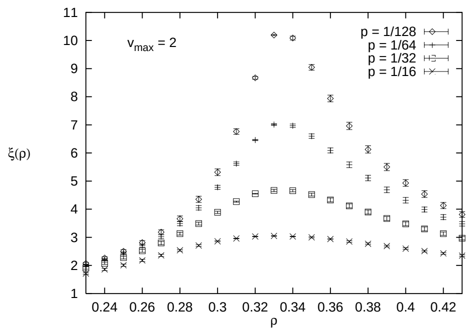


Figure 4.7: Density dependence of the correlation length in the vicinity of the transition density.

In fact, this picture can be confirmed analytically for $v_{max} = 1$ [71]. Using the results of [42] one obtains $\xi_{max}^{-1} = \ln\left(\frac{1-p}{1-p-\sqrt{p}}\right)$ for the correlation length $\xi_{max}$ at $\rho = 1/2$. Therefore $\xi_{max} \propto 1/\sqrt{p}$ for small $p$. This exponent seems to be independent of $v_{max}$ although the particle-hole symmetry is broken for $v_{max} > 1$.

## 4.4 Headway and Cluster-Size Distributions

The two-point correlation function presented in the previous section is able to describe the ordering mechanism, i.e. the efficient use of gaps near $\rho = 1/(v_{max}+1)$, which governs the stationary state in the vicinity of $\rho_c$ for small values of $p$. On the other hand for larger values of $p$, the cluster formation dominates the dynamics already at low densities. In this section we present other quantities, which can characterize the typical cluster size and the typical size of a free flow regime.

In particular the behavior of the headway distribution, i.e the number of empty cells in front of a car, as well as the cluster-size distribution is discussed. It is also interesting to study the distance between consecutive standing cars. This quantity gives a quantitative measure for the magnitude of the free-flow regime. Fig. 4.9 shows a log-plot of typical

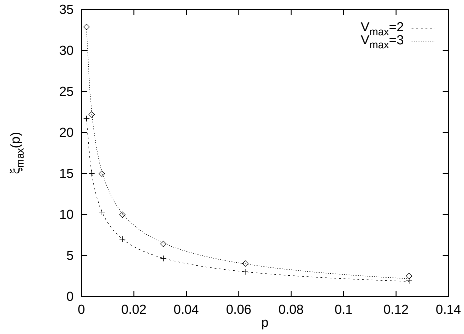


Figure 4.8: Noise dependence of $\xi_{max}$ for different maximum velocities. Independent of the maximum velocity $\xi_{max}(p) \sim 1/\sqrt{p}$ holds in the limit $p \to 0$.

distance distributions in the free-flow and in the jammed phase. For low densities a pronounced maximum of the distance distribution is observable. This is due to the fact that distances smaller than $v_{max}$ are avoided due to the distance rule **R2**. For larger densities it is no longer possible to avoid small distances between cars. Therefore the distance distribution is a monotonously decreasing function. For large distances one finds a pure exponential decay of the distance-distribution with a finite length scale. Next, we also measured the cluster-size distribution, i.e. the sizes of compact clusters of cars. Analogous to the distance distribution, one asymptotically finds a pure exponential decay for the cluster-size distribution with finite length-scale for all densities $\rho < 1$. Although both, the distance and the cluster-size distribution, lead to finite length-scales in the whole parameter regime it still has been argued that a diverging length-scale at the transition density can be found [77]. In particular, the definition of jam-sizes is controversial discussed, because in particular for large values of the braking noise jams are not compact. But nevertheless alternative definitions of the jam, i.e. counting all cars with less then two empty cells in front, lead to analogous results. In contrast to that, it is much simpler to give a correct description of the typical size of a free-flow regime. This can be done via measurements of the distance between con-

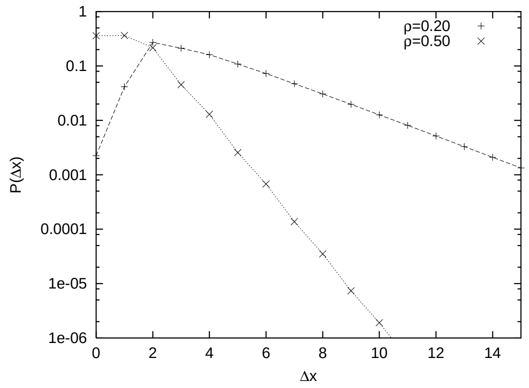


Figure 4.9: Log-plot of the distance distributions for $v_{max} = 2$, $p = 0.10$ and $\rho = 0.20, 0.50$.

secutive standing cars only, which corresponds to the distances between jams, or vice versa the typical size of a free-flow region. Fig. 4.11 shows distributions of distances between jams for $v_{max} = 2$ and $p = 0.10$. Also for the jam-gap distribution asymptotically one gets a pure exponential decay, with finite length scales in the whole high density regime. But also near as well as below the transition density an exponential decay of the jam-gap distribution for large distances is observable.

## 4.5 Discussion

The numerical results suggest a consistent picture of the jamming transition in the NaSch model. Measurements of the order parameter and the correlation function show that critical behavior only occurs in the deterministic limit where the transition density is given by $\rho_c = (v_{max} + 1)^{-1}$ (see also [72, 73]). The presence of noise destroys long-range correlations even close to the deterministic limit. The behavior is analogous to a second-order phase transition in finite systems [80]. However, it has been checked carefully that the results are not affected by finite-size effects and are solely due to the presence of noise.

The order parameter does not vanish exactly, but the transition density could be determined from the scaling behavior. This suggests that

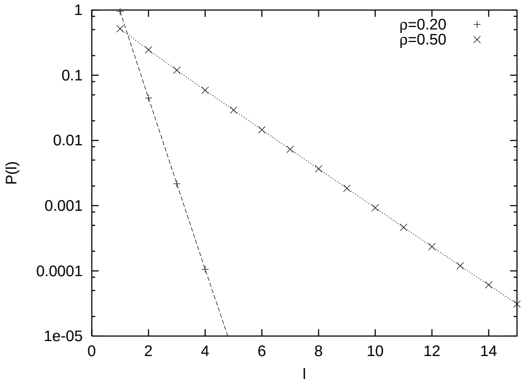


Figure 4.10: Log-plot of the cluster-size distributions for $v_{max} = 2$, $p = 0.10$ and $\rho = 0.20, 0.50$.

the system is not critical in a strict sense. Measurements of the density-density correlation function and the correlation length confirm this picture. We find a finite correlation length in the presence of noise ($p > 0$). The maximum correlation length diverges in the deterministic limit like $\frac{1}{\sqrt{p}}$ for all values of $v_{max}$ we investigated ($v_{max} = 2, 3, 5$). For the case $v_{max} = 1$ this result can also be confirmed by analytical calculations.

Our conclusions have to be compared with those of other investigations where signals of a second-order transition also in nondeterministic cases have been found. From our point of view these results are either a consequence of a special limit considered or the methods chosen. Nagel and Paczuski [74] showed the existence of self-organized critical behavior for the outflow region of a large jam in the cruise-control limit. They found a scale-invariant size distribution of jams from measurements far downstream of the mega-jam. In this region most of the cars propagate without any fluctuations such that this limit is also an example for scale-invariance in deterministic flow. Very recently an investigation of the probabilistic version of the NaSch model has been performed [77] and it has been argued, that at the jamming transition critical behavior occurs also for the nondeterministic cases. However, the order parameter introduced in [77] does also not vanish exactly below the transition density. All the data presented in [77] are consistent with our interpre-

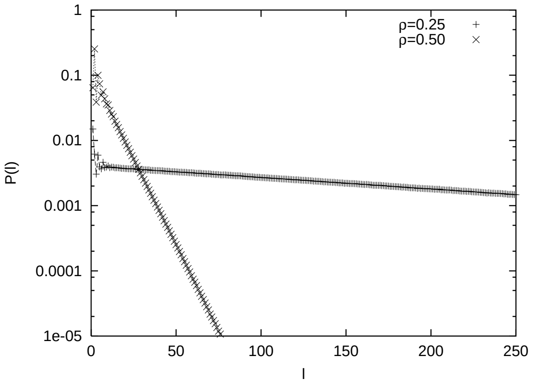


Figure 4.11: Log-plot of the jam-gap distributions for $v_{max} = 2$, $p = 0.10$ and $\rho = 0.25, 0.50$.

tation of the nature of the transition. In contrast to the view of [77] we expect true phase separation only in the limit $p \to 1$.

Another indication for the absence of critical behavior is the well-established fact (see e.g. [75] and Fig. 4.5) that the density of maximum flow $\rho(q_{max})$ and the transition density $\rho_c$ are different. Correlations obviously favor states with higher flow (see e.g. Fig. 4.6, which show that occupancies of cells in front of a car are suppressed which is the generalization of the particle-hole attraction observed in [42, 69] for $v_{max} = 1$). Therefore one should expect that the state with the strongest correlations is also the state with the highest flow as in the deterministic case. It would be rather surprising if the system exhibits a genuine second order phase transition with diverging correlation length at $\rho_c \neq \rho(q_{max})$.

# Chapter 5

# Spatial Disorder in Single-Lane Systems

In this chapter the effect of quenched disorder in driven stochastic systems, i.e. the TASEP and the NaSch model, is analyzed. The quenched disorder is implemented via so-called "defect sites". At defect sites the capacity of the lattice is locally reduced. In the first section the generic behavior of such systems is studied using the TASEP with parallel dynamics and periodic boundary conditions as an example. It turns out that already a single defect site, i.e. a site where the hopping probability of the particles is reduced, leads to a change of the macroscopic behavior.

This setup is generalized in the following sections. In the second section extended defects are analyzed as well as a distribution of quenched disorder. In the third section of this chapter the stationary behavior of the NaSch model on an inhomogeneous lattice will be discussed.

## 5.1 The TASEP with "Slow" Sites

The first investigation of driven systems on a periodic lattice with a local defect has been performed by Janowsky and Lebowitz [81, 82]. They studied the effect of one slow site for the TASEP with periodic boundary conditions and random-sequential update. A similar setup is considered in this section for the TASEP with parallel dynamics. Fig. 5.1 shows a typical fundamental diagram for a system with a spatial defect. The

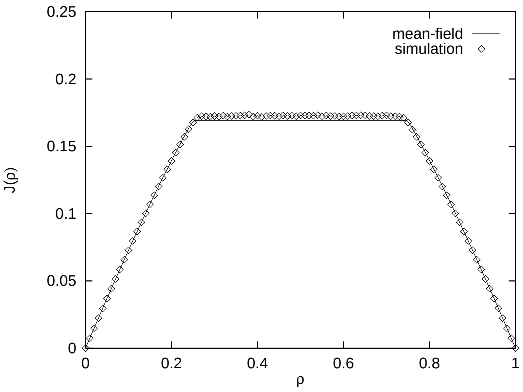


Figure 5.1: Fundamental diagram for the TASEP with parallel update and one stationary defect. The hopping probability in the bulk is given by $q = 0.75$ and at the defect by $q = 0.25$.

*hopping probability* at a regular site is given by $q = 0.75$ and at the impurity site (which is located at $x_d = 1$) by $q = 0.25$. As shown in fig. 5.1 one can distinguish three different density regimes with respect to the flow. At high densities ($\rho > \rho_h$) as well as at low densities ($\rho < \rho_l$) the flow of the homogeneous system is recovered, while the flow takes a constant value at intermediate densities $\rho_l < \rho < \rho_h$.

The underlying mechanism can be understood from the form of the density profile in the different density regimes (see fig. 5.2). In the high and low density regime the defect leads only to a local inhomogeneity in the density profile. At low densities $\rho < \rho_l$ the system organizes such that the density at the defect site is increased which compensates the reduced mobility at that site. In the high density phase the flow is limited by the number of empty cells. Therefore the average density behind the defect has to be reduced to achieve the flow of the regular sites at the defect. For intermediate densities the reduced capacity of the slow site can no longer be locally compensated. Therefore the system self-organizes in a macroscopic high and low density region.

So far, an exact solution for the stationary state of this process was only found for a sub-lattice parallel update and deterministic motion in the bulk [83] and for the TASEP with random-sequential dynamics for

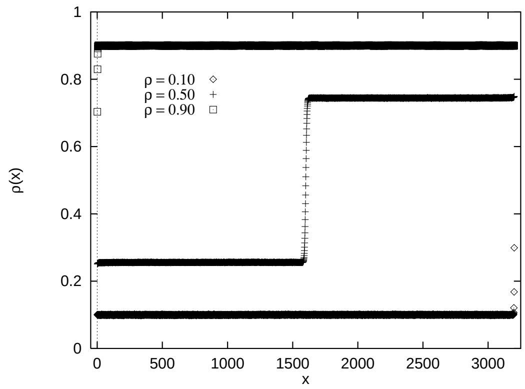


Figure 5.2: Density profiles for the TASEP with parallel update for different values of $\rho$. The hopping probability in the bulk is given by $q = 0.75$ and at the defect (located at site 1) by $q = 0.25$.

small system sizes [82].

Therefore a phenomenological approach is applied [81, 84] which is based on the form of the density profile in the phase separated state. In the bulk of the high density region one expects that the flow of the homogeneous system is recovered, i.e. the current in the high-density region is given by $J_h = (1 - \sqrt{1 - 4q\rho_h(1-\rho_h)})/2$. The flow in the low density region is given by the same expression replacing $\rho_h \to \rho_l$. If one assumes that the high- and low-density regimes are extended to the defect site the flow at the impurity is given by:

$$J_d = \frac{1 - \sqrt{1 - 4q_d\rho_h(1-\rho_l)}}{2}. \tag{5.1}$$

Now the plateau value can be calculated using $J_l = J_d = J_h$ which follows directly from the continuity equation. Explicitly one gets:

$$J_d = \frac{1}{2}\left(1 - \frac{1}{q+q_d}\sqrt{(q+q_d)^2 - 4q^2 q_d}\right) \tag{5.2}$$

for the plateau value of the flow. The bulk value of the density in the high (low) density region is given by $\rho_h = \frac{q}{q+q_d}$ ($\rho_l = \frac{q_d}{q+q_d}$). The shock is located at $r = x_d - \frac{\rho - \rho_h}{\rho_h - \rho_l} L$ (if $r < 0$ the shock is located at $r' = L + r$).

Fig. 5.1 shows that this approach indeed gives a good estimate for the stationary flow in the segregated regime. Also $\rho_l$ and $\rho_h$ as well as the average shock position are well estimated.

In contrast, the fluctuations of the shock-position are not described by the phenomenological approach and have to be determined numerically. Janowsky and Lebowitz used a so-called "second-class particle" in order to locate the shock position [81]. The dynamics of the second class particle is determined by the following rules: If a pair of sites contains a regular particle on the left and a second-class particle on the right, the position of both particles is exchanged. On the other hand, if the second-class particle interacts with an empty site, the second-class particle behaves like a regular particle. Therefore the second-class particle is typically located at the shock, because in a high density region the second-class particle moves typically to the left and in a low density region typically to the right. This method of detecting the shock position leads to the following results. For densities $\rho \neq 0.5$ in the phase-separated regime the size of the fluctuations of the shock position scales according to $\sqrt{L}$. In contrast the fluctuations of the shock are suppressed for $\rho = 0.5$. For that case the fluctuations scale according to $L^{\frac{1}{3}}$. The same results have also been obtained using a more direct method by analyzing the exponential decay of the density profile in the vicinity of the shock position. Janowsky and Lebowitz argued that the special behavior of the fluctuations at $\rho = 0.5$ is a consequence of the particle-hole symmetry of the model [81].

## 5.2 Extended Defects and a Distribution of Impurity Sites

In this section we generalize the setup of the previous section. Here, we consider extended defects, i.e. a few consecutive impurity sites. The second part of the section shortly reviews the results obtained by Tripathy and Barma [85, 86] who investigated the stationary behavior of the TASEP with randomly distributed impurity sites.

Fig. 5.3 shows fundamental diagrams for the TASEP with defects of different length. It turns out that the plateau value of the flow is continuously reduced and for large defects asymptotically reaches the maximum flow of the homogeneous system with the hopping probability

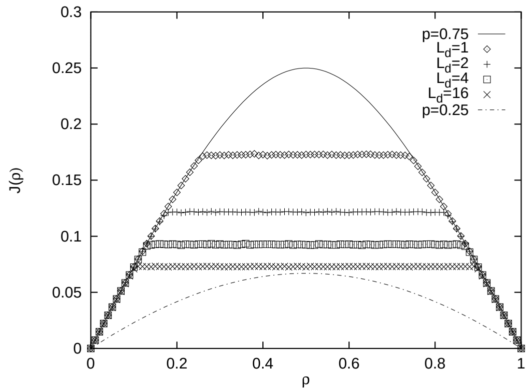


Figure 5.3: Fundamental diagram for the TASEP with parallel update and defects of different length $L_d$. Again $q = 0.75$ and $q_d = 0.25$ is chosen. For comparison the fundamental diagram of the "fast" $(q = 0.75)$ and "slow" homogeneous systems are shown.

of the defect site. Then the defect system and the homogeneous system with "slow" sites differ in that sense, that the maximum value of the flow is reached not only for a single density, but for a large density regime.

This suggests that the phenomenological approach is also valid for extended defects in the sense that one can simply iterate the ansatz which has been made for the single impurity site. Again the results of the generalized approach are in good agreement with simulations. Note, that this behavior of the system can only be found if the length of the defect is small compared to the system size. For lengths comparable to the system size deviations of the "fast" fundamental diagram are observed already before the plateau value is reached.

Analogous observations have also been made for the density profile. The densities in the high- and low-density regime of the phase-separated states, correspond to the densities of the "fast" homogeneous system where the plateau value of the flow is obtained. Therefore the reduction of the flow due to the extended defects leads to a larger difference of $\rho_h$ and $\rho_l$ in the segregated phase (see fig. 5.4).

As mentioned above Tripathy and Barma [85, 86] studied systems with randomly position quenched impurities. The TASEP with random

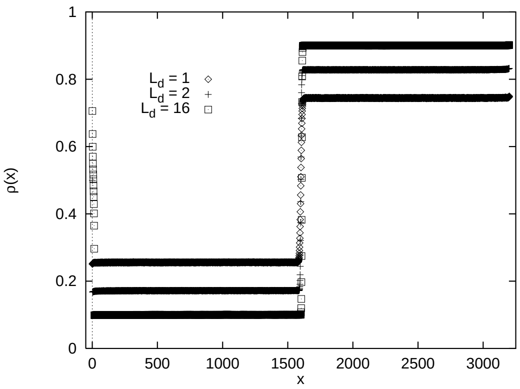


Figure 5.4: Density profiles for different length of the defect. Again $q = 0.75$ and $q_d = 0.25$ are used and the average density is given by $\rho = 0.50$. The defect extended over the first $L_d$ sites of the system.

sequential update was studied where the impurity sites were drawn from a binary distribution. The hopping rate on the fast sites was set to one and on the slow sites to $q = 0.5$.

The simulations results for this setup show that again a density regime with constant flow exists. Fig. 5.5 shows density profiles for the TASEP with randomly distributed impurities in the high density regime ($\rho = 0.80$) as well as the phase separated states ($\rho = 0.60$, $\rho = 0.50$). The distribution of impurity sites leads to a "rough" density profile for all densities, but nevertheless in the segregated phase a macroscopic high and low density regime can be identified. The right part of the figure shows the density profile for a small part of the system. Again the results of the phenomenological approach are in reasonable agreement with the simulated density profile.

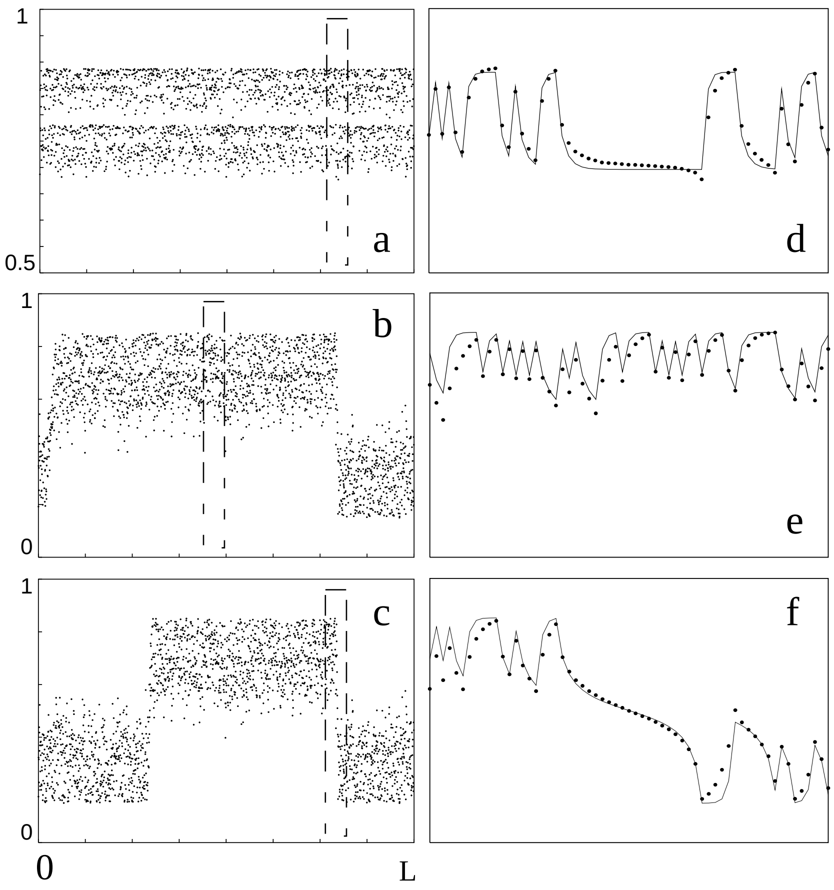


Figure 5.5: Density profiles for the TASEP with randomly distributed impurity sites at different densities ((a) $\rho = 0.80$, (b) $\rho = 0.60$, (c) $\rho = 0.50$). The hopping rate of the "slow" sites are given by 0.5 and on the "fast" sites by one. The length of the system is $L = 8000$. The right part of the figure shows clippings of the density profile at the corresponding densities in comparison with the phenomenological results. (from [86])

## 5.3 The NaSch Model and Local Impurities

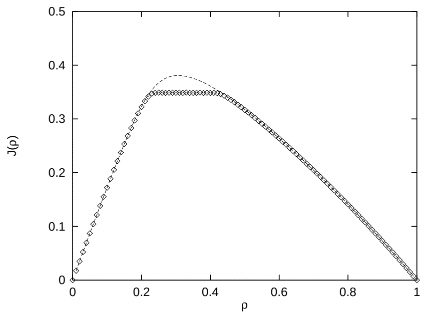


Figure 5.6: Fundamental diagram of the NaSch model with a single defect site. The model parameters are given by $v_{max} = 2$, $p = 0.25$, $p_d = 0.75$ and $L = 3200$.

As already mentioned above, in this section we show simulation results of the NaSch model on a lattice with defect sites. For the NaSch model with $v_{max} > 1$ different parameterizations of the defect sites are possible. Csahok and Vicsek [87] the defect sites where $v_{max}$ is reduced. In contrast, here the defect is implemented as a part of the chain where the braking noise $p_d$ is increased. Fig. 5.6 shows the fundamental diagram of a system with a *single* defect site. Analogous to the results for the TASEP a density regime exists where a constant value of the flow is observable.

Also the results obtained for the density profile are similar to the density profiles of the TASEP as shown in fig. 5.7. Again in the low and high density regime the local defect leads only to a local perturbation of the density profile close to the defect, while segregation effects are visible at intermediate densities.

Qualitative differences to the density profile of the TASEP have been found close to the defect site. There oscillations of the density profile occur, which correspond to the long-ranged correlations between cars for the NaSch model with $v_{max} = 2$.

Finally, the scaling behavior of the fluctuations of the shock position has been analyzed. For $v_{max} > 1$ a determination of the shock position using a second-class particle is not possible, because both $\rho_h$ and $\rho_l$ can

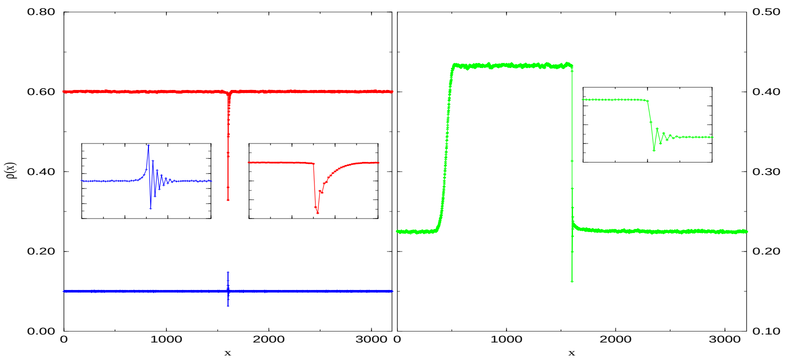


Figure 5.7: Density profiles in the three phases. In the left part of the figure density profiles in the high- ($\rho = 0.60$) and low-density ($\rho = 0.10$) phase are shown, while the right part of the figure shows a density profile of the segregated phase ($\rho = 0.30$). The defect site is located at $x_d = 1600 = L/2$. We used the same parameters as in Fig. 5.6.

be smaller than 0.5. This implies that the second-class particle moves in both parameter regimes from left to right. Therefore we analyzed the exponential decay of the density profile directly. The numerical results show that for all densities in the phase separated regime, the fluctuations scale proportional to $\sqrt{L}$. This result indicates that the sub-diffusive scaling of the fluctuations of the shock position for the TASEP at $\rho = 0.5$ is indeed a consequence of the particle-hole symmetry.

## 5.4 Discussion

In this chapter the stationary state of the TASEP and the NaSch model on inhomogeneous lattices was analyzed. It turned out that already a single impurity site or "weak bond" determines the macroscopic behavior of the system in a wide density regime. For densities $\rho_l < \rho < \rho_h$ a constant value of the flow is observed. The system organizes into a phase separated state where a macroscopic high and low density regime can be found.

Exact solutions for the stationary state of the TASEP with quenched impurities exist only in some special cases [82, 83]. For the general case to date only approximative results have been found. Nevertheless good estimates for the fundamental diagram and the density profiles can be obtained, i.e. the position of the shock as well as the densities in the phase separated states can be calculated with high accuracy. On the other hand, the fluctuations of the shock profile cannot be described by the phenomenological approach. Therefore the scaling behavior of the fluctuations of the shock must be calculated numerically. It turned out that for the TASEP and $\rho \neq 0.5$ the fluctuations of the shock profile scale according to $L^{1/2}$ while for $\rho = 0.5$ a scaling according to $L^{1/3}$ is observed.

For extended defects the flow in the segregated regime converges to the capacity of the homogeneous system containing exclusively slow sites with increasing length of the defect. Nevertheless, one does not recover the fundamental diagram of the homogeneous "slow" system, but gets a fundamental diagram which has the same form as for the single defect, which differs only by the reduced plateau value. Moreover, the smaller plateau value leads to a larger difference between $\rho_h$ and $\rho_l$ in the phase separated states.

The organization into a macroscopic high- and low-density regime is also observable for the NaSch model. Compared with the TASEP only two qualitative differences occur. First, closely behind the defect oscillations of the density profile oscillations of the density profile exist and second, the numerical results indicate that the fluctuations of the shock profile scale according to $L^{1/2}$ for all densities in the segregated regime. This supports the view that the reduced fluctuation for the TASEP at $\rho = 0.5$ are a result of the particle-hole symmetry.

# Chapter 6

# Systems with Open Boundaries

The results of the previous chapter have shown that even *local* lattice impurities may give rise to a change of the macroscopic behavior of the system. In this chapter the TASEP and the NaSch model on a lattice with open boundary conditions are investigated. It turns out, that the boundaries can also change the macroscopic behavior of the system, i.e. boundary-induced phase transition can be observed.

In the first section the exact analytical results for the stationary states of the TASEP with different updates are presented [43, 56, 58, 60]. Then a phenomenological approach [88] is introduced in the second section. These results are compared with the rigorous results. Finally, the approach is applied for the NaSch model with open boundary conditions.

## 6.1 The TASEP and Open Boundary Conditions

The TASEP shows a surprisingly rich physical behavior when open boundary conditions are considered. Depending on the in- and output rates $\alpha$ and $\beta$ different phases and different kinds of phase transitions occur.

Fig. 6.1 shows the phase diagram of the TASEP with random sequential dynamics which is generic also for the sequential and the parallel

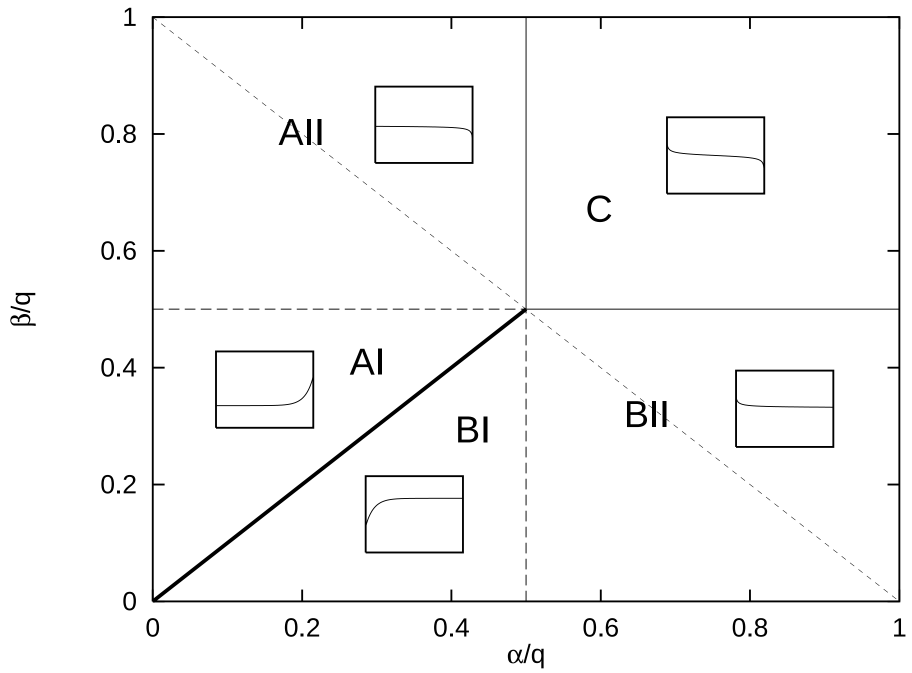


Figure 6.1: Phase diagram of the TASEP with open boundary conditions. The insets show typical density profiles of the corresponding phases.

update procedures. One can distinguish five different phases in the $\alpha-\beta$ plane. $AI$ and $AII$ label the low density phases, $BI$ and $BII$ the high density phases and $C$ the maximum current phase. Within phases $AI$ and $AII$ the flow is governed by the particle input at the left boundary, while the particle-output determines the behavior of the system in the high density phases. If both $\alpha$ and $\beta$ are larger than the critical value $\alpha_c$ the maximum current is reached. The decomposition of the high and low density phases into two sub-phases is due to the different asymptotic behavior of the density profile which will be discussed later.

### 6.1.1 Parameter Dependence of the Current

#### Random Sequential Update

The exact solution of the stationary master equation using the MPA (see chapter 3) allows for the explicit calculation of the current via

$$J = q\frac{\langle W|C^{i-1}DEC^{L-i-1}|V\rangle}{\langle W|C^L|V\rangle} = q\frac{\langle W|C^{L-1}|V\rangle}{\langle W|C^L|V\rangle}, \tag{6.1}$$

where $L$ denotes the length of the chain and $C = E + D$. Evaluating this formula one can give explicit analytical expressions for the flow for arbitrary system sizes and parameter combinations.[1] It is necessary to calculate $\langle W|C^N|V\rangle$ (without loss of generality it is assumed that $\langle W|V\rangle = 1$) first. This can be done either using the explicit representations for $\langle W|, |V\rangle, E, D$ or directly via the algebraic equations (3.19-3.20). Then an explicit analytical expression for $J$ and the TASEP with random sequential update is given by [43]:

$$\langle W|C^N|V\rangle = \sum_{n=1}^{N} \frac{n(2N-1-n)!}{N!(N-n)!}\frac{\beta^{-n-1}-\alpha^{-n-1}}{\beta^{-1}-\alpha^{-1}} \tag{6.2}$$

In the limit of large $N$ one gets [43]:

$$\begin{aligned}
\langle W|C^N|V\rangle &= [\alpha(1-\alpha)]^{-N} && \text{for} \quad \alpha < \frac{1}{2}, \quad \beta > \alpha && (6.3)\\
\langle W|C^N|V\rangle &= [\beta(1-\beta)]^{-N} && \text{for} \quad \beta < \frac{1}{2}, \quad \alpha > \beta && (6.4)\\
\langle W|C^N|V\rangle &= N^{-3/2}4^N && \text{for} \quad \alpha > \frac{1}{2}, \quad \beta > \frac{1}{2} && (6.5)
\end{aligned}$$

Now using the asymptotic expressions for $\langle W|C^N|V\rangle$ one easily calculate the current for large system sizes $L \gg 1$. The current in the three

[1] From now on we denote both the hopping rates and probabilities by $q = 1 - p$. As far as the random sequential update is considered, we choose $q = 1$ if $q$ is not explicitly given.

different parameter regimes is given by:

$$
\begin{aligned}
J(\alpha) &= \alpha(1-\alpha) && \text{for} \quad \alpha < \frac{1}{2}, \quad \beta > \alpha && (6.6)\\
J(\beta) &= \beta(1-\beta) && \text{for} \quad \beta < \frac{1}{2}, \quad \alpha > \beta && (6.7)\\
J_{max} &= \frac{1}{4} && \text{for} \quad \alpha \geq \frac{1}{2}, \quad \beta \geq \frac{1}{2} && (6.8)
\end{aligned}
$$

As long as one is only interested in the limit of large system sizes and the structure of the phase diagram one can also use a mean-field approach, which is known to be exact on the line $\beta = p - \alpha$.

### Parallel Update

Also for the parallel update the current can be calculated using eq. (6.1) [58, 60]. It turns out that in contrast to the continuous time update the current as well as the phase boundaries depend non-trivially on the hopping probability $q$. This is due to the fact that for updates in discrete-time the hopping rate is a real parameter of the model and cannot be absorbed into the time-scale of the process. For the parallel update the critical input probability is given by $\alpha_c = 1 - \sqrt{1-q}$. Explicitly, the flow for the TASEP with parallel update for large systems sizes is given by:

$$
\begin{aligned}
J(\alpha) &= \alpha\frac{(q-\alpha)}{(q-\alpha^2)} && \text{for} \quad \alpha < \alpha_c, \quad \beta > \alpha, && (6.9)\\
J(\beta) &= \beta\frac{(q-\beta)}{(q-\beta^2)} && \text{for} \quad \beta < \alpha_c, \quad \alpha > \beta, && (6.10)\\
J_{max} &= \frac{1-\sqrt{1-q}}{2} && \text{for} \quad \alpha \geq \alpha_c, \quad \beta \geq \alpha_c. && (6.11)
\end{aligned}
$$

Again one can identify a line in the $\alpha - \beta$-plane given by $1 - q = (1 - \alpha)(1 - \beta)$, where a solution analogous to the periodic system using a 2-cluster approach [42, 69] is possible [58]. The solution on this line gives the exact result for the flow for all parameter combinations in the thermodynamic limit since it touches all three phases.

**Sequential Update**

For the case of the (backward) sequential update one has to use a slightly different ansatz in order to calculate the stationary flow. Here, the flow is determined by the weights of $D\hat{E}$. Explicitly one finds:

$$J_{\leftarrow}(j) = \frac{q}{Z_L}\langle W|C^{j-1}D\hat{E}C^{L-j-1}|V\rangle \quad , \tag{6.12}$$

where $Z_L = \langle W|C^L|V\rangle$. This form of the current formula (6.12) suggests that that the flow depends on the position $j$, but inserting the relation (7.14) one can show that $J_{\leftarrow}$ is independent of $j$. This result is in accordance with the continuity equation. Also for the sequential update one can identify a line in the $\alpha-\beta$ plane where a one-dimensional solution of the algebra can be found, given by $(1-\alpha)(1-\beta) = 1-q$, as for the parallel update. Moreover, the parameter dependence of the phase boundaries turns out to be the same as for the parallel update [58]. Using the one-dimensional representation one gets the following expressions for the flow

$$\begin{aligned} J(\alpha) &= \frac{\alpha}{q}\frac{(q-\alpha)}{(1-\alpha)} && \text{for} \quad \alpha < \alpha_c, \quad \beta > \alpha, && (6.13) \\ J(\beta) &= \frac{\beta}{q}\frac{(q-\beta)}{(1-\beta)} && \text{for} \quad \beta < \alpha_c, \quad \alpha > \beta, && (6.14) \\ J_{max} &= \frac{1-\sqrt{1-q}}{1+\sqrt{1-q}} && \text{for} \quad \alpha \geq \alpha_c, \quad \beta \geq \alpha_c, && (6.15) \end{aligned}$$

which are exact for large systems sizes in the whole parameter regime.

### 6.1.2 Density-Profiles

So far, we can only distinguish three different phase in the $\alpha-\beta$ plane with respect to the flow. The division of the high- and low density phases into two phase $AI/AII$ or $BI/BII$ is due to the different asymptotic behavior of the density-profile, i.e. the average densities $\langle\tau_i\rangle$ at the sites $i = 1, \ldots, L$.

The density-profile can be calculated using the results of the exact stationary solution. In terms of the weights given by the MPA the density profile can be calculated from:

$$\langle \tau_i \rangle = \frac{\langle W|C^{i-1}DC^{L-i}|V\rangle}{\langle W|C^L|V\rangle}, \tag{6.16}$$

for all types of update schemes. An evaluation of eq. (6.16) for the random sequential update was performed in [43, 56] for arbitrary in- and output rates, and system sizes. Here we concentrate on the limit of large system sizes and discuss the parameter dependence of the bulk densities and the relevant length scales. Analyzing the explicit results for the density profiles one finds that the system is governed by two independent length scales $\xi_\alpha$ and $\xi_\beta$ which represent the influence of the boundaries. For the case of the random sequential update $\xi_\sigma = \ln(4\sigma(1-\sigma)), (\sigma = \alpha, \beta)$ holds. At the critical value of $\alpha$ and $\beta$ these length scales diverge and a phase transition occurs.

**Profiles in the Low Density Phases**

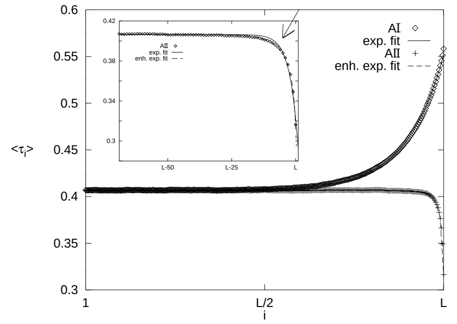


Figure 6.2: Density profiles for the parallel update (q=0.75) in the low-density phases $AI - AII$. The inset shows that deviations from a pure exponential decay are observable in phase $AII$.

Fig. 6.2 shows typical density profiles for the low density phases $AI/AII$. Both profiles differ in the way how the constant bulk value is reached. In phase $AI$ one observes a pure exponential decay, while in $AII$ an enhanced exponential decay according to $\exp(-(L-x)/\xi_\alpha)/\sqrt{L-x}$ is given. Both, the enhanced and the pure exponential decay, are governed by the length scale $\xi$ where

$$\xi^{-1} = \left|\xi_\alpha^{-1} - \xi_\beta^{-1}\right|. \tag{6.17}$$

Thus the correlation length $\xi$ remains finite at the transition line from $AI$ to $AII$ such that the divergence of $\xi_\beta$ at the transition line $AI - AII$ is not directly observable. In contrast to the divergence of $\xi_\beta$, the asymptotics of the density profile can be checked against the numerical results. The inset of Fig. 6.2 shows that the enhanced exponential asymptotics must be applied in order to match the simulation results for the density profile in phase $AII$.

Another characteristic line crossing the low-density phase $AII$ is the mean-field line, where the density profile is completely flat. This line separates the monotonously decreasing density profiles from the monotonously increasing ones. Nevertheless the asymptotic behavior is unchanged.

### Transition between High- and Low-Density Phase

The transition between the high- and low-density phases is driven by the diverging length scale $\xi$. This divergence occurs although both length scales are finite because at the transition line $\xi_\alpha$ and $\xi_\beta$ coincide. The qualitative agreement of the density profile of the random sequential update with the density profiles for the discrete time updates strongly suggest that the relevant length scale in the low-density phase is given by (6.3) also for discrete-time updates. Moreover, the comparison of the numerically estimates shows that the correlation lengths (as a function of $\alpha - \alpha_c$) of the parallel and ordered sequential update are identical and differ from those obtained for the random sequential only by a constant factor (see Fig. 6.3). Exactly at the transition line $\alpha = \beta$ one finds a linear density profile as shown in Fig. 6.3. This linear profile is the result of a fluctuating shock front which separates (for a given time) a high-density region from a low-density region. The position of the shock front fluctuates through the whole lattice such that a time average over all single time profiles gives a linear profile. An extensive discussion of the dynamics of the shock front will follow in the next section.

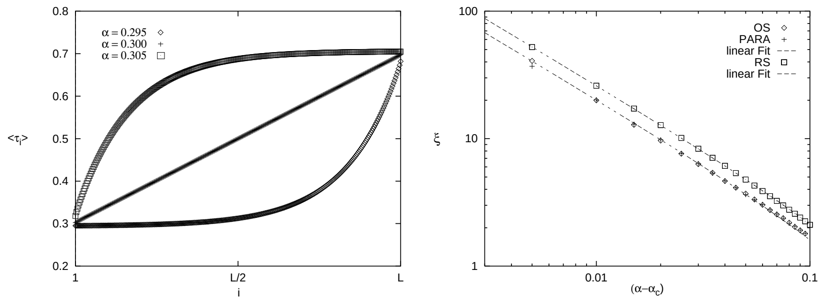


Figure 6.3: The left part of the figure shows exact density profiles for the random sequential update near the transition at $\alpha = \beta = 0.3$. The input rates are chosen such that $\alpha + \beta = 0.6$ holds. The right part of the figure shows a log-log plot of the correlation length for different types of updates (OS=ordered sequential, PARA=parallel, RS=random sequential). The length scales are obtained from an exponential fit of the density profile. Again $\alpha$ and $\beta$ are chosen such that $\alpha + \beta = 0.6$ holds ($\alpha_c = 0.3$). For the TASEP with random sequential update $q = 1$, while for the parallel and the ordered sequential update $q = 0.75$ was used.

### Maximum-Current Phase

The transition from the low- (high-) density phase AII (BII) to the maximum current phase is characterized by a change of the asymptotic behavior of the density profile from the enhanced exponential to a pure algebraic decay. The transition is driven by the divergence of the length scale $\xi_\alpha$ ($\xi_\beta$) for $\alpha \to \alpha_c$ ($\beta \to \beta_c$). Both length scales are infinite not only at the transition line but for all values of $\alpha$ and $\beta$ larger than the critical value. Therefore an algebraic decay of the density profile can be observed in the whole maximum current phase. Fig. 6.4 shows the diverging correlation length for different update types. Again the length scales of the updates with discrete time agree. The length scales produced by the random sequential update are larger if one considers the same in- and output rates (Note that for $q = 0.75$ for the parallel and

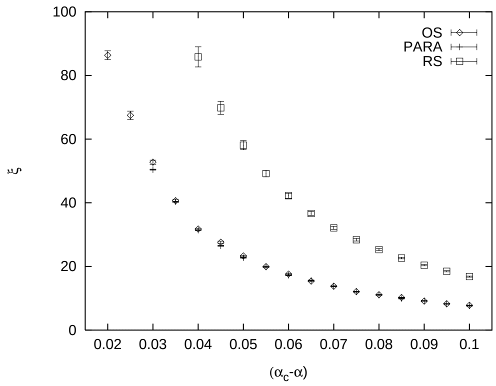


Figure 6.4: Divergence of the correlation length $\xi_\alpha$ near the transition to the maximum current phase ($\beta = 0.75$).

ordered sequential update and $q = 1$ for the random sequential update the same values for $\alpha_c$ are obtained).

## 6.2 A Phenomenological Approach

In a recent work [88] a phenomenological approach was suggested which turns out to very useful for an intuitive understanding of the physical mechanisms. Moreover, a quantitative description, e.g. the calculation of the correlation length, is possible.

The basic idea is that stochastic processes like the TASEP with open boundary are dominated by domain wall dynamics. The domain walls, which separate a high and low density regime, perform a biased random through walk the lattice. It turns out that the phase boundaries are determined by the drift velocity of the random walk while the length scales are governed by the diffusion constant. Now one has to determine the parameter dependence of the drift velocity as well as of the diffusion constant. This will be done in the remaining part of the section by using the example of the TASEP with random sequential update.

### Determination of the Drift Velocity

In order to illustrate the basic mechanism of the domain wall dynamics [88] we consider the case $\alpha L \ll 1, \quad \beta L \ll 1$ and $q = 1$ first. In this particular limit two domains can be identified easily, one consisting of empty sites and a second domain where a compact jam is present, because on the typical time scale of the particle injection and removal the particles move almost instantaneously through the lattice. If a particle leaves the system the domain wall moves one step to the right and one step to the left if a particle enters the system (again on time scales which are large compared to the typical time scale of the bulk dynamics). Therefore the dynamics of the domain wall is governed by the in- and output rates $\alpha, \beta$. If $\alpha < \beta$ the domain wall typically moves to the right and the high density region is pinned at the right end of the chain.

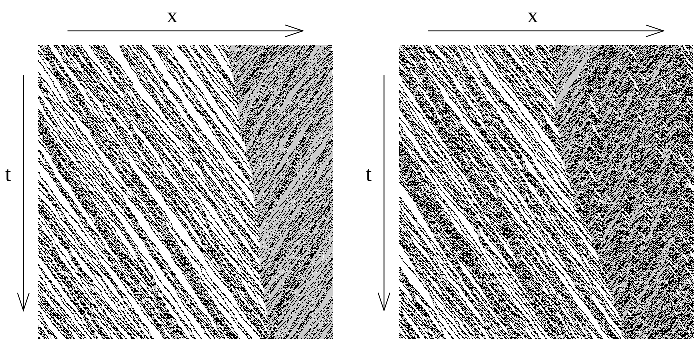


Figure 6.5: Space-time diagrams for the TASEP with open boundary conditions and parallel update ($q = 0.75$) in the low density phases ($\alpha = 0.20$, $\beta = 0.30$ (left), and $\beta = 0.60$ (right)).

For larger values of the in- and output rates one has distinguish between two types of domain walls in the low density phase, as shown in Fig. 6.5 for the TASEP with parallel update and $q = 0.75$. The left part of Fig. 6.5 shows a space-time diagram for ($\alpha = 0.20$, $\beta = 0.30$) corresponding to $AI$. Here both $\alpha$ and $\beta$ are smaller than the critical value $\alpha_c = 0.50$. Therefore a low- and a high-density regime is present in the system. In contrast to that in the right part of the figure $\beta = 0.60$ is considered such that the domain wall separates a low-density and a maximum current regime.

From now on we introduce a coarse grained picture in order to obtain quantitative results. Therefore a slightly different view of the particle in- and output is introduced. Instead of controlling the particle in- and output via the probabilities $\alpha$ and $\beta$ we couple the chain to a particle reservoir of density $\rho^+$ at the right boundary and $\rho^-$ at the left and of a chain. The densities of the particle reservoirs must be viewed as effective densities, e.g. $\rho^- = \min(\alpha, 1/2)$ and $\rho^+ = \max(1-\beta, 1/2)$ for the TASEP. For more general cases, $\rho^\pm$ is considered as bulk density which is given if the system is controlled by the input (output) probability. Both the high and low density reservoir generate a characteristic flow $j^\pm$, which is identical to what is found for the periodic system for a given density $\rho^\pm$. Now if $j^- > j^+$ one gets a high density state stationary state because at least far from the boundaries the domain wall typically moves to the left boundary of the chain.

In order to obtain an explicit expression for the drift velocity $V$, the continuity equation

$$\frac{d}{dt}\rho(x,t) = j_{x-1}(t) - j_x(t) \tag{6.18}$$

is analyzed. Introducing a coarse grained picture one obtains the well known form of the continuity equation $\partial\rho/\partial t + \partial j/\partial x = 0$, with a traveling wave solution $\rho(x,t) = \rho(x - Vt)$. Now the drift velocity $V$ of the domain wall is simply given by

$$V = \frac{j^+ - j^-}{\rho^+ - \rho^-}. \tag{6.19}$$

### Diffusion Constant

So far only the parameter dependence of the phase boundaries were established by analyzing the drift velocity of the random walk. As a next step also the fluctuations of the biased random walk are taken into account. The domain wall motion can be view as Poisson process with an effective jump rate to the right (left) given by $D_{r(l)} = j^\pm/(\rho_+ - \rho_-)$, leading to a diffusion constant

$$D = \frac{1}{2}(D_r + D_l) = \frac{1}{2}\frac{j_+ + j^-}{\rho_- - \rho_+}. \tag{6.20}$$

Then one can identify a localization length given by $\xi = \ln(D_r/D_L)$ if a sharp domain wall exists, e.g. for the TASEP. For arbitrary processes a scaling argument leads to a localization length which is approximately given by

$$\xi \approx D/|V|. \tag{6.21}$$

At this point one has to mention that the domain wall approach fails in the maximal current phase where the drift velocity vanishes and the diffusion constant is infinite. On the other hand, the phase transition between the $AI/AII$ is well described. In that case one gets a finite value for the diffusion constant, but a vanishing drift velocity of the domain wall. This implies that the domain wall is not localized anymore as expected from the exact solution.

Finally, one can state that the domain wall approach gives a qualitative explanation of the phase diagram and moreover the predictions concerning the phase boundaries and the correlation length reproduce the analytical for the TASEP results exactly. In the next section this picture will be applied to the NaSch model with $v_{max} > 1$.

## 6.3 NaSch Model and Open Boundary Conditions

The results presented in this section have been obtained exclusively by computer simulations because an analytical treatment of the NaSch model for $v_{max} > 1$ is restricted to approximative methods even for periodic boundary conditions.

In contrast to the case of $v_{max} = 1$ where particle input and removal is possible only on the sites 1 and $L$, for higher velocities a few natural choices exist. For the case of parallel update, which is applied in the NaSch model, it turns out that the maximum flow of the periodic system can only be achieved if one allows for particle input on the first $v_{max}$ sites. In contrast, if particle injection is only possible at the first site the flow is limited to $J = 0.5$ because injection of particles is only possible in every second time-step. Also the particle output at the right boundary has to be considered in an analogous fashion. Here we coupled the left

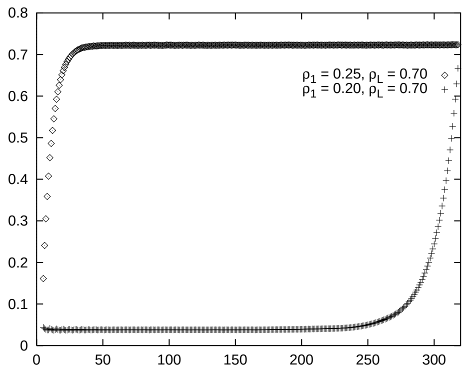


Figure 6.6: Typical density profiles in the low ($\rho_1 = 0.20, \quad \rho_L = 0.70$) and high density phase ($\rho_1 = 0.25, \quad \rho_L = 0.70$) for the NaSch model ($v_{max} = 5$, $p = 0.25$, $L = 320$).

end of the open chain with a particle reservoir of a given density. More explicitly an extra site is added at the left end of the chain, where a particle with a random velocity $v_r > 0$ is injected with probability $\rho_1$. The removal of particles is also controlled by an additional site which is occupied with probability $\rho_L$. In the following the regular sites of the chain as well as the additional sites, are updated according to the rules of the NaSch model. Fig. 6.6 shows typical density profiles for the NaSch model in the low and high density phase. Analogous to what was found for the TASEP at the left (right) part of the chain a constant bulk density is achieved in the low (high) density phase. Towards the right (left) end of the chain an exponential increase (decrease) of the average density is found. In that sense the results for the TASEP are recovered. A difference to the case of $v_{max} = 1$ is observable at the left boundary of the chain for a low density profile. Then oscillations of the density profile exist. This is due to the presence of long-ranged correlations for

$v_{max} > 1$.

In order to apply the phenomenological picture, first the effective densities $\rho^{\pm}$ which are obtained for a given density of the particle reservoirs must be determined. The effective densities $\rho^{\pm}$ are considered as the bulk densities for a chain which is governed by the right (left) particle reservoir. Following the phenomenological approach discussed in the

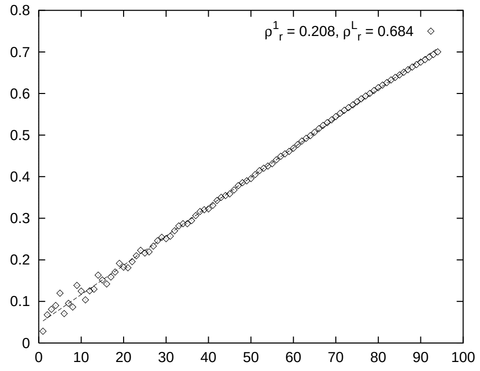


Figure 6.7: Linear density profile on the transition line $AI/BII$ for the NaSch model ($v_{max} = 5$, $p = 0.25$, $L = 96$).

previous section, one expects a linear density profile analogous to the $\alpha = \beta$ line for the TASEP, if $j^+ = j^-$. This was checked for the NaSch ($v_{max} = 5$, $p = 0.25$) model for densities of the particle reservoirs where $j^+ = j^-$ holds. Fig. 6.7 shows that one gets a linear density profile as expected apart from fluctuations at the left boundary.

Another sensitive check for the phenomenological approach is the determination of the correlation length via the diffusion constant. The results obtained by the phenomenological approach are in reasonable agreement with length scales established by exponential fits of the density profiles. A better quantitative agreement is expected if the diffusion constant for a Poisson process in discrete time is taken into account.

In terms of the effective densities the phase diagram can be obtained directly from the fundamental diagram of the periodic system. For all

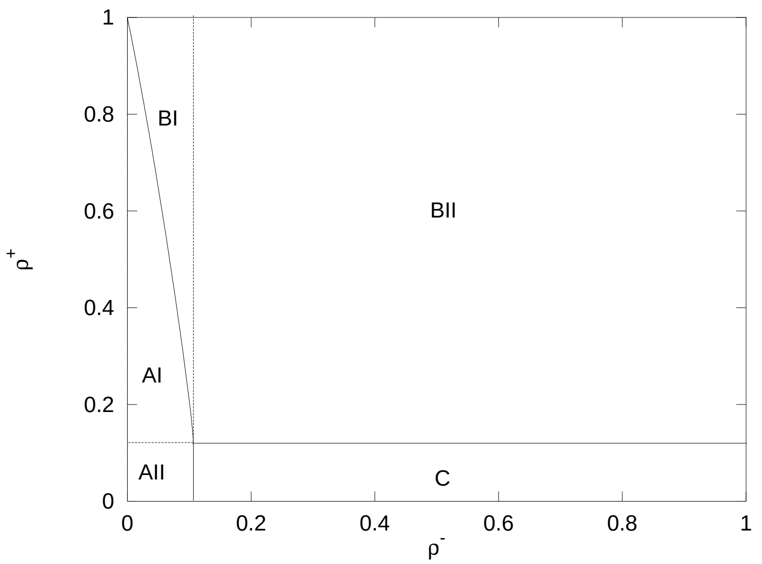


Figure 6.8: Phase diagram of the NaSch model for $v_{max} = 5$ and $p = 0.25$ with open boundary conditions dependent on the effective densities of the particle reservoirs.

currents $J < J_{max}$ two densities $\rho^+, \rho^-$ can be identified, where $J = J(\rho^+) = J(\rho^-)$. As argued above, these densities fix the transition line between $AI$ and $BI$. The endpoint of this line is given by $\rho^- = \rho_{max} = \rho^+$, where $J(\rho_{max}) = J_{max}$. Fig. 6.8 shows the phase diagram for the NaSch model with open boundary conditions, obtained by this procedure.

## 6.4 Discussion

In this chapter we discussed the effect of open boundary conditions for the TASEP and the NaSch model with $v_{max} = 5$. For all kind of models which have been considered the phase diagram has the same structure. For an infinite system one can distinguish three different phases with respect to the flow.

- Low density phase: The flow is determined by particle injection at the left boundary.
- High density phase: The flow is determined by particle removal at the left boundary.
- Maximum current phase: The flow is governed by the capacity of the chain.

The left and the right boundary of the system impose two independent length scales which determine the behavior of the density profile. If one length scale diverges a change of the asymptotic behavior of the density profile emerges. A transition from $AI \to AII$ ($BI \to BII$) is obtained if one length scale is still finite while the divergence of the second length scale leads to a transition from $AII \to C$ ($BII \to C$).

In [88] a phenomenological approach was introduced, which is able to explain the structure of the phase diagram. The behavior of the system is described in terms of the domain wall dynamics. It turned out that the analytical results for the TASEP in the thermodynamic limit can be recovered. Moreover, a correct description of the phase diagram as well as of the characteristic length scales for the NaSch model with $v_{max} > 1$ was given. The phenomenological approach also explains the universal structure of the phase diagram, i.e. the occurrence of five different phases, for all processes where one local maximum of the fundamental diagram is found.

# Chapter 7

# CA Models with "Slow-to-Start" Rules

Measurements on real traffic have revealed the existence of meta-stable states with very high flow [8]. In particular the maximum flow which can be reached in a homogeneous state is significantly higher than the maximum outflow from a jam. It turns out that this observation is crucial for an understanding of the underlying mechanism. It also explains the failure of the NaSch model where the outflow from a jam only slightly differs from the maximum value.

In the first section of this chapter a detailed description of meta-stable states in traffic flow will be given. It will be shown that meta-stable state are related to hysteresis effects. Then in the following sections three variants of the NaSch model are discussed which show meta-stable states and hysteresis effects. For all variants we discuss here the reduction of the outflow from a jam is due to a slow-to-start (s2s), i.e. the acceleration of standing cars is explicitly reduced. The first generalization of the NaSch model which is considered the model proposed by Takayasu and Takayasu [37] where a *spatial* s2s rule is introduced. Alternative implementations of s2s rules have been introduced by Benjamin and Hui [38] who considered a temporal s2s rule, and by Barlovic et al. [39, 40], where the s2s rule is implemented by a velocity-dependent randomization parameter.

## 7.1 Meta-Stable States and Hysteresis Effects

### Description of the Phenomenon

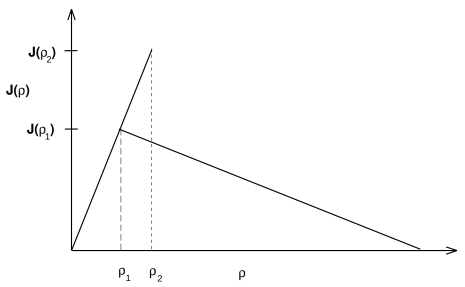


Figure 7.1: The figure shows the typical form of a stationary fundamental diagram. In a certain density regime the flow does not depend uniquely on the average density.

As mentioned above meta-stable states are an important effect established by experimental observations. In order to illustrate the basic mechanism a stationary fundamental diagram showing meta-stable states is drawn schematically in Fig. 7.1. The fundamental diagram consists of two linear branches. The low density branch corresponds to homogeneous free-flow states, while the high density branch corresponds to configurations where jammed states are present. Obviously a density regime exists extending from the intersection point of the two branches ($\rho = \rho_1$) to the density where the optimum value of the flow is obtained ($\rho = \rho_2$), where the flow depends non-uniquely on the global density.

A second feature characterizing meta-stable states is found by analyzing the time-series of flow measurements [8]. Fig. 7.2 shows that a hysteresis loop can be traced if the occupancy of the road varies continuously close to the density where the optimum value of the flow is reached. More explicitly, starting from a homogeneous state, first the flow increases with the density until the optimum value of the flow is reached. A further increase of the density leads to a significant reduction of the flow because jams emerge. Now, if jams are present in the

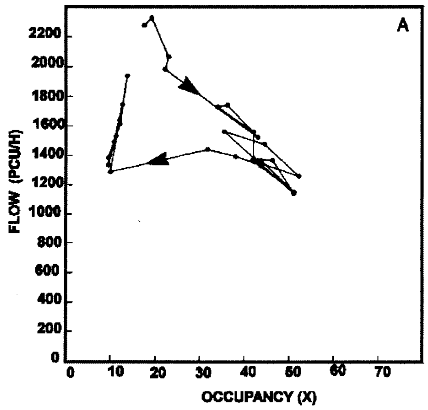


Figure 7.2: Time-traced measurements of the flow (from [8]). Each data point corresponds to a time-averaged value of the flow and density obtained from a local measurement. The average was performed over five minute intervals.

system the homogeneous states can only be recovered if the density is reduced below the intersection point of the two branches, where the jams dissolve.

The reduced outflow of a jam leads to phase separated states at high densities, which can be illustrated as follows. If the outflow from a jam is reduced, the density in the free-flow regime is smaller than the density of maximum flow. Therefore the cars can propagate freely in the outflow regime of the jam and no spontaneous formation of jams is observable in the stationary state, if fluctuations in the free-flow regime are rare.

### Simulation Strategies

In order to establish the existence of meta-stable states one can follow two basic strategies. In the first method, the density of cars is changed adiabatically by adding or removing vehicles from the stationary state at a certain density. Starting in the jamming phase (large densities) and removing cars, one obtains the lower branch of the hysteresis curve. On the other hand, by adding cars to a free flowing state (low densities), one obtains the upper branch. This method is closely related to the experimental situation where the occupancy of the road varies continuously.

The second method does not require to change the density. Instead one starts from two different initial conditions, the mega-jam and the homogeneous state. The mega-jam consists of one large, compact cluster of standing cars. In the homogeneous state, cars are distributed equidistantly (with one larger gap for incommensurate densities). Then, for $\rho_1 < \rho < \rho_2$ the homogeneous initialization leads to a free-flow state while the mega-jam initialization leads to jammed high-density states.

## 7.2 T$^2$ Model

Takayasu and Takayasu (T$^2$) [37] have first suggested a CA model with a s2s rule. Here we investigate the generalization introduced in [89], where the following extension of the NaSch model was given: A standing car with exactly one empty cell in front accelerates with probability $q_t = 1 - p_t$, while all other cars accelerate deterministically. The other update rules (R2-R4) of the NaSch model are unchanged. Due to this modification already for $v_{max} = 1$ the particle-hole symmetry is broken.

In Fig. 7.3 we show the fundamental diagram of the T$^2$ model with $v_{max} = 5$, $p = 0.01$ and $p_t = 0.75$. The system size used for the simulation was $L = 10000$. In order to equilibrate the system, 100000 lattice updates have been performed. The data shown in Fig. 7.3 represent an average over 100000 sweeps through the lattice.

Comparing the simulation results with those for the NaSch model, two qualitative differences have to be discussed. First, the fundamental diagram has an inflection point for densities close to one and second the flow behavior is non-unique in a density regime below the density of maximum flow $\rho_{max}$[1].

The existence of an inflection point for large $p_t$ has first been noticed in [89] for the case $v_{max} = 1$. In contrast, the fundamental diagram of the NaSch model is always convex. The different behavior of the T$^2$ model for large $p_t$ and large densities $\rho$ is related to the fact that space is not used as efficiently as in the NaSch model. One finds a similar

[1] Close to $\rho_1$ finite-size effects are observable in the high density branch. The origin of the finite-size effects will be discussed later.

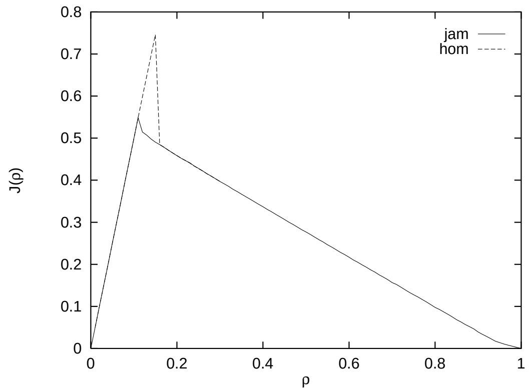


Figure 7.3: Fundamental diagram of the $\mathrm{T}^2$ model ($v_{max} = 5$, $p = 0.01$, $p_t = 0.75$) obtained by starting from two different initial conditions, i.e. a completely jammed state (full line) and a homogeneous state (broken line).

behavior in space-continuous models [90]. There is some experimental evidence that in certain situations the shape of the fundamental diagram differs from the convex form. This behavior of the average flow can be easily obtained tuning the parameter $p_t$ [67, 89].

The non-unique behavior of the flow for densities just below $\rho_{max}$ is due to the fact that for these densities the average flow still depends on the initial configuration. The measurements in Fig. 7.3 have been performed by applying the second method described in the introduction. The lower branch of the fundamental diagram corresponds to measurements starting from a initially completely jammed configuration while the upper branch has been obtained starting with a homogeneous initialization. It should be mentioned that the same result can also be obtained by applying the first method, i.e. by changing the density adiabatically.

For low densities the stationary state consists of homogeneous configurations which are completely jam-free. At higher values of the global density the configurations contain one large jam. In contrast to the NaSch model, no spontaneous formation of jams in the outflow region of the large jam has been observed for the system sizes we took into account. Therefore the jammed states are phase separated states, unlike for the case of the NaSch model.

It should be noted that the maximum value of the average flow depends on the number of updates as well as on the system size. Therefore we can not exclude that the stationary value of the average flow is unique in the thermodynamic limit. Nevertheless the meta-stable states are extremely stable, even for large systems. Moreover, in contrast to standard problems of statistical mechanics, not the thermodynamic limit is relevant for practical purposes, but the behavior of systems of finite length (note that 10000 lattice sites correspond to a road of length 75 km). Since in reality roads and observation times are always finite, the above results are sufficient for all practical purposes.

### The $T^2$ Model at $v_{max} = 1$ - a Deterministic Limit

In Fig. 7.4 we show the fundamental diagram for $v_{max} = 1$, $p = 0.5$ and $p_t = 1$, i.e. stopped cars can only move if there are at least two empty cells in front. Obviously completely blocked states exist for densities $\rho \geq 0.5$, where the number of empty cells in front of each car is smaller than two. Since fluctuations are absent in those states, they have an infinite lifetime. Therefore the flow in the stationary state is zero. In the region $0.5 \leq \rho \lesssim 0.66$ states with a finite flow exist. Although these states are not stationary one has to perform an extremely large number of update steps until the flow vanishes for large system sizes and densities slightly above $\rho = 0.5$ because the number of blocked configurations is very small compared to the total number of configurations. Precisely at $\rho = 0.5$, there are only two blocked states the typical time to reach these states diverges exponentially with the system size. Therefore we used very small systems in order to obtain the lower branch of the fundamental diagram.

Note that the mechanism for meta-stability in the case $p_t = 1$ is different from the meta-stable states discussed before. The hysteresis curve in Fig. 7.4 has been obtained by starting from two different *homogeneous* states, differing only in the velocity of the cars. The jammed branch is reached by starting with a configuration where all cars $j$ have a velocity $v_j(t = 0) = 0$, whereas the upper branch corresponds to an initialization $v_j(t = 0) = v_{max}$. In contrast, by following the first method described in the introduction, one would not find hysteresis since a mega-jam initialization would also yield the high-current branch.

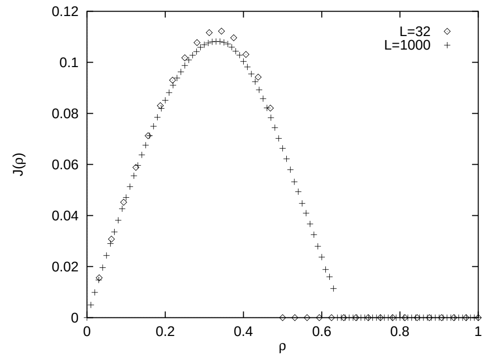


Figure 7.4: Fundamental diagram of the T$^2$ model ($v_{max} = 1$, $p = 0.5$, $p_t = 1$) for two system sizes. For densities slightly above $\rho = 0.5$ the stationary state could only be reached for the smaller system.

The reason for the occurrence of hysteresis in the limit $v_{max} = 1$ and $p_t = 1$ is the existence of a "geometrical" phase transition, in contrast to the hysteresis effects near $\rho_1$. If the critical density is exceeded, the cars can no longer move since there is not enough free space. The "geometrical" phase transition makes it possible to find hysteresis even in the case $v_{max} = 1$.

Finally we want to remark that the $p_t = 1$ limit of the T$^2$ model is in some sense complementary to the cruise-control limit [74] of the NaSch model. In the T$^2$ model the completely blocked state is stabilized due to the absence of fluctuations whereas in the cruise-control limit one finds the absence of fluctuations for homogeneous states at low densities.

## 7.3 BJH Model

The s2s rule of the T$^2$ model is a 'spatial' rule. The range of interaction for standing cars is larger than in the NaSch model and the restart behavior depends only on the spatial arrangement of the vehicles. However, there are other ways of implementing a s2s behavior. In the Benjamin-Johnson-Hui (BJH) model [38] cars which had to brake due to the next car ahead will move on the next opportunity only with probability $1-p_s$.

Note that in contrast to the $T^2$ this slow-to-start rule requires 'memory', i.e. it is a 'temporal' rule depending on the number of trials and not on the free space available in front of the car.

For higher maximum velocities we expect the occurrence of meta-stable states, since also in the BJH model the outflow from a jam is smaller than the maximal flow, while for the case of $v_{max} = 1$ no meta-stable states exist [38, 89].

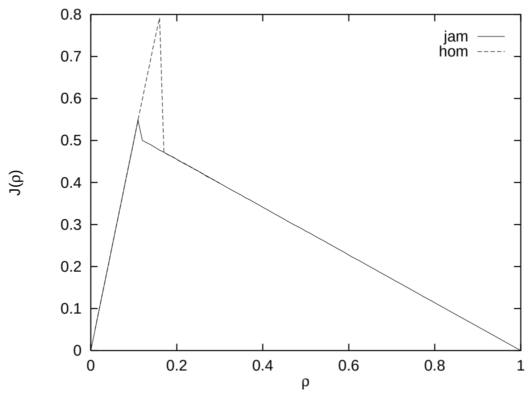


Figure 7.5: Fundamental diagram of the BJH model ($v_{max} = 5$, $p = 0.01$, $p_s = 0.75$) obtained using two different initial conditions, namely a completely jammed state (full line) and a homogeneous state (broken line).

Our simulations show that for $v_{max} > 1$ the overall behavior of the BJH model is very similar to that of the $T^2$ model (for $p_t < 1$). In Fig. 7.5 we show a typical fundamental diagram. There is, however, no inflection point and the fundamental diagram is convex for all $p_s$. This supports the view that the existence of an inflection point is a 'spatial' effect.

The existence of meta-stable states corresponds to phase separated high density states, containing a macroscopic jam and a macroscopic free-flow regime at a time. Fig. 7.6 shows a comparison of the cluster size distribution and the distribution of distances between jams for both models at $\rho = 0.50$. The cluster size distribution shows an exponential decay for large distances for both models, but the length scale which

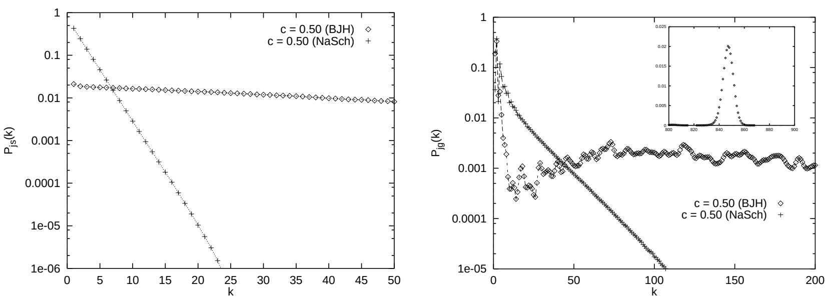


Figure 7.6: The left hand side of the figure show the cluster-size distribution for the BJH model, while on the right hand side of the figure the jam-gap distribution is depicted ($p = 0.05, p_s = 0.50, v_{max} = 5$). The inset of the right figure shows the peak of the jam-gap distribution, which corresponds to the macroscopic free-flow regime.

governs the decay is much larger for the BJH model than for the NaSch model. From what was discussed before a qualitatively different behavior of the cluster distribution for the BJH models was expected, because a macroscopic jam should lead to a peak in the cluster-size distribution at a length of the order of $L$. Nevertheless this observation is not inconsistent to what was claimed before, but it only indicates that the macroscopic jam is not compact. Then measurements of the cluster-size distribution do not detect the complete large jam, but decompose the macroscopic high density region into multiple clusters of finite length. Therefore a direct observation of the size of the jammed regime is difficult.

In contrast, it is simpler to identify the typical size of the macroscopic free-flow regime. This can be done by measuring the headway between standing cars, i.e. the jam-gap distribution. For small headways the behavior of the jam-gap is analogous to the cluster-size distribution. However, a macroscopic free-flow regime can be identified because a peak occurs for headways of the order of the system size (see the inset of the right part of Fig. 7.6). The position of the peak indicates the typical size of the macroscopic free-flow regime.

## 7.4 NaSch Model with Velocity-Dependent Randomization

In the third modified model a velocity-dependent randomization (VDR) parameter $p = p(v(t))$ is introduced in order to reduce the outflow from a jam. This parameter has to be determined *before* the acceleration step R1 (see chapter 2 for the definition of the original model). For simplicity here we study only the case

$$p(v) = \begin{cases} p_0 & v = 0 \\ p & v > 0 \end{cases} \tag{7.1}$$

which already contains the most important features of the general case [39, 40]. Since we are interested in hysteresis phenomena, we restrict ourselves to the case $p_0 \geq p$. Note that for $p_0 = p$ the NaSch model is recovered.

In the following we will use a maximum velocity $v_{max} = 5$, a braking probability $p = 1/64$ of the moving cars and a higher value $p_0 = 0.75$ for the braking probability of stopped cars. Simulation runs have been performed for periodic systems with $L = 10000$ lattice sites.

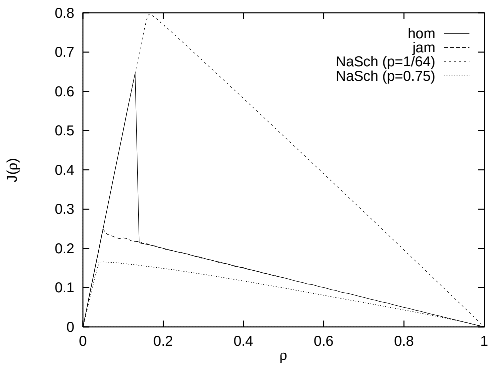


Figure 7.7: Fundamental diagram of VDR model ($v_{max} = 5$, $p_0 = 0.75$, $p = 1/64$, $L = 10000$). For comparison the fundamental diagrams of the NaSch model with $p = 0.75$ and $p = 1/64$ are given.

Fig. 7.7 shows the fundamental diagram of the modified model. Obviously the average flow $J(\rho)$ can take two values in the density interval between $\rho_1$ and $\rho_2$ depending on the chosen initialization. Again the larger values of the average flow can be obtained using a homogeneous initialization of the system. The lower branch is obtained starting from a completely jammed state. Moreover, varying the particle number adiabatically, one can trace a hysteresis loop analogous to what was found for the two other models. For a fixed value of $p$, $\Delta J = J(\rho_2) - J(\rho_1)$ depends linearly on $p_s$ for wide a range of parameters.

Increasing the system size, we observe a decrease of the density $\rho_2$ towards the branching density $\rho_1$. The jammed states become stable for densities $\rho \geq \rho_1$ even for global densities very close to $\rho_1$. Again it should be noted that the homogeneous states are extremely stable and therefore should be relevant for realistic systems.

It is instructive to compare the fundamental diagram of the VDR model with those of the corresponding NaSch models. For small densities $\rho \ll 1$ there are no slow cars in the VDR model since interactions between cars are extremely rare. Here the flow is given by $J(\rho) \approx \rho(v_{max} - p)$, i.e. identical to the NaSch model with randomization $p$. For large densities $1 - \rho \ll 1$, on the other hand, the flow is given by $J(\rho) \approx (1 - p_0)(1 - \rho)$ which corresponds to the NaSch model with randomization $p_0$. For densities close to $\rho = 1$, only cars with velocities $v_j = 0$ or $v_j = 1$ exist. The number of moving cars goes to zero so that asymptotically the flow is completely determined by $p_0$.

The microscopic structure of the jammed states in the VDR model differs from those found in the NaSch model. While jammed states in the NaSch model contain jams with an exponential size-distribution, one can find phase separation in the VDR model. This picture is supported by a simple phenomenological approach. Obviously the flow in the homogeneous branch is given by $J_{hom} = \rho(v_{max} - p) = \rho v_f$, because every car can move with the free-flow velocity $v_f$. Assuming that the high density states are phase separated, we can obtain the second branch of the fundamental diagram. The phase separated states consist of a large jam and a free flow regime, where each car moves with velocity $v_f$. The density in the free-flow regime $\rho_f$ is determined by the average waiting time $T_w = \frac{1}{1-p_0}$ of the first car in the jam and $v_f$, because, neglecting interactions between cars, the average distance of two consecutive cars is given by $\Delta x = T_w v_f + 1 = \rho_f^{-1}$. Using the normalization $L = N_J + N_F \Delta x$

($N_{F(J)}$ is the number of cars in the free-flow regime (jam)) we find that the flow is given by

$$J_{sep}(\rho) = (1 - p_0)(1 - \rho). \tag{7.2}$$

Obviously $\rho_f$ is precisely the lower branching density $\rho_1$, because for densities below $\rho_f$ the jam-length is zero. It should be noted that this approach is only valid for $p_0 \gg p$ and $v_{max} > 1$. The condition $p \ll 1$ guarantees that interactions of cars due to velocity fluctuations are rare. As a consequence, the jam is compact in that limit. For increasing $p$, the jam becomes less dense. In the case $v_{max} = 1$, cars can stop spontaneously even in the free-flow regime. If $p_0$ is large enough, these cars might initiate a jam. This is the basic reason why hysteresis is usually not observed for $v_{max} = 1$.

**Stability of the Phase-Separated States**

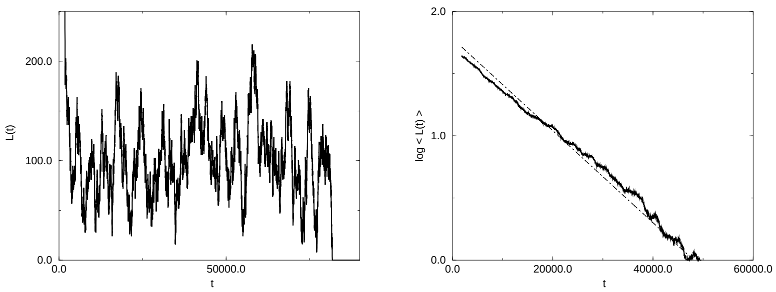


Figure 7.8: Time-dependence of the length $L(t)$ of the jam for $\rho = 0.095$. The left part of the figure shows the time evolution of the length $L(t)$ of one sample. The average $\langle L(t) \rangle$ over 10000 samples (right part of the figure) shows an exponential decay.

Measurements of the average flow show that the lower branch of the fundamental diagram is not stable near the density $\rho_1$, if small system sizes are considered. Therefore we performed a more detailed stability analysis of the homogeneous and the jammed state near $\rho_1$ and $\rho_2$. Close to $\rho_1$, the large jam present in the initial configuration resolves and the average length $\langle L(t) \rangle$ decays exponentially in time (Fig. 7.8). It should be noted that this behavior is not the consequence of a continuous "melting" of the large jam. In contrast, the jam-length $L(t)$ is strongly fluctuating without any obvious systematic time-dependence (Fig. 7.8). Once a homogeneous state without a jammed car is reached, no new jams are formed. Therefore the homogeneous state is stable near $\rho_1$. For large system sizes the jammed states are stable for $\rho \geq \rho_1$, also for densities only slightly above $\rho_1$, because the average length of the jam is proportional to the system size while the fluctuations grow sub-extensive.

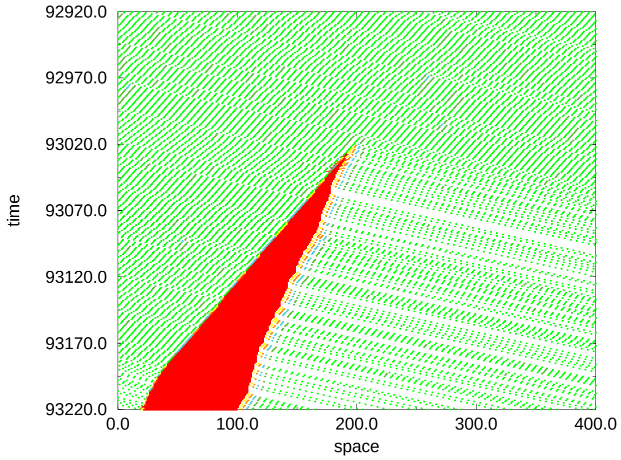


Figure 7.9: Space-time diagram of the VDR model for $\rho = 0.15, L = 400, p = 0.01$ and $p_0 = 0.5$. The homogeneous initial state is not destroyed immediately, but after approximately 93000 lattice updates. In the outflow regime of the jam the density is reduced compared to the average density.

Analogous to the meta-stable jammed states near $\rho_1$, homogeneous initializations for densities slightly above $\rho_2$ lead to meta-stable homogeneous states with short lifetimes. Fig. 7.9 shows the spontaneous formation of jams due to velocity fluctuations. The finite lifetimes of the homogeneous states are the qualitative difference between this model and the cruise-control limit [74] of the NaSch model, where the time evolution of homogeneous states at low densities is completely deterministic.

For large system sizes the density difference $\Delta\rho = \rho_2 - \rho_1$ decreases. This can be explained by looking at the mechanism of an emerging jam. Jams emerge due to velocity fluctuations in dense regions of the homogeneous states, where the distance $d_j + 1$ between consecutive cars is less than $v_{max}$. In this regions all following cars have to slow down if a car in front breaks in the randomization step. Over-reactions of following cars finally can cause jams. The probability to find clusters of an appropriate length for a given density is proportional to the system size. Therefore we expect that all homogeneous states are unstable for $\rho > \rho_1$ in the thermodynamic limit.

For higher values of $p$ the lifetime of homogeneous states at densities $\rho > \rho_1$ is very small. Nevertheless one can observe the same microscopic structure of the high density states as long as the outflow of a jam is sufficiently reduced. A *rough* estimate for the minimal difference between $p_0$ and $p$ necessary to observe phase separation can be obtained from the following arguments based on the features of a typical fundamental diagram of the VDR model at small $p$ and large $v_{max}$ (see Fig. 7.10). In

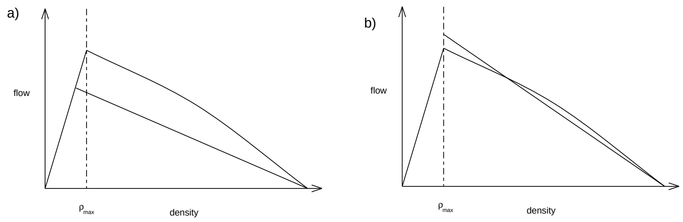


Figure 7.10: Illustration of the flow branches a) in the presence of phase separation and b) without phase separation.

the following we assume that the fundamental diagram is perfectly linear up to $\rho_2$, i.e. $J_{hom}(\rho) = \rho(v_{max} - p)$. As mentioned before, the phase-separated branch is described by $J_{sep}(\rho) = (1 - p_0)(1 - \rho)$ (see eq. (7.2)). In order to find phase separation, the flow in the phase-separated branch at density $\rho_2$ must be lower than the flow in the homogeneous branch, i.e. $J_{hom}(\rho_2) > J_{sep}(\rho_2)$ (left part of Fig. 7.10). For a situation as depicted in the right part of Fig. 7.10 (i.e. for $J_{hom}(\rho_2) < J_{sep}(\rho_2)$), no phase-separation would be found. In the following we approximate $\rho_2$ by $\rho_{max}$, the maximum of the corresponding NaSch model with randomization $p$. Using the estimate $\rho_{max} = (1-p)/(v_{max}+1)$ [78], the inequality for the current at $\rho_2 \approx \rho_{max}$ can be used to obtain an estimate for the minimal difference $p_0 - p$ necessary to observe phase separation (see Fig. 7.11). Near the deterministic limits ($p = 0$ and $p = 1$) and for large values of $v_{max}$, already a small difference $p_0 - p$ suffices to generate phase separation. For all nondeterministic cases the states of maximum flow are not completely homogeneous and the flow in the high density branch is somewhat lower than $J_{sep}(\rho) = (1 - p_0)(1 - \rho)$ for larger values of $p$, because the large jam is not compact anymore.

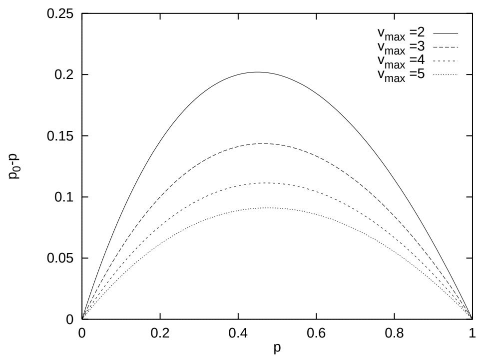


Figure 7.11: Estimates for the minimum difference $p_0 - p$ necessary to observe phase separation.

In order to substantiate this picture we performed simulation runs for different values of $p$ and a fixed value of $p_0$. During the simulations measurements of the average density of standing cars $\langle v_0 \rangle$ as well as the gap-distance distribution have been made. Here, we concentrate on the verification of phase-separated states. Therefore we used mega-jam initializations for all simulation runs.

Figure 7.12 shows the results of $\langle v_0(\rho) \rangle$ for different values of $p$, $p_0 = 0.50$, and $v_{max} = 5$. If a particular choice of $p$ leads to phase separated high density states, one observes that $\langle v_0(\rho) \rangle = 0$ if $\rho < \rho_1$

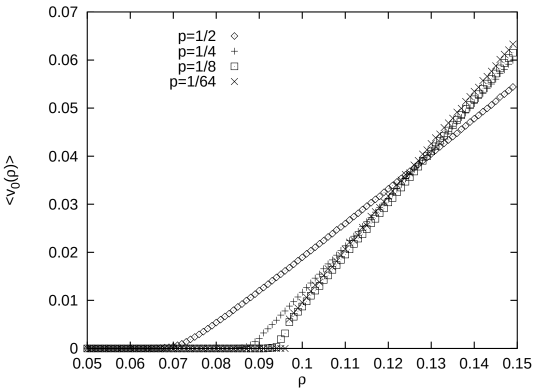


Figure 7.12: Density of standing cars $\langle v_0(\rho)\rangle$ for different values of $p$

while for larger values of the densities $\langle v_0(\rho)\rangle$ linearly increases. For densities slightly beyond $\rho_1$ $\langle v_0(\rho)\rangle = 0$ drops from a finite value to zero. This is due to the finite-size effects discussed before, because for finite systems the homogeneous states are stable in that region. Although the branching density $\rho_1$ could not be identified using $\langle v_0(\rho)\rangle$ an identification of phase-separation is possible, because this behavior is qualitatively differs from what was found for the NaSch model. There a smooth behavior of $\langle v_0(\rho)\rangle$ for also for small values is observed. Then the results clearly indicate that phase separation is already absent for $p = 0.25$, where a "NaSch-like" behavior of $\langle v_0(\rho)\rangle$ is observable.

This interpretation of the result was confirmed by measurement of the jam-gap distribution. For all values of $p_0$, we identified as phase separated from the results of $\langle v_0(\rho)\rangle$ a macroscopic free-flow regime could be identified (as shown in in Fig. 7.13).

Comparing the numerical result with the estimated difference, we conclude the minimal difference between $p_0$ and $p$ is indeed much larger than expected. This is due to the fact that already noticeably below the density of maximum flow fluctuations can cause jams.

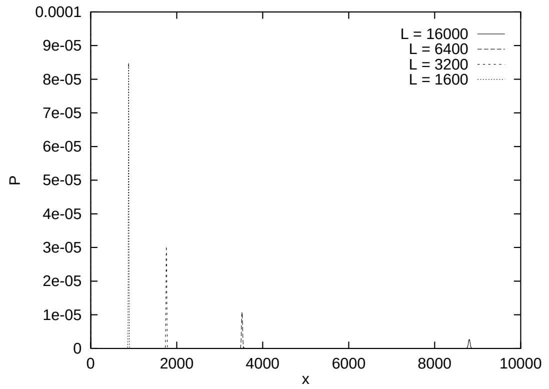


Figure 7.13: Peaks of the jam-gap distribution at macroscopic distances.

### Flow-Optimization and Meta-Stable States

Hysteresis effects and meta-stable states are not only of theoretical interest, but also have interesting applications. From the previous discussion of the s2s models it is evident that one can optimize the maximum flow, if the homogeneous state is stabilized. This implies that the density of the system must be controlled, that it never exceeds $\rho_1$.

A famous application of this strategy are the Lincoln- and the Holland-tunnels in New York, where the number of incoming cars is controlled by traffic lights [91]. Before the traffic lights were affixed jams typically emerged within the tunnel, because inside the tunnel drivers behave more carefully. This gives rise to an increase of the fluctuations. Therefore the tunnel effectively acts as a bottleneck and determines the capacity of the system.

Now a better performance can be achieved if the homogeneous state inside the tunnel is stabilized. This was done analogous to the realistic example by the use traffic lights at the entry of the tunnel.

Here we want to mimic this situation in the following way. The tunnel is considered as part of the road where both braking parameters $p^t, p_0^t$ are increased compared to the remaining part of the lattice $(p, p_0)$. Therefore, if one allows for an uncontrolled inflow of the cars, jams typically appear inside the "tunnel" and the system capacity is governed by $p_0^t$.

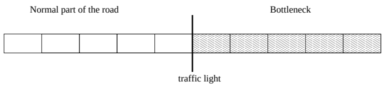


Figure 7.14: Setup used for the simulation of the “tunnel”. At the left part of the road $p = 0.01, p_0 = 0.20$ is used, while on the right part larger values of the braking parameters are applied ($p^t = 0.15, p_0^t = 0.60$).

The situation differs drastically if traffic lights are implemented. As shown in Fig. 7.15, an considerable increase of the maximum capacity can be achieved for an optimal combination of the red-/green-signal periods. The gain of capacity we obtained for the optimal intervals of the signal is of the same order as for the realistic examples [91].

## 7.5 Discussion

The ability to describe the existence of hysteresis is a serious test for any traffic flow model. In this chapter we have investigated several variants of the NaSch model and showed numerically the existence of meta-stable states in a density region close to the maximum flow.

The hysteresis in the fundamental diagram is related to the existence of meta-stable states. The latter are a consequence of phase separation in a certain density regime. The reason for this phase separation, on the other hand, is a reduced outflow from jams which destabilizes clusters forming in the outflow region. Such a reduction can be incorporated most easily by introducing slow-to-start rules which try to model the restart behavior of standing vehicles more realistically. The three models presented here used different s2s rules which can be classified as spatial, temporal and velocity-dependent, respectively. For maximum velocity $v_{max} > 1$ the models exhibit a similar behavior (see below). For $v_{max} = 1$ the spatial s2s rule of the $T^2$ model is exceptional since it leads to the existence of a phase transition to a completely jammed state in the limit $p_t \to 1$.

The NaSch model with velocity-dependent randomization shows the coexistence of phase-separated and homogeneous states in a density interval near the density $\rho_2$ of maximum flow. Near $\rho_2$ interactions be-

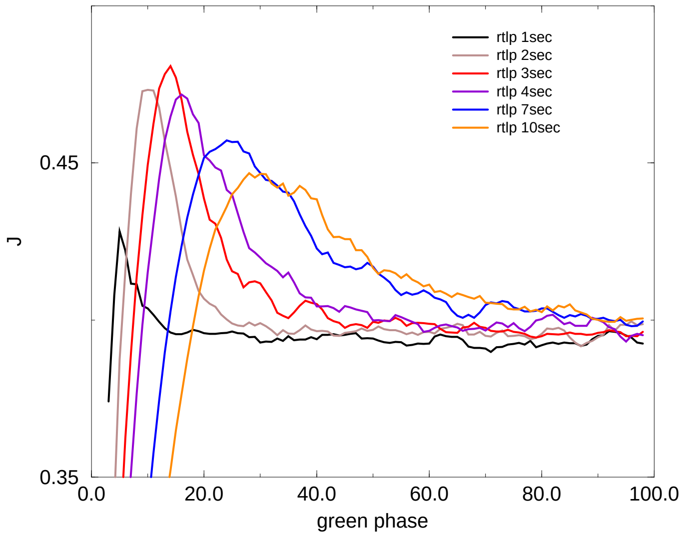


Figure 7.15: Average flow for different combinations of the red-/green-signal periods. The length of the system was given by $L = 1000$ and the maximum velocity by $v_{max} = 5$. Inside the tunnel $p^t = 0.15, p_0^t = 0.60$ and outside $p = 0.01, p_0 = 0.20$ has been used.

tween cars become important and one can find spontaneous formation of jams. Therefore the reduction of the density in the outflow regime of a jam leads to stable phase separated states. The reduction of interactions between cars in the free-flow regime can be confirmed by a phenomenological approach, which gives very accurate results. In contrast to the cruise-control limit of the NaSch model [74], where also metastable states can be found, fluctuations are present in both coexisting states.

The results presented here have interesting applications. In real traffic one is usually interested in stabilizing the homogeneous branch of the fundamental diagram in order to maximize the throughput. This can be done using signals to control the inflow, as in the case of the Lincoln tunnel in New York [91].

In [92] a family of space-continuous models has been investigated. Depending on the values of the maximum acceleration and deceleration three classes can be distinguished. Class III shows no realistic behavior since no spontaneous jams are formed. A continuous analogue of the NaSch model belongs to class II (high deceleration limit). Here one finds spontaneous formation of jams, but no meta-stable states. Finally, in class I spontaneous jamming as well as meta-stable states are found. On a macroscopic level, models in classes I and II can be distinguished by the ordering of the densities $\rho_f$, the density of the outflow from a jam, and $\rho_c$, the density where the homogeneous flow becomes unstable[2]. The discrete models discussed here have very simple braking rules, but nevertheless exhibit the behavior of class I. The existence of meta-stable states is therefore not related to the use of continuous space coordinates or "realistic" braking rules [90, 93] (e.g. anticipation of the behavior of the driver ahead).

Already the NaSch model has a tendency towards the formation of meta-stable states. The outflow from a mega-jam is maximal only in the deterministic case $p = 0$ and in the so-called cruise-control limit [74]. In the generic case $p > 0$ the outflow is not maximal [94], but organizes itself towards the 'critical' current $J_c$ where the correlation length becomes maximal [78]. Since the difference between $J_{max}$ and $J_c$ is rather small, it is very difficult to observe meta-stable states in the NaSch model.

The considerations in this chapter show the flexibility of the CA approach to traffic flow problems. A rather simple and natural extension of the rules of the NaSch model allows us to describe the formation of meta-stable states in the fundamental diagram. The introduction of a velocity-dependent randomization $p(v)$ makes it possible to control the properties of the free-flow and congested flow independently. Experimentally it has been found [12] that for real traffic the reduction of the outflow $J_{out}$ compared to the maximum flow $J_{max}$ is approximately $J_{max}/J_{out} \approx 1.5$. This value can be used to determine a realistic value

[2] Often it is not easy to define these quantities properly, especially in the presence of noise.

of $p_0 - p$.

If one is willing to give up an overly realistic description of the interactions between the vehicles one can obtain rather simple CA models capable of describing even the fine-structure of traffic flow in a satisfactory way.

# Chapter 8

# Two-Lane Traffic

The aim of this chapter is to study the effects of different kind of particles in multi-lane systems. For pedagogical reasons the results for single-lane systems with different types of particles are presented first. In the following the necessary extensions of the NaSch model for multi-lane systems will be presented and a short review of the results for one kind of particles will be given.

The main part of this chapter deals with multi-lane systems where different kind of particles, i.e. cars with different maximum velocities, are included. It turns out that in particular for the NaSch model with the standard choice of lane-changing rules at least qualitatively the results of the one-lane systems are recovered. Therefore several variants of the basic model are discussed and also variants of the basic lane-changing rules are taken into account.

## 8.1 Particle-Disorder in Single-Lane Systems

The effect of particle disorder for the NaSch model and in particular for the TASEP was studied in several investigations. In this section the basic phenomenon will be shortly discussed.

The influence of slow particles in one-lane systems was first studied by Krug and Ferrari for the TASEP [95] with random-sequential dynamics. It is illustrative to study a system with one slow car, i.e. one car with a reduced hopping rate first. At low densities the slow car determines the behavior of the system, because the faster cars cannot overtake the slow car. Therefore at low densities all cars move with the free-flow velocity of the slow particle. Increasing the density of the system the length of the jam behind the slow car increases. If the length of the jam is of the order of the system size also the slow car cannot move with its free-flow velocity. Therefore at high densities a homogeneous microscopic state is obtained.

For this setup and also for distributions of hopping rates exact analytical results exist. An analytical solution can be obtained if the process is described in terms of distance variables. Then the stationary distribution is given as a product measure [95]. It turns out that dependent on the asymptotic of the distribution of hopping rates near $c = \min(p_i)$, where $p_i$ denotes the hopping rate of a particle $i$, different kind of phase transitions occur. More explicitly if the hopping rates are drawn from the distribution

$$f(p) = \frac{n+1}{(1-c)^{n+1}}(p-c)^n \tag{8.1}$$

phase separated states can be observed below the critical density

$$\rho^* = \frac{n(1-c)}{n+c}. \tag{8.2}$$

Now the order of the phase transition depends on the exponent $n$ of the distribution of hopping rates. For $n > 1$ a first order phase transition occurs at $\rho^*$ in the sense that $\frac{\mathrm{d}v}{\mathrm{d}\rho}$ has a finite limit as $\rho \to \rho^*$ from above, while for $0 < n \leq 1$ the first derivative of the average velocity vanishes in that limit. For $n \leq 0$ no phase transition occurs [95].

These results have been generalized for the TASEP with parallel update [96] as well as for the NaSch model [97]. In both cases the same universal behavior as for TASEP with random-sequential dynamics was found.

## 8.2 Basic Models for Two-Lane Traffic

A realistic description of traffic networks obviously demands for the generalization of the single-lane CA models to multi-lane traffic. Following the same strategy as for single lane traffic this has to be done with a simple set of rules which govern the lane changing rules [98]. Then the update step is divided into two sub-steps: In the first sub-step the lanes are update independently according to the rules of the NaSch model. In the second sub-step cars may change lanes in parallel if the following criteria are satisfied:

- Incentive criterion:
  1. $v_{hope} > gap$, where $v_{hope} = \min(v + 1, v_{max})$.
- Safety criteria:
  2. $gap_{other} > gap$.
  3. $gap_{back} \geq v_{max}$.

Here $gap$, $gap_{other}$, $gap_{back}$ denote the number of free cells between the car and its predecessor on the actual lane and its two neighbor cars on the desired lane, respectively.

The lane-changing rules can be symmetric or asymmetric with respect to the lanes and to the cars. Recently, asymmetric rule sets have been proposed for the description of highway traffic on the German "Autobahn" where overtaking on the right lane is forbidden. These rule sets are able to reproduce the lane-usage inversion[1] observed experimentally in excellent agreement with measurements [98–104].

As mentioned above it is necessary to choose an appropriate lane-changing rule set depending on the experimental situation. First symmetric lane-changing rules are considered which are relevant for traffic in towns and on highways where overtaking on both lanes is allowed.

Fig. 8.1 shows the fundamental diagram of a periodic two-lane system and the density dependence of the lane-changing frequency. The simulations reproduce well known results, e.g. an increase of the maximum flow per lane compared to the flow of a single-lane road. In addition, one finds surprising new results like a local minimum of the lane-changing frequency near the density of maximum flow for small braking probabilities $p$. Obviously jams can be partially avoided by changing the lanes and therefore the capacity of the system is slightly increased.

[1]Above a certain density most of the cars are on the left lane.

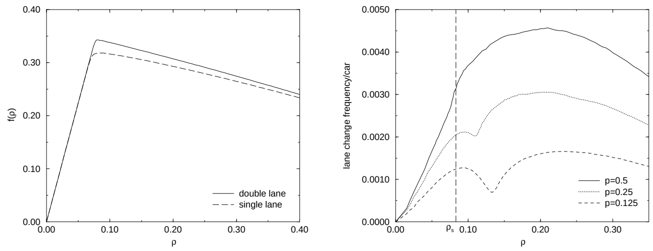


Figure 8.1: Left: Flow per lane of the single lane model compared with the two lane model for systems with $v_{max} = 5$ and $p = 0.5$. Right: Lane change frequency in the two lane model for different braking parameters $p$.

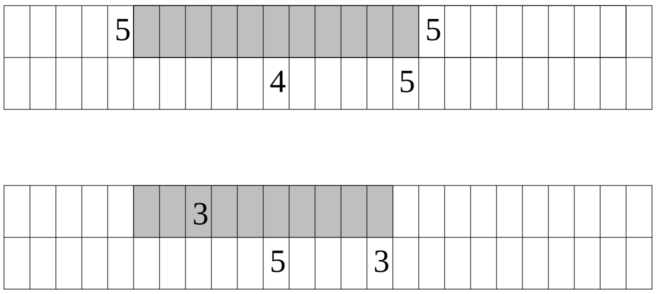


Figure 8.2: Top: Necessary safety gap for a lane change in the free flow regime. Bottom: Possible positions of slow cars which lead to a plug. The cars are driving from left to right.

The behavior of the lane-changing frequency can be explained if one takes into account the number of empty cells necessary for a lane-changing procedure. Two prerequisites have to be fulfilled in order to initiate a lane change. First the situation on the other lane must be more convenient and second the safety rules must be fulfilled. Therefore one needs typically $2v_{max} + 1$ empty cells on the destination lane for a lane-changing maneuver in the free flow regime (Fig. 8.2). Hence, one finds a

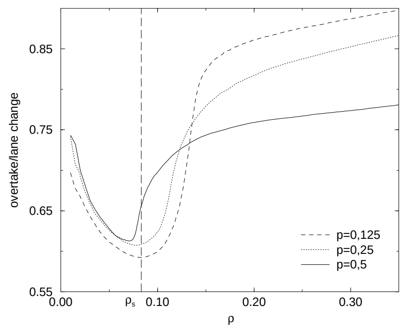


Figure 8.3: Fraction of lane changes which are overtake maneuvers for different braking parameters $p$.

local maximum of the lane-changing frequency near $\rho_s = \frac{1}{2}\frac{1}{v_{max}+1}$ if the cars are ordered homogeneously, which typically happens for small values of $p$. For larger values of the braking noise (i.e. $p = 0.5$) no local maximum is observable. Increasing the density for sufficiently small values of $p$, one finds a pronounced minimum of the lane changing frequency. This can be understood in the limit $p \to 0$ where, for $\rho = \frac{1}{v_{max}+1}$, the cars are perfectly ordered with a gap of $v_{max}$ sites between consecutive vehicles. Obviously in this case both the incentive and the safety criteria are never fulfilled and the lanes are completely decoupled. For small noise the ordering mechanism is still present and therefore the number of lane changes is drastically reduced near $\rho = \frac{1}{v_{max}+1}$. For large values of $p$ this kind of ordering is suppressed since fluctuations of the distance between consecutive cars become larger. Therefore large gaps become more likely than in the deterministic limit and lane changes become possible again. A further increase of the average density reduces the probability to find a gap on the other lane which is large enough for a lane change. Obviously the global maximum is reached at much higher values of $\rho$, because the incentive criterion is fulfilled for more and more cars at higher densities, and at intermediate densities large gaps are still present because the microscopic states are inhomogeneous.

This intuitive picture can be confirmed by measuring the number of "successful" lane changes where a car actually overtakes its former predecessor (Fig. 8.3) in the next time-step. Overtaking means that following and leading car have changed their role. Again a local minimum near $\rho_s$ is found. For densities $\rho > \rho_s$ the efficiency of lane changes increases monotonously which implies that the cars can improve their average velocity due to changing the lane.

## 8.3 Particle Disorder in Two-Lane Traffic

After this short review of the results for homogeneous systems, now different types of cars are considered which is obviously more relevant for practical purposes. As a first step towards realistic distributions of free flow velocities two types of cars are chosen, e.g. slow cars ('trucks') with $v_{max}^{slow} = 3$ and fast cars with $v_{max}^{fast} = 5$, analogous to Ref. [99]. The simulations have been carried out with 5% of slow cars, which are initially positioned randomly. The fast as well as the slow cars may use both lanes, e.g. both cars are treated equally with respect to the lane-changing behavior.

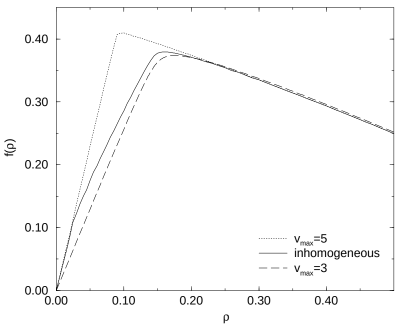


Figure 8.4: Comparison of the flow per lane of the inhomogeneous model with the corresponding homogeneous models for $p = 0.4$.

In Fig. 8.4 the effects of the slow cars on the average flow of the two-lane system is compared with the fundamental diagram of a single lane road with one slow car. Since passing is not allowed for a single-lane system, clearly the slow car dominates the average flow at low densities and platoon formation is observable [95–97]. Surprisingly the two-lane system shows a quite similar behavior, although passing is allowed and the fraction of slow cars is rather small, which is consistent with the results of Ref. [99].

In [100] it was shown that two trucks driving side by side can form a "plug" and blockade the following traffic. Similar observations have been made in [99, 105]. For constituting such a plug it is not necessary that both cars are driving side by side. A fast car with velocity $v = v_{max}^{slow}$ driving behind a slow car needs $v_{max}^{slow} + 1$ empty cells in the driving direction and $v_{max}^{fast}$ empty cells as safety gap on the other lane for a successful lane change. Therefore two trucks are able to form a plug even with a gap of 9 cells between them (Fig. 8.2).

These plugs lead to platoon formation analogous to a single-lane system. Obviously the average velocity of such platoons is limited by the free flow velocity of the slow cars. Therefore, if the plugs have long lifetimes, the total flow can not exceed the capacity of a homogeneous system of slow cars.

In fact, plug configurations are quite stable because the slow cars generically will have a large gap in front such that the incentive criterion hardly ever will be fulfilled. Therefore the leading vehicle of a platoon rarely changes the lane. Moreover both leading cars of the plug drive with the same average velocity and therefore larger distances between the slow cars only occur due to velocity fluctuations. This means that plugs have strong influence on the stationary state.

In many respects the situation is analogous to single-lane traffic. This can be exemplified by looking at the density profiles of both lanes relative to a slow car on one of the lanes. Obviously the flow is dominated by plugs. Along with several small jams one big jam parallel on both lanes occurs, comparable to the density profile of a single-lane road (Fig. 8.5). Note, however, that in contrast to one-lane systems [95] the variance of the distance distribution does not diverge.

For densities $\rho > \rho_{max}$, where $\rho_{max}$ is the density where the flow becomes maximal, also the slow cars will not always find a sufficient large gap in front. Therefore the average flow is limited by the number of empty cells but not by the low maximum velocity of the slow cars and the flow of the homogeneous system is recovered at high densities.

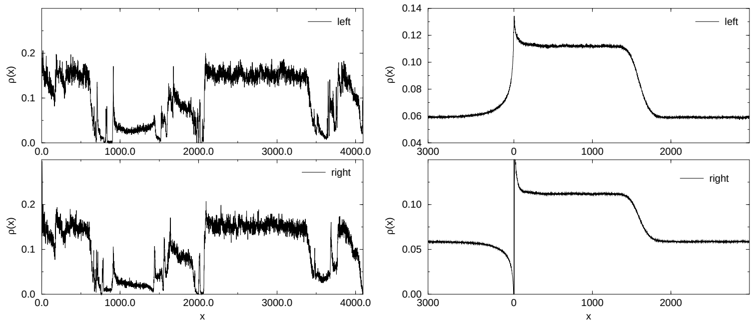


Figure 8.5: Left: Density profile relative to a slow car on one lane in the inhomogeneous model (with 5% slow cars) at $\rho = 0.1$ and $p = 0.4$. Right: Density profile of both lanes in a system with just one slow car relative to the slow car for $\rho = 0.08$ and $p = 0.125$. The system size in both cases is $L = 4096$.

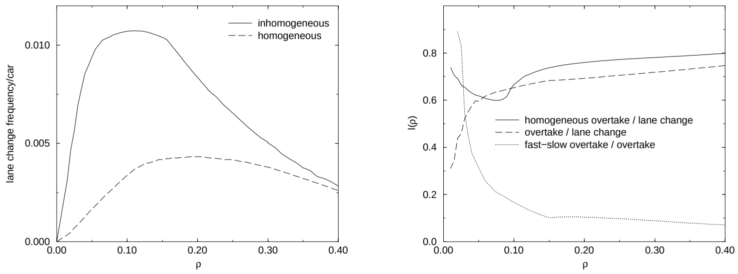


Figure 8.6: Left: Lane-changing frequency of the inhomogeneous model compared to the corresponding homogeneous model for $p = 0.4$. Right: Fraction $l(\rho)$ of lane changes which are overtaking maneuvers in the homogeneous (full line) and inhomogeneous system (broken) line. The dotted line shows the fraction of overtaking maneuvers where a slow car is passed by a fast car. $p = 0.4$ in all cases.

Fig. 8.6 shows a comparison of the lane-changing frequency and the fraction of successful overtaking maneuvers for the homogeneous and the inhomogeneous models. For small densities the lane-changing frequency in the inhomogeneous model is increased drastically. For very small densities most of the overtaking maneuvers are those where fast cars pass a slow car. This corresponds to the regime where the trucks do not have a significant effect on the flow. With increasing density the fraction of fast-slow overtaking maneuvers decreases although the fraction of successful overtaking maneuvers increases.

As a next step the effect of a *single* slow car on the behavior of the system is studied. This slow car with $v_{max}^{slow} = 3$ always moves on the same (right) lane, i.e. it is not allowed to change the lane. In contrast to the former example, one would expect that this slow car disturbs the system only locally and therefore should not have any effects on e.g. the fundamental diagram.

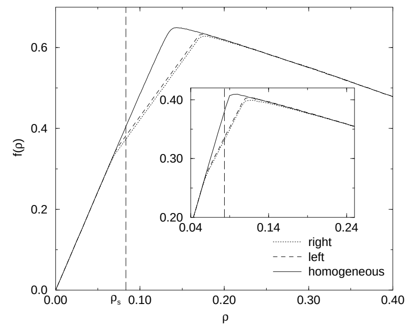


Figure 8.7: Comparison of the flow per lane of a two-lane system with one slow car with the homogeneous system, $p = 0.125$. The inset shows the same situation for $p = 0.4$.

Simulations show, however, that above a certain density $\rho_T$ already one slow car is sufficient to dominate the flow on both lanes (Fig. 8.7). The transition density $\rho_T$ depends on the maximum velocity of the fast cars and the braking parameter $p$. While $\rho < \rho_T$ the fast cars change to the left lane in order to avoid being trapped behind the slow car. With increasing density the probability for a lane change decreases and a jam behind the truck forms. This jam causes a jam on the left lane (Fig. 8.6). More and more cars change to the left and form a region of high density parallel to the jam. This region is disturbed if a jammed fast car can change to the left. The local defect, the slow car, causes a “parallel” jam on the left lane. Together with the truck this parallel jam behaves like

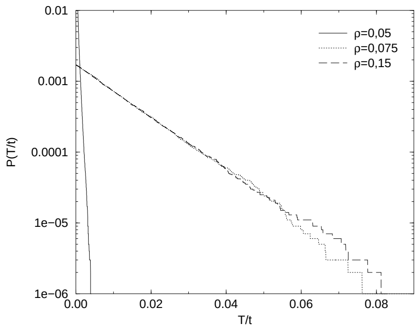


Figure 8.8: Waiting time $T$ distribution for $p = 0.125$. $t$ denotes the measure time.

a plug. Therefore the flow on both lanes is dominated by this plug for $\rho > \rho_T$, the slow car “synchronizes” the flow on both lanes. The effect of vehicles trapped behind the slow car can be illustrated by measurements of the waiting time distribution of the first fast car behind the slow one until it can change the lane (Fig. 8.8). Close to $\rho_T$ the waiting time $T$ increases strongly. Our simulations did not allow to determine the nature of this transition very accurately. However, some understanding can be gained from the limit $p \to 0$, where the two lanes decouple (see Sec. 8.2). Here for $\rho < \rho_T$ there are no fast cars on the right lane. For $\rho > \rho_T$ the waiting time for the blocked fast cars on the right lane becomes infinite. For $p > 0$, on the other hand, lane changes are possible. The probability to find a gap large enough to allow a lane-changing maneuver for a given density depends only on $p$. From our simulations it was not possible to determine whether the transition is continuous or not.

The choice of a low braking parameter $p$, on the one hand, leads to a decrease of the lane change probability and therefore to an influence even on the homogeneous system. On the other hand, with increasing $p$ interactions between the cars increase. A slow car can easily cause a jam and form a "plug". Hence, the system is dominated by one slow car above a certain density $\rho_T$ for a wide range of braking parameters $p$. With decreasing $p$ one observes $\rho_T \to \rho_s \approx \frac{1}{2}\frac{1}{v_{max}+1}$.

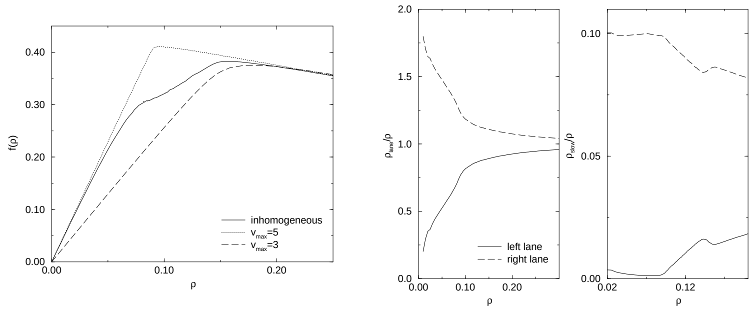


Figure 8.9: Left: Average flow of different asymmetric models with $p = 0.4$. Right: Relative densities of the lanes and slow cars for a inhomogeneous model with 5% slow cars.

In order to weaken the influence of the slow cars one can introduce asymmetric lane-changing rules. This can be done by neglecting the first rule of the symmetric rule set of Rickert et al. [98] for the change from the left to the right lane. Now the left lane is designated as the passing lane and cars are trying to change back to the right lane as soon as possible. In Fig. 8.9 the average flow of asymmetric models with $v_{max} = 5$, $v_{max} = 3$ and $v_{max}^{fast} = 5$ with 5% slow cars ($v_{max}^{slow} = 3$) is compared. For very low densities, fast cars can pass slow cars more effectively if asymmetric lane-changing rules are applied. Obviously, the flow can be increased for densities below $\rho_{max}$ although the strong influence of the slow cars is still apparent.

With asymmetric rules almost all cars drive on the right lane at low densities (Fig. 8.9). Hence, the system is divided into a "fast" and a "slow" lane. Therefore at low densities there is only a low probability for plug formation of two slow cars driving side by side. With increasing density this probability and the probability for plugs formed by a slow car and its parallel jam increases, such that platoon formation occurs and the system is dominated by slow cars. Note that the density on the fast lane is still reduced in that regime, in contrast to realistic systems, where lane inversion is observable. Therefore the increase of the system's performance is in some sense artificial.

The results presented up to now show that even very small densities of slow cars can dominate the behavior of the whole system. Since this appears to be somewhat unrealistic several modifications of the basic rule set will be investigated in the following where the influence of slow cars is reduced.

## 8.4 Modified Models

### 8.4.1 Sequential Update

The results of the previous section have shown that the safety criteria demand large gaps between consecutive cars on the destination lane for lane-changing maneuvers. This leads to plug formation and therefore a drastic flow reduction by slow cars already in the free flow regime. Much smaller gaps would be sufficient for a lane change, if the driver takes into account the behavior of the predecessor in the next time step. Such anticipation effects can be most easily considered in a discrete model if the update procedure is performed sequentially against the driving direction. This means that the driver has full information about the behavior of the predecessor in the next time step.

In order to estimate the adequacy of this approach the single-lane properties of the sequential variant of the NaSch model are briefly discussed. Using sequential update one obviously cannot ensure translational invariance. E.g. if one performs the update site by site in a fixed sequence one generates effectively a bottleneck situation analogous to a system with defect sites. Due to this shortcoming of a site oriented implementation of the update sequence the following update procedure has been chosen. The lattice update of one time step starts at a "NaSch-car", i.e. a car with $v = 0$ or $gap > v$. In the following the position of all cars are updated car by car against the driving direction[2].

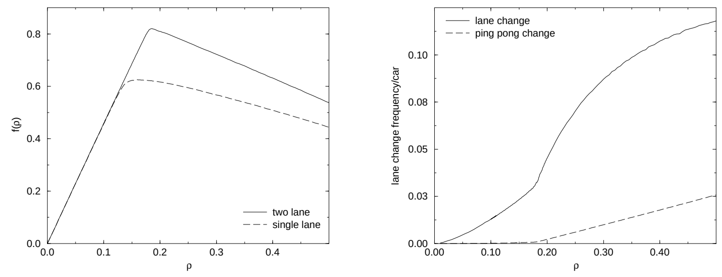


Figure 8.10: Left: Fundamental diagram of the single-lane model compared with the two-lane model for systems with $v_{max} = 5$ and $p = 0.4$. Right: lane-changing and ping-pong change frequency in the two-lane model.

Compared to the NaSch model with parallel updating one obtains generically higher values of the average flow, if the same values of $v_{max}$ and $p$ are considered. Another feature of the sequential variant is the strong $p$-dependence of $\rho_{max}$, e.g. in the limit $p \to 0$ the maximum value of the flow is reached for $\rho \approx 1$. Nevertheless for larger values of the braking noise one obtains quite realistic fundamental diagrams as shown in Fig. 8.10.

After this short description of the single-lane behavior results for the two-lane system in the presence of particle disorder are shown. Obviously the lane-changing rules can be modified because the anticipation of the drivers allows for less restrictive safety criteria. Therefore the following criteria for lane-changing have been introduced :

- Incentive criterion:

  1. $\Delta v > gap$, with $\Delta v = v_{hope} - v_{same}$

- Safety criteria:

  1. $gap_{other} \geq \Delta v$, with $\Delta v = v - v_{other}$

[2]Using a fixed sequence of cars changes the results only slightly.

2. $gap_{back} \geq \Delta v, \quad \text{with } \Delta v = v_{back} - v$

Here $v_{same}$ denotes the velocity of the preceding car on the same lane. $v_{other}$ and $v_{back}$ are the velocities of the neighboring cars on the destination lane. $gap$, $gap_{other}$ and $gap_{back}$ have the same meaning as in the definition given in Sec. 8.2.

These lane-changing rules have the same structure as for the parallel model. The first rule is the incentive criterion which corresponds to an unsatisfactory situation on the origin lane. The safety criteria are necessary for a safe lane-changing maneuver. Obviously the safety criteria differ drastically from those of the parallel case, e.g. if cars at the origin and destination lane move with the same velocity a lane change is possible also for $gap_{other} = 0$. These more aggressive lane-changing rules lead to a much more efficient gap usage in the two-lane system. Compared to the single-lane system one obtains an increase of the maximum flow of approximately 30%. Another effect of this modification is a strongly increased number of lane changes, in particular of the number of ping-pong lane changes (i.e. lane changes of the same car in two consecutive time steps). Therefore the fraction of overtakings is reduced. Moreover it is also possible to change the lane at high densities.

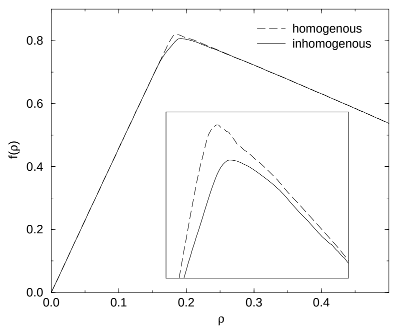


Figure 8.11: Flow per lane of the homogeneous and the inhomogeneous system with one slow car for the sequential model.

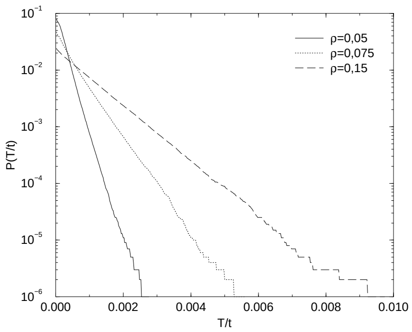


Figure 8.12: Waiting time distribution in the sequential model with one slow car.

In contrast to the parallel model the flow only slightly decreases in the presence of one slow car for densities near $\rho_{max}$ (Fig. 8.11), while for all other densities the flow of the homogeneous system is recovered. Also the waiting time distribution (Fig. 8.12) differs only slightly from the homogeneous system, because lane-changing maneuvers can be performed more effectively due to the less restrictive safety criteria.

Finally the case of 5% slow vehicles in the system has been investigated which was sufficient to dominate the system at low densities for the case of parallel update. In contrast to the model introduced by Rickert et al. [98] only small deviations from the homogeneous case can be observed (Fig. 8.13).

### 8.4.2 Anticipation models

Although the smoothing effect of the sequential update seems to be quite satisfactory other features of this approach are clearly unrealistic. Therefore a model variant with parallel update has been introduced, where anticipation effects are taken into account. Here smaller distances between consecutive fast cars are made possible by estimating the displacement of the predecessor in the next time step. The minimal movement of the predecessor is given by $\max(v_{next}, 0)$ where $v_{next}$ is given

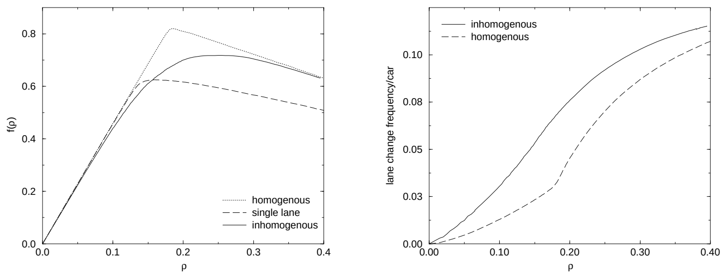


Figure 8.13: Left: Comparison of the flow per lane of two-lane systems with a single-lane system for the sequential update. Right: Comparison of the lane change frequency of the inhomogeneous two-lane system with the homogeneous system ($p = 0.4$).

by $v_{next} = \min(v_{pred}, gap_{pred}) - 1$ and $v_{pred}$, $gap_{pred}$ denote the velocity and the gap in front of the predecessor. This knowledge allows the introduction of an effective gap between the cars which is given by $gap_{eff} = gap + v_{next}$.

The anticipation leads to a slightly increased value of the maximum flow, but large parts of the fundamental diagram are left unchanged. In particular also for small values of the braking noise the fundamental diagram is still quite close to the original model.

This modified version of the NaSch model allows for a set of lane-changing rules analogous to the sequential case:

- Incentive criterion:
  1. $(v > v_{same}$ and $gap < v)$ or $(gap_{other} > gap)$
- Safety criteria:
  2. $(v_{other} > v)$ or $(gap_{other} > gap)$
  3. $v_{back} \leq gap_{back}$

All quantities have the same meaning as in the definitions given in previous sections. Now lane changes are possible at small distances, e.g.

only one empty site between the leading car on the other lane and the changing car is needed if both cars move with the same velocity. Again the minimal gap is determined by velocity differences rather than by the absolute value of the velocity. The simulation results show that such an

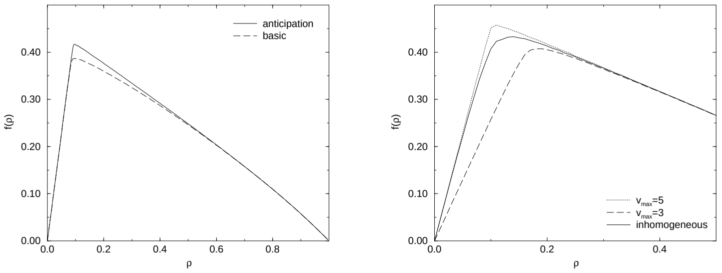


Figure 8.14: Left: Comparison of the single-lane "anticipation" and the basic model. Right: Average flow of "anticipation" two-lane models ($p = 0.4$).

implementation of anticipation effects is already sufficient to suppress the drastic influence of slow cars (Fig. 8.14). Also if 5% of slow cars are included, a reduction of the flow is observable only close to $\rho_{max}$. The increased robustness of the modified model shows that anticipation effects are essential for a realistic description of multi-lane traffic.

### 8.4.3 Other models

Several other model variants which interpolate between the sequential and the anticipation models have also been investigated. Special attention is paid on models where the lanes are updated sequentially, but the update within the lanes is parallel as in the NaSch model. This allows to incorporate lane-changing rules which are more aggressive than those of Rickert et al. [98].

In the simplest case the lane-sequential update is divided into four sub-steps: a) lane-changes from right to left, b) update of the right lane, c) lane-changes from left to right, d) update of the left lane. These steps can be carried out in different order, e.g. a-b-c-d, b-a-d-c, or a-b-d-c. The first two orderings have the disadvantage that ping-pong lane-changes without forward motion or double updates of cars are possible. The results of the simulations show, however, that there are only small differences of the fundamental diagram and the number of lane changes compared with the parallel update. Furthermore the system is still very sensitive to a small fraction of slow cars.

In all of these model variants cars move only 'side-wards' during the lane-changing sub-steps. If one allows cars also to move forward during lane-changes the situation is improved slightly. Although the cars still need the same safety distances for a lane-change, gaps can be used more efficiently.

Finally, *temporary* anticipation into the basic model of section 8.2 is introduced. Cars that changed the lane or the cars directly behind a vehicle that changed to the other lane are allowed to anticipate for the next $n$ time-steps. Therefore smaller safety distances are possible during lane changes. This reduces the effects of disorder. In comparison to the anticipation model of the previous subsection, the platoons forming behind slower cars are larger and dissolve slower. If the cars stop anticipating after $n$ time-steps they usually have a short distance to the preceding car and are likely to brake in the next update step due to the deceleration rule of the NaSch model, i.e. temporary anticipation artificially causes jams. In the limit $n \to \infty$ one recovers the fundamental diagrams of the anticipation model of the previous subsection. In general, in order for anticipation to be most effective, all cars have to anticipate.

## 8.5 Discussion

The simulation results have shown that even in two-lane systems, where fast cars can overtake slow cars, particle disorder may dominate the behavior at low densities. The strongest influence of slow cars has been observed for the NaSch model with symmetric lane-changing rules. For this model variant already one slow car leads to platoon formation on both lanes, i.e. the gap usage at low densities is not very effective. The platoon formation has obviously drastic influence on the performance of the system. If 5% slow cars are included the performance of the heterogeneous system is quite close to a homogeneous system of *slow* cars. For asymmetric lane-changing rules slow cars influence the systems performance less than in the symmetric case because the density on the "fast" (left) lane is reduced drastically an effective overtaking is possible. Therefore the flow reduction due to the slow cars has a larger magnitude only close to the maximum.

Although these results look quite realistic the distribution of cars on both lanes differs drastically from those of real traffic. Measurements on German highways show [106, 107] that already for densities below $\rho_{max}$ a higher density on the "fast" lane is observable (lane inversion).

Therefore one has to look for model variants which allow for lane changes where the application of less restrictive safety criteria is possible. An important feature of this kind of models probably is the anticipation of the behavior of the predecessor. By calculating the velocity of the leading car one can accept much smaller distances than in the NaSch model.

Anticipation is most effectively implemented with a (particle) sequential update against the driving direction. The simulation results show indeed a drastically reduced influence of slow cars, even for symmetric lane-changing rules. Analogous results can be found for a *parallel* model variant where the minimal movement of the predecessor in the next time step is taken into account in order to calculate an effective gap. Compared to the sequential model the single-lane results for this anticipation model are much more realistic and the robustness of the two-lane system against particle disorder is even larger than for the sequential variant.

The effects of a small fraction of fast cars in a system of slow vehicles also have been studied. The fundamental diagram is almost identical to that of a pure system of slow cars. The average velocity of the fast cars is larger than that of the slow cars only for small densities.

In conclusion, it has been shown that particle disorder can lead to platoon formation even in two-lane systems. Having in mind that also non-trivial lattice geometries may have strong effects on the macroscopic behavior of the system, a very careful interpretation of traffic data is necessary in order to distinguish between dynamical, multi-lane, and boundary effects.

## Chapter 9

# Summary

The aim of this work is the modeling of complex dynamical systems using one-dimensional stochastic lattice-models. In particular, discrete models for driven systems are investigated. We describe the characteristic phenomena of this models as well as their application to traffic flow.

The second chapter of this work reviews the most important empirical observations in traffic flow as well as the basic modeling concepts in that field. An approach which was introduced in 1992, and was widely used since then, is the CA model of Nagel and Schreckenberg [4]. This model and several variants are analyzed in detail in the following chapters.

From a theoretical point of view the NaSch model is a model far from equilibrium, i.e. even the stationary state of the model is not described by an equilibrium distribution. This implies that standard techniques of statistical mechanics cannot be applied here.

Recently several analytical methods were presented which allow to treat this kind of models. In chapter 3 a quantum formalism [46] is discussed which is of interest for two reasons. First, solutions of the master-equation can be obtained by mapping the stochastic process on an exactly solvable quantum system, and second, rewriting the stochastic problem using the quantum-formalism allows for the application of methods which were originally developed for quantum many-body systems. An example for the latter strategy is the generalization of the so-called matrix-product ansatz (MPA) for stochastic systems. The application of the MPA leads to the exact solution of the totally asymmetric exclusion process (TASEP) with open boundary conditions and different types of update schemes. In the context of this work the TASEP may be viewed as a simplified model for traffic flow, e.g. if a parallel update is used it is identical to the NaSch model with $v_{max} = 1$. Beyond that approximative methods are discussed.

The introductory part of this work is followed by an investigation of the phase transition in the NaSch model which is presented in chapter 4. The NaSch model for traffic flow exhibits a jamming transition from a free-flow phase to a congested phase. In the deterministic case $p \to 0$ this transition corresponds to a critical point with diverging correlation length. In the presence of noise, however, numerical simulations indicate the absence of critical behavior. The order parameter, which identifies a sharp transition density for $p = 0$, continuously increases and the relevant length scales are finite for all densities in the presence of noise. The transition of the deterministic case is smeared out and one only observes the remnants of the critical point.

In chapters 5 and 6 the stationary behavior of the TASEP on inhomogeneous lattices are discussed. First, we studied the effect of quenched impurities or defects in a periodic system. The defects are sites where the mobility of the particles is reduced. It turns out that three different phases can be distinguished with respect to the flow. At high and low densities the flow of the homogeneous system is recovered, but at intermediate densities the flow takes a constant value. The behavior of the system at intermediate densities is due to phase-separation effects, i.e. a macroscopic high and low density region exist. In contrast, at high and low densities only local inhomogeneities of the density profile occur. A good estimate for the fundamental diagram as well as for the density profile can be obtained from a phenomenological approach. This basic scenario was generalized for extended defects as well as for larger maximum velocities of the particles. Considering extended defects the same structure of the fundamental diagram was found as long as the length of the defect was small compared to the system size. Then the fundamental diagrams of the extended and the single defects differ only by the plateau value of the flow which converges for larger defects to the maximal flow of a homogeneous system with the hopping probability of the defect sites. For larger values of $v_{max}$ a density regime with constant flow is found, too. Qualitative differences exist only for the density profiles. In the low density regime as well as in the phase-separated regime oscillations of density profile are caused by the long ranged correlations of the NaSch model for $v_{max} > 1$.

In the following chapter the TASEP and the NaSch model with open boundary conditions are investigated. One observes so-called boundary induced phase transition which is a characteristic effect of driven lattice gases. In the first part of this chapter the exact results for the stationary states of the TASEP were used to discuss the phase-diagram. In particular the form of the density profiles and the parameter dependence of the flow have been analyzed. A phenomenological approach, which was suggested by Kolomeisky et al. [88], is introduced. It can be shown by comparison with the exact results that this approach gives a correct description of the phase diagram as well as for the length scales which govern the behavior of the density profiles. In the last part of the chapter the predictions of this approach were compared with simulation results for the NaSch model with open boundary conditions. It turns out that also for this case the structure of the phase diagram is well described. Therefore, the common structure of the phase diagram can be explained.

After the analysis of the fundamental properties of these models, more realistic applications for traffic flow are discussed in chapter 7 and 8. Measurements on real traffic have revealed the existence of meta-stable states with very high flow. Such states have not been observed in the NaSch model. Here a simple generalization of the NaSch model is proposed where a velocity-dependent randomization has been introduced. Several choices of the velocity-dependent randomization are possible. However, we concentrate on a a special case which belongs to the so-called slow-to-start rules. It is shown that this model exhibits meta-stable states, thus shedding some light on the prerequisites for the occurrence of hysteresis effects in the flow-density relation.

For single-lane traffic models it is well known that particle disorder leads to platoon formation at low densities. Here we discuss the effect of slow cars in two-lane systems. Surprisingly, even a small number of slow cars can initiate the formation of platoons at low densities. The robustness of this phenomenon is investigated for different variants of the lane-changing rules as well as for different variants on the single-lane dynamics. It is shown that anticipation of drivers reduces the influence of slow cars drastically.

The investigation of one-dimensional CA models for traffic flow has shown that this models are of interest for two reasons. On one hand they show characteristic non-equilibrium effects, e.g. boundary induced phase transitions, on the other hand it has been shown, that these models give a realistic description of traffic flow phenomena.

# Bibliography


[1] S. Wolfram, *Theory and Application of Cellular Automata*, World Scientific, Singapore (1986)

[2] G. Weisbuch, Complex systems dynamics, Addison-Wesley, Redwood City (1990)

[3] M. Cremer and J. Ludwig, Mathematics and Computers in Simulation **28**, 297 (1986)

[4] K. Nagel and M. Schreckenberg, J. Physique I **2**, 2221 (1992)

[5] B.D. Greenshields, Proc. Highw. Res. **14**, 448 (1935)

[6] H. Greenberg, Op. Res. **7**, 79 (1959)

[7] M. Koshi, M. Iwasaki, and I. Okuhra, in: V.F. Hurdle, E. Hauer, and G.N. Steward (eds), *Proccedings of the 8th International Symposium on Transportation and Traffic Theory*, University of Toronto Press, Toronto Ontario (1983); p. 403

[8] F.L. Hall, B.L. Allen, and M.A. Gunter, Transp. Res. A **20**, 197 (1986)

[9] D.E. Wolf, M. Schreckenberg, and A. Bachem (eds), *Traffic and Granular Flow*, World Scientific, Singapore (1996)

[10] M. Schreckenberg and D.E. Wolf (eds), *Traffic and Granular Flow '97*, Springer, Singapore (1998)

[11] B.S. Kerner, in [10], p. 239

[12] B.S. Kerner and H. Rehborn, Phys. Rev. Lett. **79**, 4030 (1998)

[13] H.Y. Lee, H.W. Lee, and D.Kim, Phys. Rev. Lett. **81**, 1130 (1998)

[14] D. Helbing and M. Treiber, Phys. Rev. Lett. **81**, 3042 (1998)

[15] B.S. Kerner, Phys. Rev. Lett. **81**, 3797 (1998)

[16] J. Treiterer: Ohio State Technical Report No. PB 246 094, (1975)

[17] B.S. Kerner, S.L. Klenov, and P. Konhäuser, Phys. Rev. E **56**, 4200 (1997)

[18] M.J. Lighthill and G.B. Withham, Proc. Roy. Soc. A **229**, 317 (1955)

[19] P.I. Richards, Op. Res. **4**, 42 (1956)

[20] H.J. Payne, in: G.A. Bekey (eds) *Mathematical Models of Public Systems (Vol. 1)*, Simulation Council, La Jolla (1971); p. 51

[21] W.F. Phillips, Transportation Planning and Technology **5**, 131 (1979)

[22] R.D. Kühne, Physik in unserer Zeit **15**, 84 (1984)

[23] H. Hilliges and W. Weidlich, Transp. Res. **B29**, 407 (1995)

[24] D. Helbing, *Verkehrsdynamik*, Springer, Berlin (1998)

[25] I. Prigogine and F.C. Andrews, Op. Res. **8**, 789 (1960)

[26] A. Reuschel, Österreichisches Ingenieur-Archiv **4**, 193 (1950)

[27] A. Reuschel, Z. d. Österr. Ing. und Arch. Vereines, **95**, 59 (1950)

[28] L.A. Pipes, J. Appl. Phys. **24**, 274 (1953)

[29] R.E. Chandler, R. Herman, and E.W. Montroll, Op. Res. **6**, 165 (1958)

[30] D.C. Gazis, R. Herman, and R.W. Rothery, Op. Res. **9**, 545 (1961)

[31] P.G. Gipps, Transp. Res. **15B**, 105 (1981)

[32] M. Bando, K. Hasebe, A. Nakayama, A. Shibata, and Y. Sugiyama, Jap. J. Indust. Appl. Math. **11**, 203 (1994)

[33] M. Bando, K. Hasebe, A. Nakayama, A. Shibata, and Y. Sugiyama, Phys. Rev. E **51**, 1035 (1995)

[34] M. Rickert and K. Nagel, Int. J. Mod. Phys. C **8**, 483 (1997)

[35] J. Esser and M. Schreckenberg, Int. J. Mod. Phys. C **8**, 1025 (1997)

[36] L. Santen, J. Esser, L. Neubert, J. Wahle, A. Schadschneider, and M. Schreckenberg, in: J. D. Griffiths (Ed.),*Proceedings of the Third International Conference on Mathematics in Transport Planning and Control*, Pergamon, Amsterdam (1998); p. 301

[37] M. Takayasu and H. Takayasu, Fractals **1**, 860 (1993)

[38] S.C. Benjamin, N.F. Johnson, and P.M. Hui, J. Phys. A **29**, 3119 (1996)

[39] R. Barlovic, L. Santen, A. Schadschneider and M. Schreckenberg, in: [10]; p. 335

[40] R. Barlovic, L. Santen, A. Schadschneider, and M. Schreckenberg, Eur. Phys. J. B **5**, 793 (1998)

[41] W. Knospe, L. Santen, A. Schadschneider, and M. Schreckenberg, Physica A **265**, 614 (1999)

[42] M. Schreckenberg, A. Schadschneider, K. Nagel and N. Ito, Phys. Rev. E **51**, 2939 (1995)

[43] B. Derrida, M.R. Evans, V. Hakim, and V. Pasquier, J. Phys. A **26**, 1493 (1993)

[44] B. Chopard and M. Droz, *Cellular Automata Modeling of Physical Systems*, Cambridge University Press, Cambridge (1998)

[45] V. Privman (ed), *Nonequilibrium Statistical Mechanics in One Dimension*, Cambridge University Press, Cambridge (1997)

[46] G. M. Schütz, Berichte des Forschungszentrums Jülich **3555**, Jülich (1998)

[47] H. Bethe, Z. Phys. **71**, 205 (1931)

[48] L.H. Gwa and H. Spohn, Phys. Rev. Lett. **68**, 725 (1992)

[49] G.M. Schütz, J. Stat. Phys. **88**, 427 (1997)

[50] A. Klümper, A. Schadschneider, and J. Zittartz, J. Phys. A **24**, L955 (1991)

[51] A. Klümper, A. Schadschneider, and J. Zittartz, Z. Phys. B **87**, 281 (1992)

[52] A. Klümper, A. Schadschneider, and J. Zittartz, Europhys. Lett. **24**, 293 (1993)

[53] H. Spohn, *Large Scale Dynamics of Interacting Particles*, Springer, Berlin (1991)

[54] J. Krug, Phys. Rev. Lett. **67**, 1882 (1991)

[55] B. Derrida, E. Domany, and D. Mukamel, J. Stat. Phys. **69**, 667 (1992)

[56] G. Schütz and E. Domany, J. Stat. Phys. **72**, 277 (1993)

[57] N. Rajewsky, A. Schadschneider, and M. Schreckenberg, J. Phys. A **29**, L305 (1996)

[58] N. Rajewsky, L. Santen, A. Schadschneider, and M. Schreckenberg, J. Stat. Phys. **92**, 151 (1998)

[59] A. Honecker and I. Peschel, J. Stat. Phys. **88**, 319 (1997)

[60] M. Evans, N. Rajewsky, and E.R. Speer, J. Stat. Phys. **95**, 45 (1999)

[61] J. de Gier and B. Nienhuis, Phys. Rev. E **59**, 4899 (1999)

[62] S.F. Edwards, Proc. Roy. Soc. **92**, 9 (1967)

[63] H. Hinrichsen, S. Sandow and I. Peschel, J. Phys. A **29**, 2643 (1996)

[64] K. Krebs and S. Sandow, J. Phys. A **30**, 3165 (1997)

[65] K. Klauck and A. Schadschneider, Physica A (in press)

[66] N. Rajewsky and M. Schreckenberg, Physica A **245**, 139 (1997)

[67] A. Schadschneider, in [10], p. 417–431

[68] A. Schadschneider and M. Schreckenberg, J. Phys. A **31**, L225 (1998)

[69] A. Schadschneider and M. Schreckenberg, J. Phys. A **26**, L679 (1993)

[70] A. Schadschneider and M. Schreckenberg, J. Phys. A **30**, L69 (1997)

[71] A. Schadschneider, Eur. Phys. J. B (in press)

[72] K. Nagel, Int. J. Mod. Phys. C **5**, 567 (1994)

[73] L.C.Q. Vilar and A.M.C. de Souza, Physica A **211**, 84 (1994)

[74] K. Nagel and M. Paczuski, Phys. Rev. E **51**, 2909 (1995)

[75] G. Csányi and J. Kertész, J. Phys. A **28**, L427 (1995), Erratum: J. Phys. A **29**, 471 (1996)

[76] M. Sasvári and J. Kertész, Phys. Rev. E **56**, 4104 (1997)

[77] S. Lübeck, M. Schreckenberg, and K. D. Usadel, Phys. Rev. E **57**, 1171 (1998)

[78] B. Eisenblätter, L. Santen, A. Schadschneider, and M. Schreckenberg, Phys. Rev. E **57**, 1309 (1998)

[79] K. Nagel, Dissertation Thesis, Universität zu Köln (1995)

[80] M. N. Barber, in: C. Domb and J. L. Lebowitz (eds) *Phase Transitions and Critical Phenomena*, Vol. 8, Academic Press, London (1983); p. 145

[81] S.A. Janowsky and J.L. Lebowitz J.L., Phys. Rev. A **45**, 618 (1992)

[82] S.A. Janowsky and J.L. Lebowitz, J. Stat. Phys. **77**, 35 (1994)

[83] H. Hinrichsen and S. Sandow, J. Phys. A **30**, 2745 (1997)

[84] S. Yukawa, M. Kikuchi and S. Tadaki, J. Phys. Soc. Jap. **63**, 3609 (1994)

[85] G. Tripathy and M. Barma, Phys. Rev. Lett. **78**, 3039 (1997)

[86] G. Tripathy and M. Barma, Phys. Rev. E **58**, 1911 (1998)

[87] Z. Csahok and T. Vicsek, J. Phys. A **27**, L591 (1994)

[88] A.B. Kolomeisky, G.M. Schütz, E.B. Kolomeisky and J.P. Straley, J. Phys. A **31**, 6911 (1998)

[89] A. Schadschneider and M. Schreckenberg, Ann. Physik **6**, 541 (1997)

[90] S. Krauß, P. Wagner and C. Gawron, Phys. Rev. E **55**, 5597 (1997)

[91] H. Greenberg, and A. Daou: Op. Res. **8**, 524 (1960)

[92] S. Krauss, in [10], p. 269

[93] S. Krauss, P. Wagner, and C. Gawron, Phys. Rev. E **54**, 3707 (1996)

[94] B. Eisenblätter: Diploma Thesis, Universität Duisburg (1996)

[95] J. Krug and J.A. Ferrari, J. Phys. A **29**, 465 (1996)

[96] M.R. Evans, J. Phys. A **30**, 5669 (1997)

[97] D.V. Ktitarev, D. Chowdhury, and D.E. Wolf, J. Phys. A **30**, L221 (1997)

[98] M. Rickert, K. Nagel, M. Schreckenberg, and A. Latour, Physica A **231**, 534 (1996)

[99] D. Chowdhury, D.E. Wolf, and M. Schreckenberg, Physica A **235**, 417 (1997)

[100] K. Nagel, D.E. Wolf, P. Wagner, and P. Simon, Phys. Rev. E **58**, 1425 (1998)

[101] P. Wagner, K. Nagel, and D.E. Wolf, Physica A **234**, 687 (1997)

[102] P. Wagner, in [9]

[103] T. Nagatani, J. Phys. A **29**, 6531 (1996)

[104] T. Nagatani, in [9]

[105] D. Helbing and B. Huberman, Nature 396, 738 (1998)

[106] W. Leutzbach and F. Busch, *Spurwechselvorgänge auf dreispurigen BAB–Richtungsfahrbahnen*, Institut für Verkehrswesen, Universität Karlsruhe (1984).

[107] U. Sparmann, *Spurwechselvorgänge auf zweispurigen BAB–Richtungsfahrbahnen*, Forschung Straßenbau und Straßenverkehrstechnik, Heft 263 (1978).

# Kapitel 10

# Deutsche Zusammenfassung

Diese Arbeit beschäftigt sich mit der Modellierung komplexer dynamischer Systeme mit Hilfe von eindimensionalen Gittermodellen. Insbesondere werden diskrete Modelle für sogenannte getriebene Systeme, d.h. Systeme, bei denen im stationären Zustand ein endlicher Strom vorliegt, behandelt. Für solche Modelle ist auch der stationäre Zustand kein Gleichgewichtszustand. Neben den grundlegenden Eigenschaften wird insbesondere auch die Anwendung dieser Modelle auf die Beschreibung von Verkehrsfluß diskutiert.

Das zweite Kapitel dieser Arbeit faßt die wichtigsten experimentellen Befunde zusammen, die bei der Beobachtung von Straßenverkehr gemacht wurden. Weiterhin werden verschiedene Modellierungsansätze diskutiert, die zur theoretischen Beschreibung von Verkehrsfluß herangezogen wurden. Ein Modell, das 1992 eingeführt wurde und seitdem breite Anwendung gefunden hat, ist das Zellularautomatenmodell von Nagel und Schreckenberg [4] (NaSch Modell). Dieses Modell und diverse Varianten des Modells werden im folgenden ausführlich analysiert.

Aus theoretischer Sicht handelt es sich bei dem NaSch Modell für Verkehrsfluß um ein System fernab vom Gleichgewicht, d.h. ein Modell, das auch im stationären Zustand nicht durch eine Gleichgewichtsverteilung beschrieben wird. Dies bedeutet insbesondere, daß auch die Methoden der Statistischen Physik des Gleichgewichts nicht angewendet werden können.

In jüngerer Zeit sind daher neue Methoden entwickelt worden, die einen analytischen Zugang auch für Nichtgleichgewichtssysteme erlauben. In Kapitel 3 wird ein Quanten-Formalismus vorgestellt, der in zweierlei Hinsicht interessant ist. Zum einen erlaubt er die Lösung von Modellen durch Abbildung auf quantenmechanische Modelle, deren exakte Lösung bekannt ist und zum anderen können durch die Umformulierung des Problems Methoden angewendet werden, die zur Lösung quantenmechanischer Modelle entwickelt wurden. Ein Beispiel für letzteres Vorgehen ist die Verallgemeinerung des sogenannten Matrix-Produkt Ansatzes (MPA) für stochastische Systeme. Die Anwendung des MPA führte auf die exakte Beschreibung des stationären Zustandes des vollständig-asymmetrischen Exklusionsprozesses (TASEP) mit offenen Randbedingungen und verschiedene Arten des Updates. Der TASEP kann als vereinfachtes Modell für Straßenverkehr angesehen werden, insbesondere bei paralleler Dynamik ist das Modell identisch zum NaSch mit Höchstgeschwindigkeit 1. Im Anschluß an die Vorstellung des MPA werden approximative Methoden diskutiert, die speziell für die Behandlung des NaSch Modells entwickelt wurden. Die Anwendung dieser Methoden beschränkt sich allerdings nicht auf das NaSch Modell.

Nach diesen einführenden Kapiteln schließt sich die Untersuchung des Phasenübergangs im NaSch Modell an. Beim NaSch Modell zeichnen sich die stationären Zustände bei niedrigen und hohen Dichten durch qualitativ verschiedenes Verhalten aus. Bei niedrigen Dichten können die Autos mit ihrer Wunschgeschwindigkeit fahren. Im Unterschied dazu beobachtet man bei hohen Dichten die Bildung von Staus. Im deterministischen Grenzfall, d.h. bei verschwindendem Trödelparameter, kann man kritisches Verhalten beobachten. Bei eingeschaltetem Rauschen ist hingegen kein kritisches Verhalten zu beobachten. Dies zeigte sich insbesondere im Verhalten des Ordnungsparameters und bei der Untersuchung der relevanten Längenskalen. Für den Ordungsparameter wurde gefunden, daß im Gegensatz zum deterministischen Fall keine eindeutige Übergangsdichte bestimmt werden konnte, sondern vielmehr ein Übergangsbereich existiert, in dem der Ordnungsparameter kontinuierlich anwächst. Die relevanten Längenskalen, die aus verschiedenen Verteilungsfunktionen sowie dem asymptotischen Verhalten der Korrelationsfunktion bestimmt werden konnten, zeigten ebenfalls die Abwesenheit von kritischem Verhalten im nicht-deterministischen Fall.

In den Kapiteln 5 und 6 wird der Einfluß von inhomogenen Gittern auf den stationären Zustand des TASEP sowie des NaSch Modells untersucht. Eine Realisierung solcher Gitter sind periodische Systeme mit sogenannten Defekten. Als Defekte werden Gitterplätze bezeichnet, bei denen die Beweglichkeit der Teilchen reduziert wird. Es zeigt sich, daß man drei verschiedene Phasen mit qualitativ verschiedenem Verhalten unterscheiden kann. Bei niedrigen und hohen Dichten nimmt der Fluß den Wert des homogenen Systems an, während bei mittleren ein Plateau im Fundamentaldiagramm auftritt, in dem der Fluß einen konstanten Wert annimmt. Dieses Verhalten ist auf Phasenseparationseffekte zurückzuführen. Bei niedrigen und hohen Dichten führt der Defekt nur zu lokalen Inhomogenitäten des Dichteprofils. Im Gegensatz dazu bilden sich bei mittleren Dichten koexistierende makroskopische Hoch- und Niedrigdichtebereiche aus. Das grundlegende Phänomen kann mit Hilfe eines phänomenologischen Ansatzes beschrieben werden, der eine gute Übereinstimmung mit den numerischen Resultaten zeigt. Dieses Szenario wurde für ausgedehnte Defekte und höhere Maximalgeschwindigkeiten verallgemeinert. Bei den ausgedehnten Defekten erhält man die gleiche Struktur des Phasendiagramms, solange die Länge des Defektes als klein gegenüber der Systemgröße angesehen werden kann. Der Plateauwert des Flusses nähert sich dabei asymptotisch dem Wert des maximalen Fluß des homogenen Systems an, das ausschließlich aus „langsamen"' Gitterplätzen besteht. Für höhere Maximalgeschwindigkeiten kann man ebenfalls das gleiche generische Verhalten beobachten, allerdings führen die langreichweitigen Korrelationen zu Oszillationen des Dichteprofils im Niedrigdichtebereich.

Im folgenden Kapitel wird der TASEP und das NaSch Modell mit offenen Randbedingungen untersucht. Bei offenen Randbedingungen kann man den Effekt sogenannter randinduzierter Phasenübergänge beobachten, die eine charakteristische Eigenschaft von getriebenen Systemen sind. Im ersten Teil dieses Kapitels werden die exakten Ergebnisse für den TASEP mit verschiedenen Dynamiken diskutiert. Insbesondere werden die Flüsse und Dichteprofile in den verschiedenen Phasen dargestellt. Danach wird ein phänomenolgischer Ansatz, der von Kolomeisky et al. [88] vorgeschlagen wurde, diskutiert. Dieser phänomenologische Ansatz erlaubt die Bestimmung des Phasendiagramms direkt aus dem Fundamentaldiagramm des periodischen Systems. Zudem können auch die Längenskalen, die das Verhalten des Dichteprofils bestimmen, aus diesem Ansatz hergeleitet werden. Für den TASEP konnte gezeigt werden, daß die phänomenologischen Ergebnisse mit den exakten Resultaten im Limes großer Systemgrößen übereinstimmen. Dieses Resultat konnte auch für das NaSch Modell mit höheren Geschwindigkeiten bestätigt werden. Somit kann durch den phänomenologischen Ansatz die gemeinsame Struktur des Phasendiagramms erklärt werden.

Im Anschluß an diese Kapitel, die die grundlegenden Eigenschaften des NaSch Modells sowie des TASEP's vorgestellt haben, folgt in den Kapitel 7 und 8 die Diskussion der Anwendung dieser Modelle zur Beschreibung von Verkehrsfluß. Messungen an realem Verkehr zeigen die Existenz von metastabilen Höchstflußzuständen. Solche Zustände können vom NaSch Modell nicht reproduziert werden. In Kapitel 7 wird eine einfache Erweiterung des NaSch Modells vorgeschlagen, das solches Verhalten zeigt. Die Modifikation des Modells besteht darin, daß der Trödelparameter geschwindigkeitsabhängig gewählt wird. Diese modifizierte Version fällt in die Klasse von Modellen mit reduzierter Startbeschleunigung, die bei geeigneter Parameterwahl metastabile Zustände zeigen. Daher zeigen diese Untersuchungen, daß die reduzierte Startbeschleunigung verantwortlich für die Existenz metastabiler Zustände ist.

Im 8. Kapitel dieser Arbeit wird der Einfluß mehrerer Fahrzeugsorten in Zweispursystemen diskutiert. Überraschenderweise zeigt sich, daß bereits ein langsames Fahrzeug zur Bildung von makroskopischen Staus bei niedrigen Dichten führen kann. Die Robustheit dieses Phänomens wird für verschiedene Varianten der Spurwechselregeln und der Einspurdynamik studiert. Es zeigt sich, daß insbesondere Antizipationseffekte den Einfluß langsamer Fahrzeuge drastisch reduzieren können.

Die Untersuchung von eindimensionalen CA Modellen für Straßenverkehr hat gezeigt, daß diese Modelle in zweierlei Hinsicht interessant sind. Zum einen kann man an ihnen charakteristische Nichtgleichgewichts–effekte studieren, wie zum Beispiel randinduzierte Phasenübergänge, zum anderen bestaetigen Vergleiche mit Messdaten, daß sich diese Modelle sich zur realistischen Beschreibung von Straßenverkehr eignen.

# Danksagung

An dieser Stelle möchte Herrn Dr. Andreas Schadschneider für die hervorragende Betreuung, unzählige Diskussionen und Tips danken, ohne die das Zustandekommen dieser Arbeit nicht möglich gewesen wäre.

Herrn Prof. Dr. Johannes Zittartz danke ich für das Interesse an dieser Arbeit und die Schaffung idealer Arbeitsbedingungen.

Während der Anfertigung dieser Arbeit habe ich stark von der freundschaftlichen und offenen Atmosphäre innerhalb unserer Arbeitsgruppe profitiert. Dafür möchte ich allen Mitgliedern der Arbeitsgruppe danken. Insbesondere gilt mein Dank Georg Diedrich, Kai-Oliver Klauck und Nikolaus Rajewsky für die konstruktive Zusammenarbeit.

Der Arbeitsgruppe von Prof. Dr. Schreckenberg, insbesondere Robert Barlovic, Bernd Eisenblätter, Wolfgang Knospe und Lutz Neubert, sowie Prof. Dr. Debashish Chowdhury möchte ich ebenfalls für die hervorragende Zusammenarbeit danken.

Ich danke Julia Meyer, Kai-Oliver Klauck, Wolfgang Knospe, Lutz Neubert und Dr. Andreas Schadschneider für das Korrekturlesen des Manuskripts.

Mein besonderer Dank gilt meiner Frau, die immer ein großer Rückhalt für mich war.

Mein Dank gilt auch meiner Familie, meinen Schwiegereltern und meiner Schwägerin Alex für die stete Unterstützung während meiner Ausbildung.

## Erklärung

Ich versichere, daß ich die von mir vorgelegte Dissertation selbständig angefertigt, die benutzten Quellen und Hilfsmittel vollständig angegeben und die Stellen der Arbeit – einschließlich Tabellen, Karten und Abbildungen –, die anderen Werken im Wortlaut oder dem Sinn nach entnommen sind, in jedem Einzelfall als Entlehnung kenntlich gemacht habe; daß diese Dissertation noch keiner anderen Fakultät oder Universität zur Prüfung vorgelegen hat; daß sie – abgesehen von unten angegebenen Teilpublikationen – noch nicht veröffentlich worden ist sowie, daß ich eine solche Veröffentlichung vor Abschluß des Promotionsverfahrens nicht vornehmen werde. Die Bestimmungen dieser Promotionsordnung sind mir bekannt. Die von mir vorgelegte Dissertation ist von Prof. Dr. J. Zittartz betreut worden.

Köln, den 20. Dezember 1998

## Teilpublikationen:

B. Eisenblätter, L. Santen, A. Schadschneider, M. Schreckenberg:
*Jamming transition in a cellular automaton model for traffic flow.*
Phys. Rev. E **57**, 1309 (1998)

N. Rajewsky, L. Santen, A. Schadschneider, M. Schreckenberg:
*The Asymmetric Exclusion Process: Comparison of Update Procedures.*
J. Stat. Phys. **92**, 151 (1998)

L. Santen, A. Schadschneider:
*Jamming transition in a cellular automaton model for traffic flow.*
In: M. Schreckenberg, A. Bachem (Ed.), *Traffic and Granular Flow '97*, Springer, Singapore (1998)

R. Barlovic, L. Santen, A. Schadschneider, M. Schreckenberg:
*Metastable States in Cellular Automata for Traffic Flow.*
In: M. Schreckenberg, A. Bachem (Ed.), *Traffic and Granular Flow '97*, Springer, Singapore (1998)

W. Knospe, L. Santen, A. Schadschneider, M. Schreckenberg:
*Disorder effects in cellular automata models for traffic flow.*
In: M. Schreckenberg, A. Bachem (Ed.), *Traffic and Granular Flow '97*, Springer, Singapore (1998)

R. Barlovic, L. Santen, A. Schadschneider, M. Schreckenberg:
*Metastable States in Cellular Automata for Traffic Flow.*
Eur. Phys. J. B **5**, 793 (1998)

L. Santen, J. Esser, L. Neubert, J. Wahle, A. Schadschneider, M. Schrek–kenberg: *Online-Simulation of Urban Traffic Using Cellular Automata.*
In: J. D. Griffiths (Ed.), *Proceedings of the Third International Conference on Mathematics in Transport Planning and Control*, Pergamon, Amsterdam (1998)

W. Knospe, L. Santen, A. Schadschneider, M. Schreckenberg:
*Disorder effects in cellular automata models for two-lane traffic.*
Physica A **265**, 614 (1999)

D. Chowdhury, L. Santen, A. Schadschneider, S. Sinha, A. Pasupathy:
*Spatio temporal organization of vehicles in a cellular automata model of traffic with 'slow-to-start' rule.*
J. Phys. A **32**, 3229 (1999)